The Static Potential in QCD

Dissertation
zur Erlangung des Doktorgrades
des Fachbereichs Physik
der Universität Hamburg

vorgelegt von
York Schröder
aus Celle

Hamburg
1999

Gutachter der Dissertation:	Prof. Dr. W. Buchmüller Prof. Dr. G. Kramer
Gutachter der Disputation:	Prof. Dr. W. Buchmüller Prof. Dr. B. Kniehl
Datum der Disputation:	28. Juni 1999
Dekan des Fachbereichs Physik und Vorsitzender des Promotionsausschusses:	Prof. Dr. F.-W. Büßer

Abstract

In quantum chromodynamics (QCD), the binding energy of an infinitely heavy quark–antiquark pair in a color singlet state can be calculated as a function of the distance. We investigate this static potential of QCD perturbatively in three and four dimensions. For the four–dimensional (4D) case, we calculate the full two-loop coefficient, correcting an earlier result. Beyond this order, the perturbative expansion breaks down. In three dimensions, already the one-loop calculation gives a new result. At two loops, we analyze the infrared behaviour in detail. We present a new type of diagrams, that can potentially cure the 3D divergences, and that are shown to vanish in four dimensions.

Zusammenfassung

Die Wechselwirkungsenergie eines unendlich schweren Quark–Antiquark Paares in einem Farbsingulett–Zustand kann in der Quantenchromodynamik (QCD) als Funktion des Abstandes berechnet werden. Wir untersuchen dieses statische Potential der QCD im Rahmen der Störungstheorie in drei und vier Dimensionen. Im vierdimensionalen (4D) Fall berechnen wir den kompletten Zwei–Schleifen Beitrag, wobei ein früheres Resultat korrigiert wird. In höheren Ordnungen bricht die Störungsreihe zusammen. In drei Dimensionen erhält man bereits mit einer Ein–Schleifen Berechnung ein neues Resultat. Das Infrarotverhalten des Zwei–Schleifen Beitrages wird detailliert diskutiert. Wir präsentieren einen neuen Diagrammtyp, welcher in der Lage sein könnte, die 3D–Infrarotdivergenzen zu beheben, der aber in vier Dimensionen verschwindet.

Contents

Introduction

The static potential of quantum chromodynamics (QCD) is subject to theoretical investigations since more than twenty years. Being the non–abelian analogue of the well–known Coulomb potential of quantum electrodynamics (QED), this interaction energy of an infinitely heavy quark–antiquark pair is a fundamental concept which is expected to play a key role in the understanding of quark confinement. Moreover, the static potential is a major ingredient in the description of non–relativistically bound systems like quarkonia, and it is of importance in many other areas, such as quark mass definitions and quark production at threshold.

It is expected that the static potential consists of two terms: a Coulomb–like term at short distances, which is calculable with perturbative methods, and a long–distance term responsible for confinement. Even though a perturbative analysis is not suited to give the full potential, such a calculation proves very useful. The short–distance part of the potential can be utilized as a refined starting point for the construction of potential models (which have been rather successful in the past for the description of quarkonia), or it could describe very heavy systems (like $\bar{t}t$) to good accuracy. Furthermore, it can be compared to the results of numerical calculations in lattice gauge theory. It is natural to define the QCD coupling constant with help of the potential as $V(r) = -\frac{4}{3}\frac{\alpha_V(1/r)}{r}$, the so-called V–scheme [1], using a physical quantity in contrast to the usual coupling definition in the $\overline{\rm MS}$ scheme [2]. In lattice calculations α_V is regarded as as the 'better' expansion parameter [3]. For these reasons, and to get a more precise determination of $\alpha_{\overline{\rm MS}}$ from the lattice, the relation between the two couplings has to be known.

A first determination of the static potential in (massless) QCD has been performed by L. Susskind in the context of a lecture about lattice gauge theory [4]. In order to demonstrate asymptotic freedom in Yang–Mills theory, he calculated the one-loop pole terms using a Wilson–loop formula for the potential, and re-derived the first coefficient of the renormalization group Beta function. This work was extended by other groups quite soon, who then added fermionic contributions [5] and two-loop pole terms [6] to the potential, as well as examined the structure of higher–order corrections qualitatively [7]. Recently, the perturbative static potential has received new interest, in particular due to its application in top–quark production at threshold [8], a process that comes within experimental reach in the near future. A complete two-loop calculation for the static potential was performed in ref. [9]. Such an important result clearly

needs confirmation. This is one of the motivations of our work on the two-loop potential. More recently, the effect of fermion masses was considered on the two-loop level in ref. [10].

There has always been discussion about whether the perturbative Wilson–loop formula is a well-defined definition of the static potential, which can be questioned due to possible infrared divergences in higher orders [7]. A redefinition was proposed recently [11], which becomes effective at the three-loop level. To study the infrared structure of the potential, one can also investigate the theory in lower dimensions (than four) [12]. Hence, while calculating the two-loop potential, we will specify the space–time dimension at a late stage only, enabling us to discuss the case of three dimensions also.

Another line of motivation for performing a three–dimensional calculation comes from finite temperature field theories [13]. Due to dimensional reduction at high temperatures, the original (4D) theory can be described by an effective theory in three (Euclidean) dimensions [14, 15]. The spectrum of the dimensionally reduced theory describes the problematic infrared sector of the full theory [16]. Since the reduced theory has a universal character in the sense that it can describe different 4D theories by choosing the parameters accordingly, the 3D static potential is interesting conceptually in its own right. Moreover, as the electroweak standard model can be mapped to a 3D SU(2)×U(1) gauge–Higgs theory [17], the symmetric phase of the SU(2) Higgs model has received a lot of interest in studies of the electroweak phase transition. In particular, the efforts to understand the spectrum of this theory as obtained in lattice simulations [18] led to the picture of an effective theory of (weakly) bound states [19], for which the knowledge of the 3D static potential is an important ingredient in a non-relativistic treatment. A most welcome observation in this respect is the following. Since in 3D the gauge coupling g^2 acquires the dimension of a mass, one expects the perturbative expansion of the potential to be of the form $V^{3D}_{\rm pert}(r) = c_1 g^2 \ln(g^2 r) + c_2 g^4 r + \ldots$, where the c_i are dimensionless coefficients. At the one-loop level, a linear term is produced automatically. This is in contrast to the behaviour in 4D, where $V^{4D}_{\rm pert}(r) = c_0 g^2/r \cdot (1 + c_1 g^2 \ln(r\mu) + \ldots)$ leads to the well–known effective (running) coupling.

Concerning the purely technical side of the work documented here, only part of the Feynman diagrams to be considered, namely the pure self-energy contributions to the static potential, are amenable to standard calculation methods [20, 21, 22, 23]. For the others, essentially being two–point functions also, but involving non–covariant propagators, the standard methods need to be generalized. We will present a general strategy to deal with these expressions, which is based on a purely algebraic reduction to a minimal set of integrals, and apply it to the two-loop case.

The outline of this work is as follows. In chapter 1 the Wilson–loop definition of the static potential is introduced. Following a discussion of the abelian model (QED), which serves to introduce the notation as well as to illustrate some conceptual problems in a simple example,

the perturbative expansion of the Wilson–loop is worked out for QCD. All Feynman diagrams that are relevant for the potential up to two loops are displayed. Chapter 2 deals with the algebraic calculation of massless two-loop two–point functions that involve static propagators. A method for the tensor reduction is worked out, and a general algorithm for the reduction of the resulting propagator–type integrals to a minimal set of basic scalar integrals is presented. Furthermore, the derivation of the applied recurrence relations is explained.

In chapter 3 the static potential is calculated to two loops. Analytic results are presented for arbitrary dimensions D. Renormalization and infrared cancelation are discussed both in the four–dimensional and in the three–dimensional theory. Chapter 4 is concerned with an analysis of the potential in coordinate space, in order to clarify issues related to the infrared sector. A new type of diagrams is shown to potentially contribute to the two-loop term in three dimensions. In chapter 5 the problems known to arise in higher orders of the perturbative expansion are briefly reviewed. In addition, one-loop results for the massive SU(N) Higgs model are given.

In the four appendices, additional reduction formulae, the complete set of massless integrals as well as some massive ones, the two-loop infrared poles of individual diagrams, and the Feynman rules are listed.

Chapter 1

The Static Potential

In this chapter, the static potential will be defined. In order to explain some general features in a simple abelian example, the potential will be discussed first in QED. Being exactly solvable, the pure abelian potential allows for an easy understanding of the perturbative treatment, which becomes inevitable in more complicated cases. For the non–abelian case of QCD, the color structure will be exploited in a compact notation, and the complete set of diagrams contributing to the potential up to two loops will be presented.

1.1 Abelian Case

In QED, the static potential $V(r)$ is defined as the interaction energy of an infinitely heavy electron–positron pair separated by a distance r. Generalizations to other theories, like QCD, are obvious. The idealization to fixed sources is necessary in order to obtain the potential as a non-relativistic, semi-classical quantity. Furthermore, this idealization allows a simple, gauge–invariant and non–perturbative definition, which is useful for analytical as well as numerical (lattice) studies.

Since the abelian potential was already analyzed in detail in the past (see, e.g., [4, 6, 9]), we will be very brief here. Giving the main arguments, this section will be used mainly to introduce some notation and set the stage for the non–abelian case.

1.1.1 Definition and Exact Solution

In the abelian case, let us start from the manifest gauge invariant definition [6]

$$V(r) = -\lim_{T\to\infty} \frac{1}{T} \ln \left\langle \mathcal{T} \exp\left(ie \oint_\Gamma dx_\mu A_\mu \right) \right\rangle \ . \tag{1.1}$$

Here, Γ is taken as a rectangular path with time extension T and spatial extension r (see fig. 1.1), and $\mathcal{T}$ denotes time ordering. The average is to be taken over the photon field in the

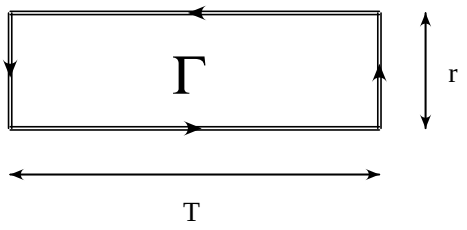

Figure 1.1: *Rectangular Wilson–loop for the definition of the static potential.*

usual way,

$$\left\langle \mathcal{O}(A) \right\rangle \;=\; \frac{\int \mathcal{D}A \, \exp\left(-S\right) \; \mathcal{O}(A)}{\int \mathcal{D}A \, \exp\left(-S\right)} \,, \tag{1.2}$$

where the Euclidean action is given by (recall that ghosts decouple here and hence cancel in the above average)

$$S = \int_x \mathcal{L} = \int_x \left[\tfrac{1}{4} F_{\mu\nu} F_{\mu\nu} + \tfrac{1}{2\eta} \left(\partial_\mu A_\mu\right)^2 \right] = \int_{\not q} \left[\tfrac{1}{2} A_\mu M_{\mu\nu} A_\nu \right] \tag{1.3}$$

with inverse propagator $M_{\mu\nu} = q^2 g_{\mu\nu} + \left(\frac{1}{\eta} - 1\right) q_\mu q_\nu$. For further notation, e.g. notations for integral measures, see appendix D. Neglecting the contributions coming from the vertical parts of the Wilson–loop, the definition becomes

$$V(r) \;=\; -\lim_{T\to\infty} \frac{1}{T} \ln \left\langle \mathcal{T} \exp\left(-\int_x J_\mu A_\mu \right) \right\rangle \,, \tag{1.4}$$

$$J_\mu(x) \;=\; iev_\mu \left[\delta(\boldsymbol{x}) - \delta(\boldsymbol{x} - \boldsymbol{r}) \right] \theta\left(T^2/4 - x_0^2\right) \tag{1.5}$$

$$\;=\; \int_{\not q} \exp(-iqx) \, iev_\mu \left[1 - \exp(i\boldsymbol{q}\boldsymbol{r}) \right] \frac{\sin(q_0 T/2)}{q_0/2} \,. \tag{1.6}$$

Since the Wilson–loop explicitly breaks Lorentz invariance, an extra vector $v_\mu = \delta_{\mu 0}$ is introduced. The functional integral is Gaussian, so it can be solved exactly. Shifting $A = A' - M^{-1} J$ and inserting all expressions in momentum-space representation, the potential reads

$$\begin{aligned} V(r) \;&=\; -\lim_{T\to\infty} \frac{1}{T} \int_{\not q} \tfrac{1}{2} J_\mu M^{-1}_{\mu\nu} J_\nu \\ &=\; \lim_{T\to\infty} \frac{1}{T} \int_{\not q} e^2 \left[1 - \exp(-i\boldsymbol{q}\boldsymbol{r}) \right] \left(\frac{\sin(q_0 T/2)}{q_0/2} \right)^2 v_\mu \left\{ \frac{1}{q^2} g_{\mu\nu} + (\eta - 1) \frac{q_\mu q_\nu}{q^4} \right\} v_\nu \\ &=\; \int_{\not\boldsymbol{q}} \left[1 - \exp(-i\boldsymbol{q}\boldsymbol{r}) \right] \frac{e^2}{\boldsymbol{q}^2} \;=\; \Sigma + V_{\text{Coul}} \,. \end{aligned} \tag{1.7}$$

In the last step, the limit was pulled inside the integral, to exploit a representation of the delta-function,

$$\lim_{T\to\infty} \frac{1}{T} \left(\frac{\sin(q_0 T/2)}{q_0/2} \right)^2 = 2\pi \delta(q_0) \,. \tag{1.8}$$

As expected, one gets an (attractive) Coulomb–potential plus an (infinite) constant, which represents the self-energy of the sources. The r–independent constant can be dropped in the definition of a potential, of course.

If one wants to include the effect of dynamic fermions (which would contribute via internal loops only), or even to go over to the non–abelian theory, it is no longer possible to derive an exact analytic result. Before dealing with these more complicated cases, it proves very useful to re-derive the above result by a perturbative analysis as a 'training exercise'.

1.1.2 Perturbative Treatment and Exponentiation

The Feynman rules can be obtained from from the path–integral representation of the vacuum expectation value in eq. (1.4). They are collected in appendix D. In addition to the usual Feynman rules of QED, one gets a source–photon coupling and a 'source propagator', the latter of which reflects the time–ordering prescription and hence is a theta–function in coordinate space, or has the non-covariant propagator form $i/(v \cdot p + i\epsilon)$ in momentum space.

The form of the static propagator coincides with the one that is used in the leading order of an effective theory of heavy electrons, which is the abelian counterpart of the heavy–quark effective theory (HQET) [24]. This comes as no surprise, since the same asymptotics of the full theory is examined in both cases, and shows the connection with another well–known approach to the potential, namely via the scattering amplitudes, which in turn even give information on spin–dependent and relativistic corrections to the potential. In the full theory, the Bethe–Salpeter kernel is constructed this way [25].

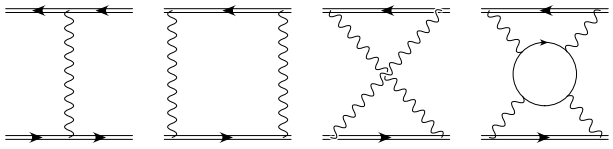

Figure 1.2: *Lowest order diagrams for the QED potential (a..c), and light–by–light scattering in a three-loop diagram (d). The double line stands for the static (source) propagator, while wavy and straight lines denote photons and electrons, respectively.*

Starting with the perturbative treatment, the Born term (see fig. 1.2) reads

$$\begin{aligned} V_{\rm tree} \;=\; \text{diag.}(a) \;&=\; \int_{\boldsymbol{q}} \exp\left(-i\boldsymbol{q}\boldsymbol{r}\right)(-)\,(iev_\mu)\,(-iev_\nu)\,D_{\mu\nu}(q)\Big|_{q_0=0} \\ &=\; -e^2 \int_{\boldsymbol{q}} \exp\left(-i\boldsymbol{q}\boldsymbol{r}\right)\frac{1}{\boldsymbol{q}^2}\,. \end{aligned} \tag{1.9}$$

Comparing with the above exact result, eq. (1.7), this seems to be the complete Coulomb

potential already. The question is now what happens to higher–order contributions.

At next–to–leading order, one finds the two ladder diagrams of fig. 1.2. They are most easily analyzed in coordinate space, due to the simple form of the source propagator (a theta function). It is immediately clear that adding the two diagrams effectively removes the time–ordering on one of the source–lines, due to $\theta(t)+\theta(-t)=1$. Adding the sum again with switched arguments removes the second time–ordering, too, and we get the product of two tree-level diagrams. The result is thus

$$\text{diag.}(b)+\text{diag.}(c)=\frac{1}{2}\left[\text{diag.}(a)\right]^2=\frac{1}{2}\,V_{\text{Coul}}^2\,. \tag{1.10}$$

In a completely analogous way, one can show that the sum of the remaining one-loop diagrams (source–self-energy insertions as well as vertex corrections) contribute $\Sigma\cdot V_{\text{Coul}}$ and $\frac{1}{2}\Sigma^2$. Now, recalling the logarithm in the definition of the potential, all one-loop contributions can be seen to cancel against the first iteration of the tree-level term.

The cancelation works in the same way in higher orders, as proven in the appendix of [6]. Again, crossing two lines always removes one time–ordering, such that the sum of all ladder diagrams at n–loop order contributes a term $V_{\text{Coul}}^n/n!$, while the others will give contributions of the form $\Sigma^k/k!\cdot V_{\text{Coul}}^{(n-k)}/(n-k)!$. Altogether, the Wilson–loop exactly builds up the exponentiated potential, so the result (1.7) gets reproduced in the perturbative treatment, indeed.

The next step would be the inclusion of electron loops (with negligible mass). This leads to the inclusion of the fermionic determinant in the path–integral representation, such that an exact solution is no longer possible. Hence, going beyond the trivial case of a pure abelian gauge theory makes the perturbative treatment the only viable algebraic tool. After identifying the non–iterative diagrams along the above arguments in coordinate space, it proves more tractable to work in momentum space. The main effect of fermion loops is the well–known vacuum polarization effect. This leads to an effective, 'running', coupling $\alpha_{\text{eff}}(\boldsymbol{q}^2)=\alpha_{\text{eff}}(0)/(1+\Pi(\boldsymbol{q}^2))$, where $\alpha_{\text{eff}}(0)$ denotes the fine structure constant $e^2/4\pi$. In the potential, however, fermion loops can also contribute via light–light scattering in three-loop and higher–order diagrams. As a result, the momentum–space potential will have the form

$$V(\boldsymbol{q}^2) \;=\; -\frac{4\pi\alpha_V(\boldsymbol{q}^2)}{\boldsymbol{q}^2}\,, \tag{1.11}$$

with $\alpha_V\neq\alpha_{\text{eff}}$ providing a useful gauge invariant definition of a 'physical' coupling, the so–called V–scheme [1].

Let us stop the discussion of the abelian case at this point. The QED potential can be obtained via simple replacements from the QCD potential, to which we now turn, so a separate calculation would be superfluous.

1.2 Non–Abelian Case

The quark–antiquark ($q\bar{q}$) potential, defined as the binding energy of an infinitely heavy $q\bar{q}$ pair in a color singlet state, needs some minor modifications of the Wilson–loop formula (1.1), due to the non–abelian nature of the gauge fields. In this section, after generalizing the above definition, we will identify the non–iterative diagram classes that have to be computed for the perturbative potential. The actual calculation of the generated list of diagrams is quite involved and will be presented in the following chapters.

1.2.1 Definition and Expansion

The modified Wilson–loop formula reads [6, 26]

$$V(r) = -\lim_{T\to\infty} \frac{1}{T} \ln \left\langle \widetilde{\mathrm{tr}}\, \mathcal{P} \exp\left(ig \oint_\Gamma dx_\mu A_\mu \right) \right\rangle \ . \tag{1.12}$$

Like in the abelian case, Γ is taken as a rectangular loop with time extension T and spatial extension r. Due to the non-commuting gauge fields A_μ, the time–ordering prescription had to be generalized to a path ordering along the loop. Also, the normalized color trace $\widetilde{\mathrm{tr}}(..) = \mathrm{tr}(..)/\mathrm{tr}\mathbb{1}$ had to be introduced in the above.

In a perturbative analysis it can be shown that, at least to the order needed here[1], all contributions to eq. (1.12) containing connections to the spatial components of the gauge fields $A_i(\boldsymbol{r}, \pm T/2)$ vanish in the limit of large time extension T. Hence, the definition can be reduced to

$$V_{\mathrm{pert}}(r) = -\lim_{T\to\infty} \frac{1}{T} \ln \left\langle \widetilde{\mathrm{tr}}\, \mathcal{T} \exp\left(-\int_x J^a_\mu A^a_\mu \right) \right\rangle \ , \tag{1.13}$$

where $\mathcal{T}$ means time ordering and the static sources separated by the distance $r = |\boldsymbol{r}|$ are given by

$$J^a_\mu(x) = ig\, \delta_{\mu 0} T^a \, [\, \delta(\boldsymbol{x}) - \delta(\boldsymbol{x} - \boldsymbol{r}) \,] \, \theta\left(T^2/4 - x_0^2 \right) \ , \tag{1.14}$$

where T^a are the generators in the fundamental representation (choosing the adjoint representation, one would get the potential for a static color–singlet gluino–pair). In the case of QCD the gauge group is $SU(3)$. Let us stay a little more general, however, and carry out the calculation for an arbitrary compact semi-simple Lie group. Definitions for the invariants C_A and C_F as well as some useful relations for performing the color traces are collected in appendix D.2. The number of massless quarks will denoted by n_f.

Expanding the expression in eq. (1.13) perturbatively, one encounters in addition to the usual Feynman rules the source–gluon vertex $ig\delta_{\mu 0} T^a$, with an additional minus sign for the antisource, like in the preceding section. Again, the time–ordering prescription generates step

[1] For a detailed discussion of this point, see sect. 4.3.

functions, which can be viewed as source propagators, in analogy to HQET. Now, an overall color trace is to be taken along the loop. The Feynman rules are collected in the appendix.

Concerning the generation of the complete set of Feynman diagrams contributing to the two-loop static potential, there are some subtleties connected with the logarithm in the definition (1.13), as already discussed in the abelian case. After working out the color trace along the static loop, one obtains

$$\begin{aligned}\left\langle ... \right\rangle \;=\; & 1 + g^2 C_F \; \text{} + g^4 C_F \Big[C_F \; \text{  } + (C_F - \tfrac{1}{2} C_A) \; \text{} + \tfrac{1}{2} C_A \; \text{} + \; \text{} \Big] \\ & + g^6 C_F \Big[(C_F - \tfrac{1}{2} C_A)^2 \; \text{  } + (C_F - C_A)(C_F - \tfrac{1}{2} C_A) \; \text{  } + \tfrac{1}{2} C_A (C_F - \tfrac{1}{2} C_A) \; \text{  } \\ & + \tfrac{1}{4} C_A^2 \; \text{  } + \tfrac{1}{4} C_A^2 \; \text{  } + (C_F - \tfrac{1}{2} C_A) \; \text{  } + \tfrac{1}{2} C_A \; \text{  } + \tfrac{1}{2} C_A \; \text{  } + \; \text{  } + \; \text{  } \\ & + C_F \; \text{} + C_F^2 \; \text{} + C_F^2 \; \text{  } + C_F (C_F - \tfrac{1}{2} C_A) \; \text{} + \tfrac{1}{2} C_F C_A \; \text{} + 0 \cdot \; \text{} \Big] \\ & + \mathcal{O}(g^8) \; . \end{aligned} \tag{1.15}$$

The diagrammatic notation is that of Susskind [4]. The outer loop stands for the source, while the inner lines are gluons. Blobs denote 1PI–insertions, containing gluons, ghosts and (light) quarks. Diagrams are conveniently collected in topological classes, from which the actual 2→2 amplitudes are generated by cutting the source loop twice. After expanding the logarithm and using the relations

$$\tfrac{1}{2} \; \text{  }^2 \;=\; \text{  } + \text{  } \tag{1.16}$$

$$\text{  } \; \text{} \;=\; 3 \; \text{  } + 3 \; \text{  } + 2 \; \text{  } + \; \text{  } \tag{1.17}$$

$$\text{  } \; \text{} \;=\; \text{  } + 2 \; \text{  } + 3 \; \text{  } \tag{1.18}$$

$$\text{  } \; \text{} \;=\; \text{  } + \text{  } \tag{1.19}$$

$$\text{  } \; \text{} \;=\; \text{} + \text{} \tag{1.20}$$

(which, using the strategy explained in the abelian case, can most easily be checked in position space due to the trivial identity $\theta(t)+\theta(-t) = 1$), some topological classes cancel completely (one class in the g^4–term, five classes in the g^6–term; compare eq. (1.15)), while only the non–abelian parts of the others remain:

$$\begin{aligned}\ln \left\langle ... \right\rangle \;=\; & g^2 C_F \; \text{} + g^4 C_F \Big[-\tfrac{1}{2} C_A \; \text{} + \tfrac{1}{2} C_A \; \text{} + \; \text{} \Big] \\ & + g^6 C_F \Big[\tfrac{1}{4} C_A^2 \; \text{} + \tfrac{1}{2} C_A^2 \; \text{} - \tfrac{1}{4} C_A^2 \; \text{} + \tfrac{1}{4} C_A^2 \; \text{} + \tfrac{1}{4} C_A^2 \; \text{} \\ & - \tfrac{1}{2} C_A \; \text{} + \tfrac{1}{2} C_A \; \text{} + \tfrac{1}{2} C_A \; \text{} + \; \text{} + \; \text{} \Big] + \mathcal{O}(g^8) \; . \end{aligned} \tag{1.21}$$

This explicitly proves the exponentiation up to the two-loop level. However, for the non–abelian case no general proof is known so far.

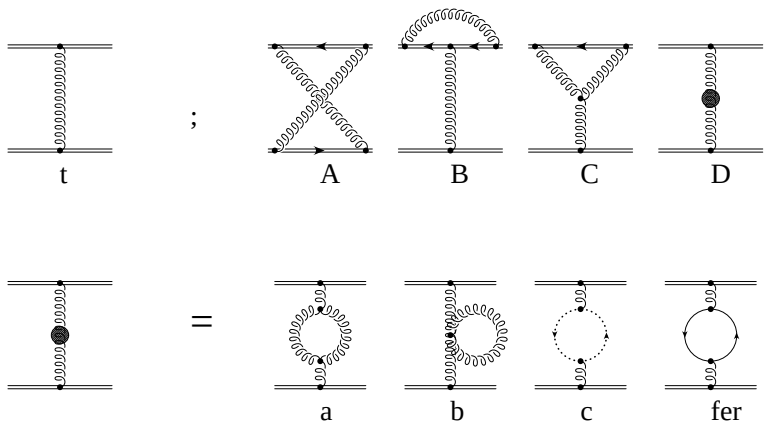

Figure 1.3: *Tree-Level (t) and one-loop exchange diagrams (A..D) contributing to the static potential. Double, curly, dotted and solid lines denote source, gluon, ghost and (light) fermion propagators, respectively. The blob on the gluon line stands for one-loop self-energy corrections, which are given in the second line.*

1.2.2 Lists of Diagrams

As mentioned above, the Feynman diagrams are generated from the topological classes of eq. (1.21) by cutting the source loop twice. By definition, only pure exchange diagrams need to be considered in the calculation of $V_{pert}(r)$, since the others (self-energy corrections of the sources) are independent of r. Hence, there is only one diagram at tree-level, namely the one–gluon exchange diagram. It is shown in fig. 1.3, together with the one-loop diagrams contributing to the potential. The set of diagrams to be considered for the two-loop correction is reduced to the diagrams of fig. 1.4. In both figures, we have omitted diagrams that differ from the ones shown by a mere rotation or reflection.

Let us already drop a word of caution here. In later stages of this work, when discussing the potential in other than four dimensions, we will find that the list of two-loop diagrams presented here is not complete. The source–self-energy corrections will become important for infrared safety, and diagrams containing couplings to the 'vertical' pieces of the Wilson–loop will start to contribute. However, returning to the physical case of four dimensions, these points are of no concern. This is why we postpone a detailed discussion of these issues to chapter 4 and turn to the calculation of the presented exchange diagrams up to the two-loop level immediately.

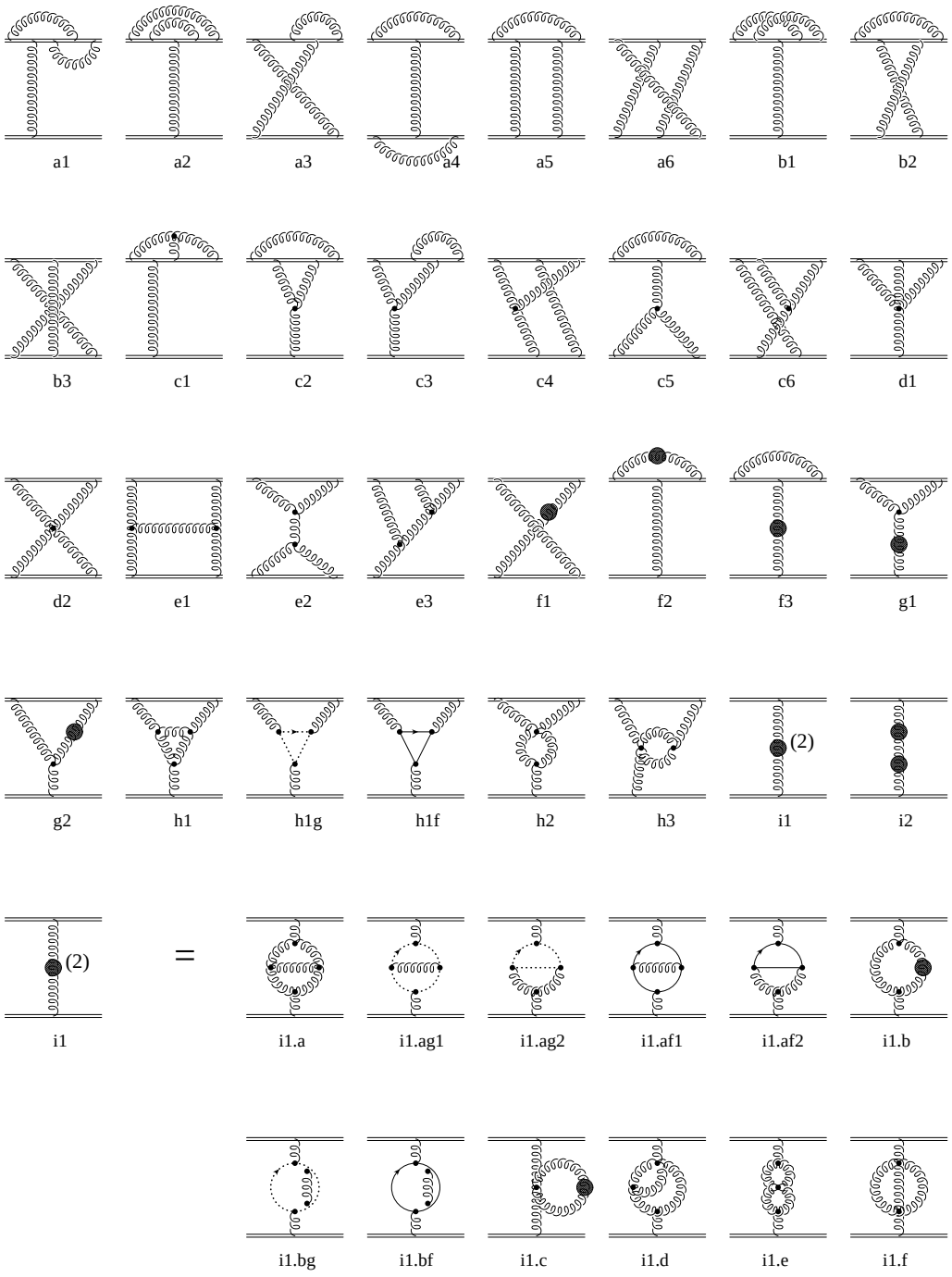

Figure 1.4: *Classes of two-loop exchange diagrams contributing to the static potential. For notation, see fig. 1.3.*

Chapter 2

Calculation Techniques

In this chapter, the calculation techniques used to reduce the analytical expressions for the Feynman diagrams to a linear combination of elements from a minimal set of basic scalar integrals are described in detail. Necessarily, the material presented here is somewhat technical. To enhance readability, graphical representations of the formulae are presented where possible.

The adopted reduction strategy is complete in the sense that neither a specialization only to integrals occurring in the calculation of the static potential nor a restriction of allowed powers of propagators or numerator structures is done. Hence, the algorithm may well be used to treat the two-loop–part of possible higher–order calculations.

An algorithm for massive two-loop two–point functions was already presented by Tarasov [23]. Treating the massless case only, the new feature added here is the inclusion of non-covariant propagators (arising from the source lines in our particular case). This effectively introduces one more 'four'–momentum, namely the vector v, into the integral, hence making a tensor reduction à la Passarino/Veltman [27] somewhat involved. To avoid the problem of singular Gram–determinants, we therefore take Tarasov's method as a basis for a generalization to source propagators.

Before presenting the reduction algorithm in detail, it is worthwhile to explicitly give the two cornerstones of the (purely algebraic) reduction strategy.

Following a trivial reduction of scalar products in the numerator, the first step is to trade the remaining scalar products for operators T, which raise the indices of the propagators as well as the dimension of the integral. This is efficiently done by generalizing Tarasov's method to include static propagators.

In a second step, pure propagator integrals with arbitrary powers of the lines are reduced in a standard way (integration by parts) [20] to a minimal set of basic scalar integrals. The new point here, as already introduced by Tarasov in his treatment of covariant propagators, is to mix in the T–operators, as to allow only integrals with the original dimension of space–time to

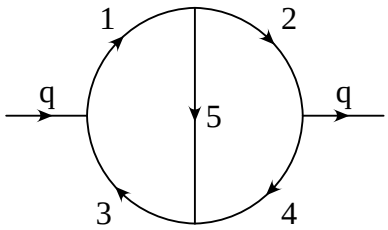

Figure 2.1: *The master two-loop two-point diagram*

build up the basic set.

This chapter is organized as follows. In section 2.1 the general notation is introduced, followed by a description of an optimal procedure for the integrand simplification. Furthermore, a method for the representation of tensor integrals as well as integrals with irreducible numerators in terms of scalar ones with shifted space–time dimensions is given. The next section describes the structure of a generic algorithm to reduce the scalar integrals with shifted dimensions to a minimal set of basic integrals. Each part of the algorithm is illustrated graphically to enhance readability. In section 2.4 the general strategy to obtain such recurrence relations is outlined, including some concrete examples.

2.1 Preparation

In this section, a description of the method to reduce the calculation of two-loop two–point integrals with boson–type as well as static–type propagators to calculating scalar integrals only will be given. The main strategy is to trade irreducible numerators for a shift in the integral's space–time dimension, using (and generalizing) the method of refs. [21, 22].

2.1.1 General Notation and Numerator Simplification

In principle, all possible numerators (containing the four vectors k_1, k_2, q, v), including scalar as well as tensor ones, can be treated directly with the method of tensor decomposition of individual integrals by certain operators T given in section 2.1.3. Nevertheless, it is useful to do some 'naive' simplifications beforehand, since the T–operators are 'costly' in the sense that they enhance the number of terms to be treated by the subsequent reduction algorithm.

There are two types of denominators,

$$D_i \equiv D(k_i) = \frac{1}{k_i^2} \quad , \quad S_i \equiv S(k_i) = \frac{1}{(k_i v) + i\epsilon} \quad \text{with} \quad v = (1, \mathbf{0}) \; , \tag{2.1}$$

the former stemming from gluon, ghost and fermion propagators, and the latter stemming from the source propagators. Adopting the conventions given in fig. 2.1, the momenta are

$$k_1\ ,\ k_2\ ,\ k_3 = k_1 - q\ ,\ k_4 = k_2 - q\ ,\ k_5 = k_1 - k_2 \quad \text{where} \quad q = (0, \boldsymbol{q})\ . \tag{2.2}$$

Due to the orthogonality of the external vectors q and v, there are only three different generic source propagators, namely S_1, S_2 and S_5. For integration measures, the abbreviation

$$\int_i \equiv \int \frac{d^D k_i}{b^{D/2}} \tag{2.3}$$

will be used frequently[1].

The generic two-loop two–point tensor integral then has the form

$$\begin{aligned}&(k_1)_{\mu_1}...(k_1)_{\mu_\tau}(k_2)_{\lambda_1}...(k_2)_{\lambda_s} \circ [abcde, xyz] \\ &= \int_1 \int_2 (k_1)_{\mu_1}...(k_1)_{\mu_\tau}(k_2)_{\lambda_1}...(k_2)_{\lambda_s}\ D_1^a D_2^b D_3^c D_4^d D_5^e S_1^x S_2^y S_5^z\ ,\end{aligned} \tag{2.4}$$

where the symbol $\circ$ means that momenta k have to be considered under the integral sign.

The evaluation of diagrams in tensor form is more involved than the evaluation of scalar diagrams. In practice, one contracts the tensor structure with the appropriate projectors (constructed from the two external vectors q_μ, v_μ and the metric tensor $g_{\mu\nu}$), resulting in scalar integrals of the form

$$\mathcal{N}(k_1k_2, k_1^2, k_2^2, k_1q, k_2q, k_1v, k_2v) \circ [abcde, xyz]\ , \tag{2.5}$$

where $\mathcal{N}(k)$ is a polynomial in the seven nonzero scalar products. Hence, it is sufficient to describe the simplification of scalar numerators only.

Anticipating the result of section 2.1.3, it is most efficient to remove the products $(k_1k_2), k_1^2, k_2^2$ in favor of $(k_1q), (k_2q)$ from the numerator polynomials $\mathcal{N}(k)$ wherever possible, since the latter scalar products result in a lower shift of the integral's space–time dimension. Scalar numerators that cannot be simplified further based on this criterion will be called 'irreducible numerators'.

Naive Simplifications

To eliminate scalar products quadratic in the loop momenta k, the following identities can be used:

$$\begin{aligned} 2(k_1k_2)\ D_5 &= (k_1^2 + k_2^2)\ D_5 - 1 \\ k_2^2\ D_2 &= 1 \end{aligned}$$

[1] Later, we will choose $b = 4\pi^2$, but let us stay more general here.

$$\begin{aligned}
k_2^2\, D_4 &= (2(k_2q) - q^2)D_4 + 1 \\
k_2^2 \circ [a0c0\underline{e}, x0z] &\overset{k_2 \to k_1 - k_2}{\longrightarrow} (k_1^2 + k_2^2 - 2(k_1k_2)) \circ [aec00, xz0] \\
k_1^2\, D_1 &= 1 \\
k_1^2\, D_3 &= (2(k_1q) - q^2)\, D_1 + 1 \\
k_1^2 \circ [0b0d\underline{e}, 0yz] &\overset{k_1 \to k_1 + k_2}{\longrightarrow} (k_1^2 + k_2^2 + 2(k_1k_2)) \circ [eb0d0, zy0]
\end{aligned} \tag{2.6}$$

An underlined variable means that the corresponding index has to be greater than zero.

Factorization

After performing the above simplifications, the scalar product (k_1k_2) remains in the numerator only if the propagator D_5 is canceled (i.e. e=0). In this case, and if there is no propagator S_5 (i.e. z=0), the substitution

$$(k_1k_2) = \frac{(k_1v)(k_2v)}{v^2} + \frac{(k_1q)(k_2q)}{q^2} + A_{12} \tag{2.7}$$

where

$$A_{12} = k_1\, P_T\, k_2 \quad \text{with} \quad P_{T,\mu\nu} = g_{\mu\nu} - \frac{v_\mu v_\nu}{v^2} - \frac{q_\mu q_\nu}{q^2}\,, \tag{2.8}$$

allows one to factorize the integral into products of one-loop integrals. Integrals containing an odd power of A_{12} vanish identically since the transverse tensor of eq. (2.8) will always be multiplied by one of the external vectors q or v. Integrals with even powers of A_{12} then factorize as

$$\begin{aligned}
&\int_1 \int_2 f_1(k_1^2, k_1q, k_1v)\; f_2(k_2^2, k_2q, k_2v)\; A_{12}^{2n} \\
&= N(2n) \int_1 f_1(k_1^2, k_1q, k_1v)\; [\,k_1\, P_T\, k_1\,]^{\,n} \int_2 f_2(k_2^2, k_2q, k_2v)\; [\,k_2\, P_T\, k_2\,]^{\,n}\,.
\end{aligned} \tag{2.9}$$

Here, the prefactor can be calculated as

$$N(2n) = \frac{T_{\mu_1\ldots\mu_{2n}}\, P_{T,\mu_1\nu_1} \cdots P_{T,\mu_{2n}\nu_{2n}}\, T_{\nu_1\ldots\nu_{2n}}}{\left(P_{T,\mu_1\mu_2} \cdots P_{T,\mu_{2n-1}\mu_{2n}}\, T_{\mu_1\ldots\mu_{2n}}\right)^2} = \frac{\Gamma\left(\frac{2n+1}{2}\right)\Gamma\left(\frac{D-2}{2}\right)}{\Gamma\left(\frac{1}{2}\right)\Gamma\left(\frac{2n+D-2}{2}\right)}\,, \tag{2.10}$$

where the $T_{\mu_1\ldots\mu_{2n}} = g_{[\mu_1\mu_2} \cdots g_{\mu_{2n-1}\mu_{2n}]}$ are totally symmetric tensors constructed from the metric tensor only.

Irreducible Numerators

After applying the above simplifications as well as the factorization of the 'mixed' scalar product (k_1k_2), 'quadratic' scalar products left in the numerator imply a certain propagator structure:

- if (k_1k_2) is left, then $e = 0$ and $z > 0$

- if k_1^2 is left, then $a = c = 0$ and either $e = 0$ or $e > 0$ and $x > 0$
- if k_2^2 is left, then $b = d = 0$ and either $e = 0$ or $e > 0$ and $y > 0$

In addition, the four 'linear' scalar products $(k_1q), (k_2q), (k_1v), (k_2v)$ will occur in the numerator polynomial. As already mentioned above, these irreducible numerators will be removed by the T–operators of section 2.1.3.

2.1.2 Simplification of the Source Structure

All eight possible combinations of source lines can be transformed to just two patterns, according to the following flow diagram. To simplify the notation, overlined indices denote a reflection of the momentum of the corresponding line, i.e. $\bar{x} \hat{=} (S_{\bar{1}})^x = 1/(-(k_1v) + i\epsilon)^x$.

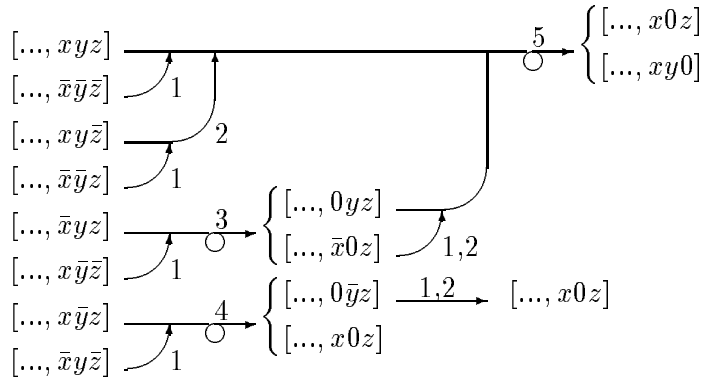

In the above, the shift $(1) : v \to -v$, the interchange of integration variables $(2) : k_1 \leftrightarrow k_2$, as well as the (possibly repeated; that's what the circle–arrows stand for in the graphical notation used here) inclusion of factors of one $(3) : 1 = -S_5 \left(S_{\bar{1}}^- + S_2^-\right)$, $(4) : 1 = S_5 \left(S_1^- + S_{\bar{2}}^-\right)$ and $(5) : 1 = S_1 \left(S_2^- + S_5^-\right)$ was used.

Furthermore, as for the boson–type propagators, some 'naive' simplifications can be made:

$$\begin{aligned} (k_1v)\, S_1 = 1 \quad &, \quad (k_1v)\, S_{\bar{1}} = -1 \ , \\ (k_2v)\, S_2 = 1 \quad &, \quad (k_2v)\, S_{\bar{2}} = -1 \ , \\ (k_2v)\, S_1 S_5 \ &= \ S_5 - S_1 \ . \end{aligned} \tag{2.11}$$

However, note that harmless–looking replacements like $S_{\bar{1}} = -S_1$ are not allowed. Written out in more detail,

$$S_{\bar{1}} = \frac{1}{-(k_1v) + i\epsilon} = -\frac{1}{(k_1v) + i\epsilon} - \frac{2i\epsilon}{(k_1v)^2 + \epsilon^2} \stackrel{\epsilon \to 0^+}{\longrightarrow} -S_1 - 2\pi i \delta(k_1v) \ , \tag{2.12}$$

this becomes immediately clear.

2.1.3 Tensor T–Operators

In this section, it will be shown how to write tensor integrals as a combination of scalar integrals with shifted space–time dimension multiplied by tensor structures made from external momenta and the metric tensor. The method for integrals with boson–type propagators originates from the one-loop work [21] and was generalized to arbitrary orders in [22]. Here, a generalization of the two-loop two–point case to boson–type and static propagators is discussed. For completeness, one-loop results are collected in appendix A.1. The concept of T–operators works for massless as well as massive propagators. Here, the derivation is shown for the massless case, but can easily be generalized to massive propagators. The 'massive' and 'massless' T–operators are exactly the same.

For an easier comparison to the work of Tarasov, it is convenient to introduce a separate notation for inverse propagators. Let $c_i = D_i^{-1}$ (i=1..5) denote the boson–type inverse propagators, while $c_6 = S_1^{-1}$, $c_7 = S_2^{-1}$ and $c_8 = S_5^{-1}$. The tensor integrals of interest are written as

$$\int_1\int_2 \frac{(k_1)_{\mu_1}\cdots(k_1)_{\mu_\tau}(k_2)_{\lambda_1}\cdots(k_2)_{\lambda_s}}{c_1^{\nu_1}c_2^{\nu_2}c_3^{\nu_3}c_4^{\nu_4}c_5^{\nu_5}c_6^{\nu_6}c_7^{\nu_7}c_8^{\nu_8}} = T_{\mu_1..\mu_\tau,\lambda_1..\lambda_s}\left(\mathbf{J}^+,\mathbf{D}^+\right)\int_1\int_2\frac{1}{c_1^{\nu_1}\cdots c_8^{\nu_8}}\ , \tag{2.13}$$

where $\mathbf{J}^+$ are operators raising the indices of specific propagators, and $\mathbf{D}^+$ is the operator shifting the value of the integral's space–time dimension by two: $\mathbf{D}^+ I^{(D)} = I^{(D+2)}$.

For a derivation of the T–operators on the right-hand side of eq. (2.13), the integral is first converted to an α–parametric representation. Using two auxiliary vectors a_1, a_2 to rewrite the tensor structure as

$$\partial_{a_1,\mu_1}\cdots\partial_{a_1,\mu_\tau}\partial_{a_2,\lambda_1}\cdots\partial_{a_2,\lambda_s}\int_1\int_2\frac{\exp\left\{(a_1k_1)+(a_2k_2)\right\}}{c_1^{\nu_1}\cdots c_8^{\nu_8}}\bigg|_{a_i=0}\ , \tag{2.14}$$

employing the α–representation for propagators (see e.g. sect. 27 in [28])

$$\frac{1}{c^\nu} = \frac{1}{\Gamma(\nu)}\int_0^\infty d\alpha\,\alpha^{\nu-1}\exp\left\{-\alpha c\right\}\ , \tag{2.15}$$

shifting the loop momenta, and solving the D–dimensional Gaussian momentum integrals

$$\int d^Dk\,\exp\left\{-Ak^2\right\} = A^{-D/2}\frac{2\pi^{D/2}}{\Gamma\left(\frac{D}{2}\right)}\int_0^\infty dk\,k^{D-1}\exp\left\{-k^2\right\} = \left(\frac{\pi}{A}\right)^{D/2} \tag{2.16}$$

(for real, positive coefficients A), the integral in (2.14) can be represented by

$$\prod_{i=1}^8\int_0^\infty d\alpha_i\,\frac{\alpha_i^{\nu_i-1}}{\Gamma(\nu_i)}\left(\frac{\pi^2}{b^2f_2(\alpha)}\right)^{D/2}\exp\left\{-\frac{Q(\alpha,a_1,a_2)+f_3(\alpha)}{f_2(\alpha)}\right\}\ , \tag{2.17}$$

where

$$f_2(\alpha) \;=\; (\alpha_1+\alpha_3+\alpha_5)(\alpha_2+\alpha_4+\alpha_5)-\alpha_5^2\ ,$$

$$
\begin{aligned}
f_3(\alpha) &= q^2\left[(\alpha_1+\alpha_2)(\alpha_3+\alpha_4)\alpha_5+(\alpha_1+\alpha_2)\alpha_3\alpha_4+\alpha_1\alpha_2(\alpha_3+\alpha_4)\right] \\
&\quad -\frac{v^2}{4}\Big[(\alpha_2+\alpha_4+\alpha_5)\alpha_6^2+(\alpha_1+\alpha_3+\alpha_5)\alpha_7^2+(\alpha_1+\alpha_2+\alpha_3+\alpha_4)\alpha_8^2 \\
&\quad +2(\alpha_2+\alpha_4)\alpha_6\alpha_8-2(\alpha_1+\alpha_3)\alpha_7\alpha_8+2\alpha_5\alpha_6\alpha_7\Big] , \\
Q(\alpha,a_1,a_2) &= (a_1q)Q_1(\alpha)+(a_2q)Q_2(\alpha)+(a_1v)Q_3(\alpha)+(a_2v)Q_4(\alpha) \\
&\quad +a_1^2Q_{11}(\alpha)+(a_1a_2)Q_{12}(\alpha)+a_2^2Q_{22}(\alpha) ,
\end{aligned}
\tag{2.18}
$$

with

$$
\begin{aligned}
Q_1(\alpha) &= \alpha_3(\alpha_2+\alpha_4+\alpha_5)+\alpha_4\alpha_5 , \\
Q_2(\alpha) &= \alpha_4(\alpha_1+\alpha_3+\alpha_5)+\alpha_3\alpha_5 , \\
-2Q_3(\alpha) &= (\alpha_2+\alpha_4+\alpha_5)\alpha_6+\alpha_5\alpha_7+(\alpha_2+\alpha_4)\alpha_8 , \\
-2Q_4(\alpha) &= \alpha_5\alpha_6+(\alpha_1+\alpha_3+\alpha_5)\alpha_7-(\alpha_1+\alpha_3)\alpha_8 , \\
-4Q_{11}(\alpha) &= \alpha_2+\alpha_4+\alpha_5 , \\
-2Q_{12}(\alpha) &= \alpha_5 , \\
-4Q_{22}(\alpha) &= \alpha_1+\alpha_3+\alpha_5 .
\end{aligned}
\tag{2.19}
$$

There are two crucial observations to be made at this point: First, the space–time dimension D only occurs at one place in eq. (2.17), which allows to write the denominator f_2 in the exponential function as the operator $\mathbf{D}^+$. Second, the entire dependence on the auxiliary vectors a_1, a_2 resides in the function Q, allowing to pull a factor of $\exp(-Q/f_2)$ out of the integral, if every α in Q is interpreted as an operator increasing the index of the corresponding line by one (recall the representation (2.15)). Hence, putting together eqs. (2.13), (2.14) and (2.17), one finally obtains an expression for the T–operator:

$$
\begin{aligned}
T_{\mu_1\ldots\mu_\tau,\lambda_1\ldots\lambda_s} &= \partial_{a_{1,\mu_1}}\ldots\partial_{a_{1,\mu_\tau}}\,\partial_{a_{2,\lambda_1}}\ldots\partial_{a_{2,\lambda_\tau}}\exp\left\{\frac{b^2\mathbf{D}^+}{\pi^2}\Big[(a_1q)Q_1+(a_2q)Q_2\right. \\
&\quad \left.+(a_1v)Q_3+(a_2v)Q_4+a_1^2Q_{11}+(a_1a_2)Q_{12}+a_2^2Q_{22}\Big]\right\}\Big|_{\substack{a_1=a_2=0\\ \alpha_j=\nu_j\mathbf{J}^+}} .
\end{aligned}
\tag{2.20}
$$

Note that, in contrast to the widely used method of tensor decomposition à la Passarino/Veltmann [27], no contractions with external momenta and the metric tensor and no solution of a linear system of equations were needed in this approach.

2.1.4 Scalar T–Operators

For the special case that one has to reduce integrals with scalar numerators of the type

$$
I^{(D)}_{rstu}=\int_1\int_2\frac{(k_1q)^r(k_2q)^s(k_1v)^t(k_2v)^u}{c_1^{\nu_1}c_2^{\nu_2}c_3^{\nu_3}c_4^{\nu_4}c_5^{\nu_5}c_6^{\nu_6}c_7^{\nu_7}c_8^{\nu_8}}
\tag{2.21}
$$

only, the T–operators simplify considerably and hence are a lot easier to implement. By either contracting the result of the previous section with the suitable combination of q_μ and v_μ, or by following the same lines as above introducing four scalar parameters instead of the two auxiliary vectors, the result is

$$I^{(D)}_{rstu} = T_{rs}\left(\mathbf{J}^+, \mathbf{D}^+\right) \widetilde{T}_{tu}\left(\mathbf{J}^+, \mathbf{D}^+\right) \int_1 \int_2 \frac{1}{c_1^{\nu_1} ... c_8^{\nu_8}} \tag{2.22}$$

with

$$T_{rs} = \partial^r_{x_1} \partial^s_{x_2} \exp\left\{ \frac{b^2 \mathbf{D}^+}{\pi^2} q^2 \left[Q_1 x_1 + Q_2 x_2 + Q_{12} x_1 x_2 + Q_{11} x_1^2 + Q_{22} x_2^2 \right] \right\} \Big|_{\substack{x_1 = x_2 = 0 \\ \alpha_j = \nu_j \mathbf{J}^+}} \tag{2.23}$$

$$\widetilde{T}_{tu} = \partial^t_{x_3} \partial^u_{x_4} \exp\left\{ \frac{b^2 \mathbf{D}^+}{\pi^2} v^2 \left[Q_3 x_3 + Q_4 x_4 + Q_{12} x_3 x_4 + Q_{11} x_3^2 + Q_{22} x_4^2 \right] \right\} \Big|_{\substack{x_3 = x_4 = 0 \\ \alpha_j = \nu_j \mathbf{J}^+}} \tag{2.24}$$

and the Q_i given in eq. (2.19).

At this point, note that the problem of numerators in two-loop integrals is solved completely by the T–operators of eq. (2.20) and eqs. (2.23), (2.24). All possible two-loop tensor and scalar integrals, (2.13) and (2.21), are transformed to pure propagator integrals, the reduction of which will be treated in the next section.

2.2 Reduction: General Strategy

Before presenting the reduction algorithm in detail, it seems to be worthwhile to give an overview over the types of integrals, the notation used and the main results.

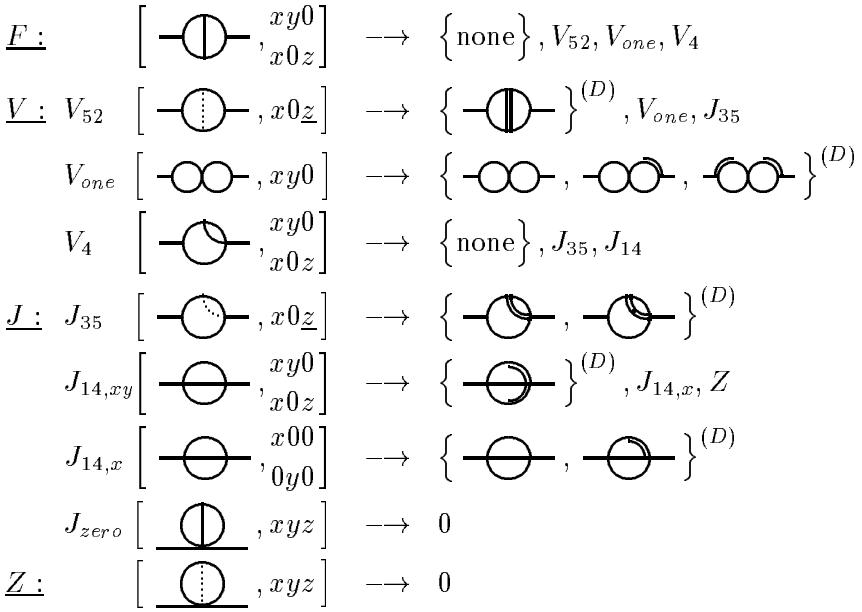

$$\left[\ \text{  }\ , xyz\right] \quad \longrightarrow \quad 0 \tag{2.25}$$

Some notation used in the above compact diagram needs to be explained. Reflecting the notation of Tarasov, the integrals are classified according to the number of different boson–type propagators they contain. Integrals with five different bosonic lines fall in the F–class, while the classes V, J and Z contain those with four, three and two (or less) different boson–lines, respectively. Classes can have a number of members, differing in topology. This is sketched by the little graphs in brackets. Boson–type lines with a non–zero index are drawn as full lines, while the static propagators can either lie on any full line, or, when the corresponding bosonic line is absent, they are indicated by dotted lines. Separated by a comma, the source–structure is explicited. Like above, an underlined index must not be zero. Furthermore, the integrals on the left–hand side of the arrows may have any powers of propagators, and the integral measure may have any dimension $D + 2n$, n being an integer.

On the right–hand sides, it is indicated what the result of the corresponding part of the reduction algorithm is. The graphs in curly brackets are the basic integrals. They form a complete set. All lines drawn have the power one. Single lines stand for bosonic–type, double lines for static propagators. The dimension of the basic integrals is reduced to the original space–time dimension D.

2.3 Reduction: The Algorithm in more Detail

In this section, the arrows of (2.25) are filled with details. A complete set of recurrence relations is given for each step. They are chosen to do the reduction in a very economical way, but of course there is no guarantee that this is *the* optimal set. A description of the derivation of these relations is postponed to the next section.

2.3.1 F–Reduction

All integrals involving five different bosonic propagators can be reduced to simpler cases, no matter what the source–structure is. This is one of the major simplifications arising from having a massless theory.

$$\begin{aligned} [abcde, x0z] &\xrightarrow{(2.27)} V_{52}\ ,\ V_{one}\ ,\ V_4 \\ [abcde, x\underline{y}0] &\xrightarrow{(2.26)} \{[abcde, x00]\ ,\ V_{one}\ ,\ V_4 \end{aligned}$$

The two recurrence relations needed are

$$c_1[abcde, xyz] = \left\{a\mathbf{1}^+\left(\mathbf{2}^- - \mathbf{5}^-\right) + c\mathbf{3}^+\left(\mathbf{4}^- - \mathbf{5}^-\right) + x\mathbf{S}_1^+\mathbf{S}_2^-\right\}[abcde, xyz] \tag{2.26}$$

$$c_2[abcde, xyz] = \left\{b\mathbf{2}^+\left(\mathbf{1}^- - \mathbf{5}^-\right) + d\mathbf{4}^+\left(\mathbf{3}^- - \mathbf{5}^-\right) + y\mathbf{S}_2^+\mathbf{S}_1^-\right\}[abcde, xyz] \tag{2.27}$$

with coefficients $c_1 = (a + c + 2e + x + z - D)$ and $c_2 = (b + d + 2e + y + z - D)$. The bold–face numbers are operators raising or lowering the indices of the corresponding propagators, e.g. $\mathbf{1}^+ [abcde, xyz] = [a{+}1\, bcde, xyz]$.

2.3.2 V–Reduction

The reduction of integrals with four bosonic propagators has to be done in three steps, reflecting the possible distinct topologies, cf. (2.25). The integrals of type V_{52} have an F–like topology due to the presence of S_5 and will be considered first. Next, products of one-loop integrals, V_{one}, will be reduced, followed by the type V_4, containing V–integrals in the sense of Tarasov.

V_{52}–Reduction

(a) Reduce the source–structure $[..., \underline{x}0\underline{z}]$ to $[..., 00\underline{z}]$.

$$[abcd0, \underline{x}0\underline{z}] \xrightarrow[\bigcirc]{(2.28)} \xrightarrow[\bigcirc]{(2.29)} \begin{cases} [abcd0, 00z] \longrightarrow \text{(see b)} \\ [abcd0, 101] \xrightarrow[\bigcirc]{(2.30)} \xrightarrow[\bigcirc]{(2.31)} \xrightarrow[\bigcirc]{(2.32)} \xrightarrow[\bigcirc]{(2.33)} \begin{cases} [abcd0, 00z] \longrightarrow \text{(see b)} \\ [11110, 101] \xrightarrow{(2.34)} V_{one} \end{cases} \\ V_{one} \\ J_{35} \end{cases}$$

The recurrence relations needed to reduce the source indices read

$$\begin{aligned} (z-1)\,[abcd0, x0z] &= \left\{2\,(b\mathbf{2}^+ + d\mathbf{4}^+)\left(\mathbf{S}_1^- - \mathbf{S}_5^-\right)\mathbf{S}_5^-\right\}[abcd0, x0z]\,, && (2.28)\\ (x-1)\,[abcd0, x0z] &= \Big\{2\,(b\mathbf{2}^+ + d\mathbf{4}^+)\,\mathbf{S}_1^-\mathbf{S}_5^- \;, \\ &\qquad -2\,(a\mathbf{1}^+ + b\mathbf{2}^+ + c\mathbf{3}^+ + d\mathbf{4}^+)\,\mathbf{S}_1^{--}\Big\}[abcd0, x0z]\,. && (2.29) \end{aligned}$$

The case $[..., 101]$ is then further reduced by

$$\begin{aligned} (a-1)\,\boldsymbol{q}^2[abcd0, xyz] &= \left\{(a-1)\,\mathbf{3}^- + \mathbf{1}^-\left(c_3 + z\mathbf{S}_5^+\mathbf{S}_1^-\right)\right\}[abcd0, xyz]\,, && (2.30)\\ (c-1)\,\boldsymbol{q}^2[abcd0, xyz] &= \left\{(c-1)\,\mathbf{1}^- + \mathbf{3}^-\left(c_4 + z\mathbf{S}_5^+\mathbf{S}_1^-\right)\right\}[abcd0, xyz]\,, && (2.31)\\ (b-1)\,\boldsymbol{q}^2[abcd0, xyz] &= \left\{(b-1)\,\mathbf{4}^- + \mathbf{2}^-\left(c_5 - z\mathbf{S}_5^+\mathbf{S}_1^-\right)\right\}[abcd0, xyz]\,, && (2.32)\\ (d-1)\,\boldsymbol{q}^2[abcd0, xyz] &= \left\{(d-1)\,\mathbf{2}^- + \mathbf{4}^-\left(c_6 - z\mathbf{S}_5^+\mathbf{S}_1^-\right)\right\}[abcd0, xyz]\,, && (2.33) \end{aligned}$$

with coefficients $c_3 = (a+2c+x-1-D)$, $c_4 = (2a+c+x-1-D)$, $c_5 = (b+2d+y+z-1-D)$ and $c_6 = (2b+d+y+z-1-D)$.

The last transformation is due to the integral's symmetry. Consider

$$[abba0, 110] = [aabb0, 1\bar{1}0] = [aabb0, 101] + [aabb0, 0\bar{1}1] = 2[aabb0, 101]\,,$$

where first the shift $k_2 \to q - k_2$ was performed, then the identity $1 = S_5(S_2^- + S_1^-)$ was used, and finally the exchange of loop momenta $k_1 \leftrightarrow k_2$ as well as the inversion $v \to -v$ was done in

the second term only. Reversing the equation chain, as a special case the relation

$$2[11110,101] \;=\; \left\{\mathbf{S}_2^+\mathbf{S}_5^-\right\}[11110,101] \tag{2.34}$$

follows, as needed in the above diagram. The right-hand side of eq. (2.34) is a product of one-loop integrals.

(b) Treat the case $[...,00\underline{z}]$ (here, $[abcd,z]$ abbreviates $[abcd0,00z]$).

$$[abcd,\underline{z}] \xrightarrow[\bigcirc]{(2.35)} \begin{cases} [abcd,2] \xrightarrow[\bigcirc]{(2.36)} \xrightarrow[\bigcirc]{(2.37)} \xrightarrow[\bigcirc]{(2.38)} \begin{cases} [a111,2] \xrightarrow[\bigcirc]{\substack{(2.39)\\ \bigcirc}} \xrightarrow[\bigcirc]{(2.36)} \begin{cases} [1111,2] \xrightarrow[\bigcirc]{(2.40)} V_{one}, J_{35} \\ V_{one}\ ,\ J_{35} \end{cases} \\ J_{35} \end{cases} \\ J_{35} \\ [abcd,1] \xrightarrow[\bigcirc]{(2.36)} \xrightarrow[\bigcirc]{(2.37)} \xrightarrow[\bigcirc]{(2.38)} \begin{cases} [a111,1] \xrightarrow[\bigcirc]{} \begin{cases} J \\ [1111,1] \xrightarrow[\bigcirc]{} \begin{cases} [1111,1]^{(D)} \\ J \end{cases} \end{cases} \\ J_{35} \end{cases}$$

In the above diagram, two arrows do not carry labels since the corresponding recurrence relations are not listed below (in fact, they are rather lengthy). However, these two relations are not needed in the calculation of the potential. The others read

$$\begin{aligned}(z-1)\,(z-2)\,\boldsymbol{q}^2[abcd0,00z] \;=\; &\Big\{4d\left((b+2d+2-D)\,\mathbf{4}^+ + b\mathbf{2}^+\left(1-\boldsymbol{q}^2\mathbf{4}^+\right)\right)\boldsymbol{q}^2\mathbf{S}_5^{--} \\ &-(z-1)\,(z-2)\,(\mathbf{2}^- - \mathbf{4}^-)\Big\}\,[abcd0,00z]\,, \end{aligned} \tag{2.35}$$

as well as

$$(c-1)\,\boldsymbol{q}^2[abcd0,xyz] \;=\; \left\{(a-c+1)\,\mathbf{3}^- + a\mathbf{1}^+\mathbf{3}^-\left(\boldsymbol{q}^2-\mathbf{3}^-\right)+(c-1)\,\mathbf{1}^-\right\}[abcd0,xyz]\,, \tag{2.36}$$

$$(d-1)\,\boldsymbol{q}^2[abcd0,xyz] \;=\; \left\{c_7\mathbf{4}^- + a\mathbf{1}^+\mathbf{4}^-\left(\mathbf{3}^- - \boldsymbol{q}^2\right) + (d-1)\,\mathbf{2}^-\right\}[abcd0,xyz]\,, \tag{2.37}$$

$$(b-1)\,\boldsymbol{q}^2[abcde,xyz] \;=\; \left\{c_8\mathbf{2}^- + a\mathbf{1}^+\mathbf{2}^-\left(\mathbf{3}^- - \boldsymbol{q}^2\right) + (b-1)\,\mathbf{4}^-\right\}[abcde,xyz]\,, \tag{2.38}$$

with $c_7 = (a+2b+2c+d+x+y+z-1-2D)$ and $c_8 = (a+b+2c+2d+2e+x+y+z-1-2D)$, and finally

$$\begin{aligned} 4c_9\boldsymbol{q}^2[a1110,002] \;=\; &\Big\{(a-1)\mathbf{3}^- - (a-2)\,\mathbf{1}^- - \mathbf{3}^+\mathbf{1}^{--} - \boldsymbol{q}^2\,(a\mathbf{1}^+\mathbf{3}^- + \mathbf{2}^+\mathbf{4}^- + \mathbf{4}^+\mathbf{2}^-) \\ &+ \boldsymbol{q}^4\,(a\mathbf{1}^+ + \mathbf{3}^+)\,\mathbf{S}_2^{++}\mathbf{S}_5^{--}\Big\}\,[a1110,002]\,, \end{aligned} \tag{2.39}$$

$$\begin{aligned} 4\,(4-D)\,[11110,002] \;=\; &\Big\{(\mathbf{2}^+ + \mathbf{4}^+)\,\boldsymbol{q}^2\mathbf{S}_1^{++}\mathbf{S}_5^{--} - \mathbf{1}^+\mathbf{3}^- - \mathbf{2}^+\mathbf{4}^- \\ &- \mathbf{3}^+\mathbf{1}^- - \mathbf{4}^+\mathbf{2}^-\Big\}\,[11110,002]\,, \end{aligned} \tag{2.40}$$

where $c_9 = (a+3-D)$.

$\mathbf{V}_{one}$–Reduction

The integrals V_{one} are products of one-loop–integrals. They are reduced according to (here, $[abcd,xy]$ abbreviates $[abcd0,xy0]$)

$$[abcd,xy] \xrightarrow[\bigcirc]{(2.41)} \xrightarrow[\bigcirc]{(2.42)} [abcd,{}^{1\,1}_{0\,0}] \xrightarrow[\bigcirc]{(2.43)} \xrightarrow[\bigcirc]{(2.44)} \xrightarrow[\bigcirc]{(2.45)} \xrightarrow[\bigcirc]{(2.46)} [1111,{}^{1\,1}_{0\,0}] \xrightarrow[\bigcirc]{(2.47)} [1111,{}^{1\,1}_{0\,0}]^{(D)}$$

To reduce the source–line indices of the one-loop integrals to 0 or 1, one uses

$$(x-1)\,[abcd0,xy0] = \left\{-2\,(a\mathbf{1}^+ + c\mathbf{3}^+)\,\mathbf{S}_1^{--}\right\}[abcd0,xy0]\,, \tag{2.41}$$

$$(y-1)\,[abcd0,xy0] = \left\{-2\,(b\mathbf{2}^+ + d\mathbf{4}^+)\,\mathbf{S}_2^{--}\right\}[abcd0,xy0]\,. \tag{2.42}$$

In the next four steps, all boson–line indices can be reduced to 1 by

$$(c_{10}-2c)\,(a-1)\,\boldsymbol{q}^2[abcd0,xy0] = \{(a+c+x-D)\,(c_{10}-2)\,\mathbf{1}^-\}\,[abcd0,xy0]\,, \tag{2.43}$$

$$(c_{10}-2a)\,(c-1)\,\boldsymbol{q}^2[abcd0,xy0] = \{(a+c+x-D)\,(c_{10}-2)\,\mathbf{3}^-\}\,[abcd0,xy0]\,, \tag{2.44}$$

$$(c_{11}-2d)\,(b-1)\,\boldsymbol{q}^2[abcd0,xy0] = \{(b+d+y-D)\,(c_{11}-2)\,\mathbf{2}^-\}\,[abcd0,xy0]\,, \tag{2.45}$$

$$(c_{11}-2b)\,(d-1)\,\boldsymbol{q}^2[abcd0,xy0] = \{(b+d+y-D)\,(c_{11}-2)\,\mathbf{4}^-\}\,[abcd0,xy0]\,, \tag{2.46}$$

where $c_{10} = (2a+2c+x-D)$ and $c_{11} = (2b+2d+y-D)$. Finally, the integral's dimension is restored by

$$4\,(x+1-D)\,(y+1-D)\,\mathbf{D}^+[11110,xy0]^{(D)} = \boldsymbol{q}^4[11110,xy0]^{(D)}\,. \tag{2.47}$$

V_4–Reduction

The V_4–type integrals are V–integrals in the sense of Tarasov. This type of four–boson integrals can again be removed completely, due to the masslessness of the propagators.

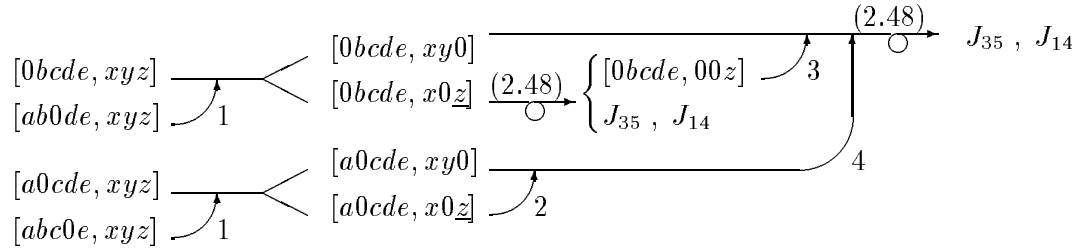

Here, the shifts (1) : $k \to k+q$; $q \to -q$, (2) : $k_2 \to k_1 - k_2 + q$ and (3) : $k_1 \to k_2 - k_1 + q$; $v \to -v$ as well as the interchange of integration variables (4) : $k_1 \leftrightarrow k_2$ had to be used, as well as the relation

$$(2c+e+x-D)\,[0bcde,xyz] = \left\{e\mathbf{5}^+\,(\mathbf{4}^- - \mathbf{3}^-) - z\mathbf{S}_5^+\mathbf{S}_1^-\right\}[0bcde,xyz]\,. \tag{2.48}$$

2.3.3 J–Reduction

Integrals with three different bosonic propagators are treated in four steps. The integrals J_{35} are, topologically, of V–type. $J_{14,xy}$ denotes sunset–type integrals with two different source–lines, while $J_{14,x}$ collects those with at most one source–line. Finally, J_{zero} collects the tadpoles.

J_{35}–Reduction

(a) Transformation to the standard type $[ab0d0, 00z]$.

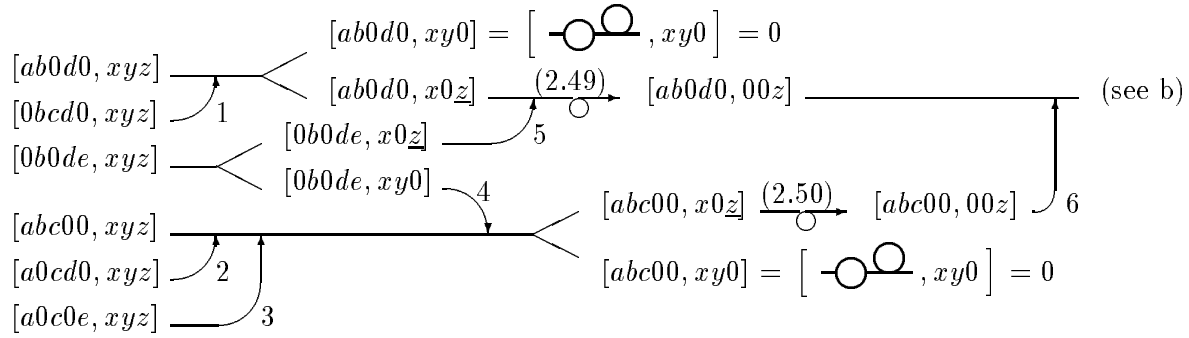

The shifts needed are (1) : $k_1 \to k_1 + q$, (2) : $k_2 \to k_2 + q$, (3) : $k_2 \to k_1 - k_2$, (4) : $k_1 \to k_1 - k_2$, $k_2 \to k_1$, (5) : $k_1 \to k_1 - k_2 + q$, $k_2 \to q - k_2$ and finally (6) : $k_1 \to q - k_2$, $k_2 \to -k_1$. Two of the integrals are identically zero, because they are a product of a one-loop–bubble– and a one-loop–tadpole–integral, the latter of which vanishes (in the massless case at hand) in dimensional regularization due to the absence of a dimensionful parameter. The two recurrence relations used are

$$(2a + x - D)\,[ab0d0, xyz] = \left\{-z\mathbf{S}_5^+\mathbf{S}_1^-\right\}[ab0d0, xyz]\,, \tag{2.49}$$

$$(2b + y + z - D)\,[abc00, xyz] = \left\{z\mathbf{S}_5^+\mathbf{S}_1^-\right\}[abc00, xyz]\,. \tag{2.50}$$

(b) Reduction

$$[ab0d0, 00\underline{z}] \xrightarrow{(2.51)} [ab0d0, 00^2_1] \xrightarrow{(2.52)} \xrightarrow{(2.53)} \xrightarrow{(2.54)} [11010, 00^2_1] \xrightarrow{(2.55)} [11010, 00^2_1]^{(D)}$$

The source–line is reduced by

$$(z-1)\,(z-2)\,[ab0d0, 0yz] = \left\{(2a+2-D)\,2a\mathbf{1}^+\mathbf{S}_5^{--}\right\}[ab0d0, 0yz]\,, \tag{2.51}$$

while relations for the bosonic lines read

$$(d-1)\,(c_{12}-b+d)\,\boldsymbol{q}^2[ab0d0, xyz] = \{c_{12}\,(c_{12}+b+d-2)\,\mathbf{4}^-\}\,[ab0d0, xyz]\,, \tag{2.52}$$

$$(b-1)\,(c_{12}+b-d)\,\boldsymbol{q}^2[ab0d0, xyz] = \{c_{12}\,(c_{12}+b+d-2)\,\mathbf{2}^-\}\,[ab0d0, xyz]\,, \tag{2.53}$$

$$(a-1)\,(2a-D)\,\boldsymbol{q}^2[a1010, 00z] = \{-2c_{13}\mathbf{1}^-\}\,[a1010, 00z]\,, \tag{2.54}$$

with $c_{12} = (2a+b+d+x+y+z-2D)$ and $c_{13} = (2a+z-2-D)(2a+z+1-2D)$. A reduction of the integral's dimension is then accomplished by

$$4c_{14}\,(z-D)\,\mathbf{D}^+[11010, 00z]^{(D)} = -\,(2-D)\,\boldsymbol{q}^4[11010, 00z]^{(D)}\,, \tag{2.55}$$

where $c_{14} = (z+1-2D)(z+3-2D)$.

$\mathbf{J}_{14,xy}$–Reduction

(a) Reduction of source–lines.

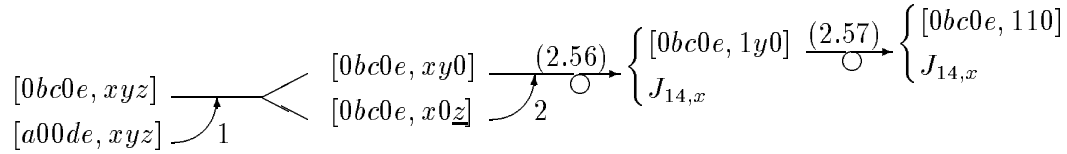

Where the shifts needed are $(1): k \to k+q;\ q \to -q$ and $(2): k_2 \to k_1 - k_2$, and two recurrence relations can be used:

$$(x-1)\,[0bcde,xy0] = \left\{-2e\mathbf{5}^+\left(\mathbf{S}_1^- - \mathbf{S}_2^-\right)\mathbf{S}_1^- - 2c\mathbf{3}^+\mathbf{S}_1^{--}\right\}[0bcde,xy0]\,, \tag{2.56}$$

$$(y-1)\,[abc0e,xy0] = \left\{\ 2e\mathbf{5}^+\left(\mathbf{S}_1^- - \mathbf{S}_2^-\right)\mathbf{S}_2^- - 2b\mathbf{2}^+\mathbf{S}_2^{--}\right\}[abc0e,xy0]\,. \tag{2.57}$$

(b) Reduction of bosonic lines. To save space, here only $[bce]$ will be displayed instead of $[0bc0e,110]$.

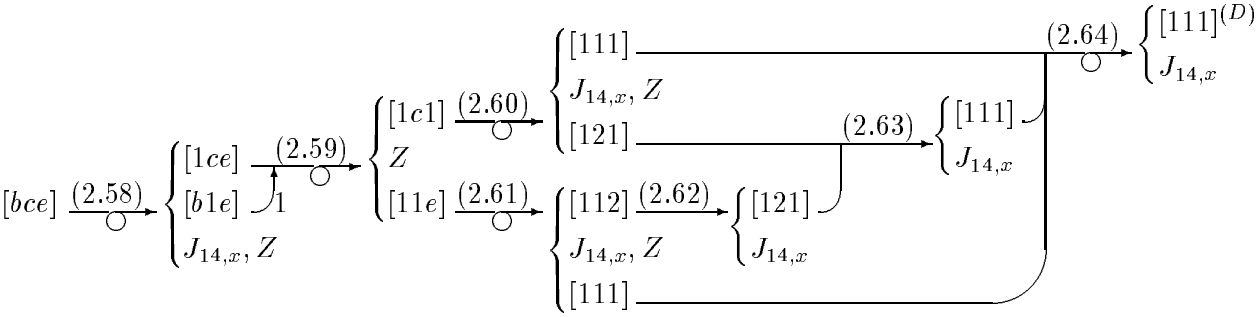

The shift reads $(1): k_1 \to q - k_2,\ k_2 \to q - k_1;\ v \to -v$. The recurrence relations are

$$\begin{aligned}
(b-1)(c-1)\,\boldsymbol{q}^2[0bc0e,xy0] &= \{(c-1)(c_{15}+c)\,\mathbf{2}^- + (b-1)(c+2e+x-1-D)\,\mathbf{3}^- \\
&\quad + (b-1)\left((c-1)\,\mathbf{5}^- - x\mathbf{S}_1^+\mathbf{S}_2^-\mathbf{3}^-\right)\}[0bc0e,xy0]\,, && (2.58)\\
(c-1)(e-1)\,\boldsymbol{q}^2[0bc0e,xy0] &= \{(e-1)(c_{15}+b)\,\mathbf{3}^- + (c-1)(2b+e+y-1-D)\,\mathbf{5}^- \\
&\quad + (c-1)(e-1)\,\mathbf{2}^-\}[0bc0e,xy0]\,, && (2.59)\\
c_{16}(c-1)(c-2)\,\boldsymbol{q}^2[0bc0e,xy0] &= \{c_{17}(c-2)\,\mathbf{3}^- \\
&\quad + ex\left(-(c-2)\,\boldsymbol{q}^2 + (c_{18}+e+x)\,\mathbf{3}^-\right)\mathbf{3}^-\mathbf{5}^+\mathbf{S}_1^+\mathbf{S}_2^- \\
&\quad + e(c-2)(c_{19}+2)\,\mathbf{2}^-\mathbf{3}^-\mathbf{5}^+\}[0bc0e,xy0]\,, && (2.60)\\
c_{19}(e-1)\,\boldsymbol{q}^2[0bc0e,xy0] &= \left\{c_{17}\mathbf{5}^- + x\left((e-1)\,\boldsymbol{q}^2 - (c_{18}-c-2+D)\,\mathbf{5}^-\right)\mathbf{S}_1^+\mathbf{S}_2^- \right. \\
&\quad \left. + c(c_{16}+2)\,\mathbf{2}^-\mathbf{3}^+\mathbf{5}^-\right\}[0bc0e,xy0]\,, && (2.61)\\
(4+x-D)\,[0b1d2,xy0] &= \left\{(4+x-D)\,\mathbf{3}^+\mathbf{5}^- + x\mathbf{S}_1^+\mathbf{S}_2^-\right\}[0b1d2,xy0]\,, && (2.62)\\
(5-D)\,\boldsymbol{q}^2[01201,110] &= \left\{(4-D)(11-3D)\,\mathbf{3}^- + \mathbf{D}^+\left(9(3-D)\,\mathbf{5}^+\mathbf{S}_1^{++++}\right.\right. \\
&\quad \left.\left. + 2(11-3D)\left(2\mathbf{5}^{++}\mathbf{S}_2^{++} + \mathbf{3}^+\mathbf{5}^+\mathbf{S}_2^{++} - \mathbf{5}^{++}\mathbf{S}_1^{++}\right)\right.\right.
\end{aligned}$$

$$+ 3\,(5-D)\,\mathbf{2}^{+}\mathbf{S}_1^{++++}\Big)\,\mathbf{3}^{-}\mathbf{S}_1^{-}\mathbf{S}_2^{-}\Big\}\,[01201,110]\,, \quad (2.63)$$

with coefficients $c_{15} = (b+c+2e+x+y-1-2D)$, $c_{16} = (2c+x-D)$, $c_{17} = (c+e+x-D)(4b+2c+2e+x+2y-2-3D)$, $c_{18} = (2b+c+e+y-2D)$ and $c_{19} = (2e+x-D)$. In the last step, the dimension is reduced by

$$\begin{aligned} 3c_{20}\mathbf{D}^{+}[01101,110]^{(D)} &= \Big\{-(7-3D)\,\mathbf{5}^{+}\mathbf{S}_1^{+}\mathbf{S}_2^{-}\,\Big[\boldsymbol{q}^2\mathbf{D}^{+} + 6\mathbf{D}^{++}\Big((5-3D)\,(\mathbf{2}^{+}+\mathbf{5}^{+}) \\ &\quad + 3\,(3-2D)\,\mathbf{S}_1^{++}\Big)\Big] + (3-D)\,\boldsymbol{q}^4\Big\}\,[01101,110]^{(D)}\,, \end{aligned} \quad (2.64)$$

with $c_{20} = (2-D)(5-3D)(7-3D)$.

$\mathbf{J}_{14,x}$–Reduction

$$[0bc0e,x00] \xrightarrow{(2.65)} \begin{cases} [0bc0e,100] \longrightarrow [01101,100]^{(D)} \\ [0bc0e,000] \xrightarrow{(2.66)} \xrightarrow{(2.67)} \xrightarrow{(2.68)} [01101,000] \xrightarrow{(2.69)} [01101,000]^{(D)} \end{cases}$$
$$[0bc0e,0y0] \xrightarrow{1}$$

Here, all relations used in the lower line can be obtained by Tarasov's relations in the massless limit, of course. Like above, four recurrence relations corresponding to the unlabeled arrow are not listed, because they are not needed for calculating the potential. They will be relevant for higher–order calculations only. The shift is given by $(1): k_1 \to q-k_2,\ k_2 \to q-k_1;\ v \to -v$, the relations read

$$c_{21}\,(x-1)\,[0bc0e,x00] = \Big\{-\left((2b+2-D)\,b\mathbf{2}^{+} + 2c_{21}c\mathbf{3}^{+}\right)\mathbf{S}_1^{--}\Big\}\,[0bc0e,x00] \quad (2.65)$$

with $c_{21} = (b+e+1-D)$, as well as

$$\begin{aligned} (b-1)\,(2b-D)\,\boldsymbol{q}^2[0bc0e,000] &= \{c_{22}\mathbf{2}^{-}\}\,[0bc0e,000]\,, & (2.66)\\ (c-1)\,(2c-D)\,\boldsymbol{q}^2[0bc0e,000] &= \{c_{22}\mathbf{3}^{-}\}\,[0bc0e,000]\,, & (2.67)\\ (e-1)\,(2e-D)\,\boldsymbol{q}^2[0bc0e,000] &= \{c_{22}\mathbf{5}^{-}\}\,[0bc0e,000]\,, & (2.68)\\ (2-3D)\,(3-3D)\,(4-3D)\,\mathbf{D}^{+}[01101,000]^{(D)} &= (2-D)\,\boldsymbol{q}^4[01101,000]^{(D)}\,, & (2.69) \end{aligned}$$

with $c_{22} = (2b+2c+2e-3D)(b+c+e-1-D)$.

$\mathbf{J}_{zero}$–Relations

The remaining three–boson–integrals are identically zero:

$$[ab00e,xyz] = \Big[\ \underline{\bigoplus}\ ,xyz\Big] = 0 \qquad [00cde,xyz] = \Big[\ \underline{\bigoplus}\ ,xyz\Big] = 0$$

This is obvious from the little graphs, since massless tadpoles vanish in dimensional regularization.

2.3.4 Z–Relations

All integrals with two (or less) bosonic lines are identically zero, independent of their source structure. From the ten possible boson structures, for eight of them this is immediately clear because they are special cases of the J_{zero}–relations:

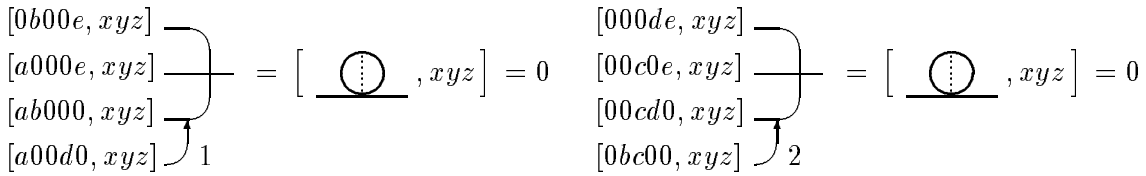

The shifts needed here are (1) : $k_2 \to k_2 + q$ and (2) : $k_2 \to k_2 - q$.

For the remaining two integral types, we have

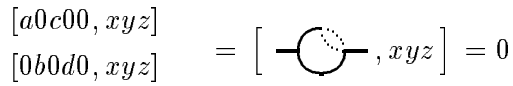

This zero is a consequence of a simple integration by parts (see next section for notation):

$$\begin{aligned} 0 &= \left\{\partial_{k_{2,\mu}} k_{2,\nu}\right\} \circ [a0c00, xyz] = \left\{g_{\mu\nu} + k_{2,\nu}\partial_{k_{2,\mu}}\right\} \circ [a0c00, xyz] \\ &= \left\{g_{\mu\nu} + k_{2,\nu} v_\mu \left(-y\mathbf{S}_2^+ + z\mathbf{S}_5^+\right)\right\} \circ [a0c00, xyz] \\ 0 &= \left\{\partial_{k_{1,\mu}} k_{1,\nu}\right\} \circ [0b0d0, xyz] = \left\{g_{\mu\nu} + k_{1,\nu}\partial_{k_{1,\mu}}\right\} \circ [0b0d0, xyz] \\ &= \left\{g_{\mu\nu} + k_{1,\nu} v_\mu \left(-x\mathbf{S}_1^+ - z\mathbf{S}_5^+\right)\right\} \circ [a0c00, xyz] \end{aligned} \tag{2.70}$$

Eliminating the terms proportional to v_μ by contracting with either q_μ, $q_\mu q_\nu$ or $(g_{\mu\nu} - v_\mu v_\nu / v^2)$, one can conclude that $[a0c00, xyz] = 0$ and $[0b0d0, xyz] = 0$, indeed.

2.4 Derivation and some Examples

All recurrence relations listed in the preceding section can be derived by a combination of two methods: first, a generalization of the traditional method of integration by parts [20] to include the static propagators, and second, the use of T–operators (see section (2.1)).

2.4.1 Traditional Method

From the trivial identity [2]

$$\begin{aligned} 0 &= \int_1 \int_2 \partial_{k_{1,\mu}} \mathcal{P}_\mu(k_1, k_2, q, v) D_1^a D_2^b D_3^c D_4^d D_5^e S_1^x S_2^y S_5^z \\ &\equiv \left\{\partial_{k_{1,\mu}} \mathcal{P}_\mu(k_1, k_2, q, v)\right\} \circ [abcde, xyz] \end{aligned} \tag{2.71}$$

[2] There is a similar identity with ∂_{k_2} , of course.

one can derive generic relations among the two-loop–integrals by choosing $\mathcal{P}_\mu$ in a clever way. Doing the derivatives, one produces a numerator containing $g_{\mu\mu} = D$ as well as scalar products of the momenta. The latter are written as inverse propagators, like $2(k_1 q) = q^2 + k_1^2 - (k_1 - q)^2 = q^2 + \mathbf{1}^- - \mathbf{3}^-$. For the inverse static propagators, the relation

$$S_1^- = S_2^- + S_5^- \tag{2.72}$$

can be used in addition to $(k_1 v) = \mathbf{S}_1^-$ and $(k_2 v) = \mathbf{S}_2^-$.

As an example, consider eq. (2.71) with $\mathcal{P}_\mu = (k_1 - q)_\mu$. Doing the derivatives, one gets the relation (2.26). Now, setting $a = b = c = d = e = 1$ and $x = y = z = 0$,

$$\begin{aligned}(4 - D)\,[11111, 000] &= [20111, 000] - [21110, 000] + [11201, 000] - [11210, 000] \\ &= 2\,[20111, 000] - 2\,[21110, 000]\,,\end{aligned} \tag{2.73}$$

where the last line follows from the integral's symmetry under an exchange of inner momentum labels. This relation can be illustrated as

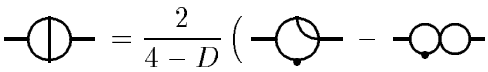

$$= \frac{2}{4 - D}\Big($$

$$\Big)\,,$$

(2.74)

where a dot on a line means it is squared. In this particular case, a non–trivial two-loop diagram is expressed through diagrams of much simpler structure, which sheds some light on the enormous power of the integration by parts method. Another explicit example was already given in eq. (2.70).

2.4.2 Additional Relations

The new idea, as introduced by Tarasov, is to replace the scalar products obtained after differentiation not only by inverse propagators, but also by T–operators. In this way, relations between integrals living in different space–time dimensions can be obtained in addition to the 'traditional' ones. For numerators containing the integration momenta only linearly, the scalar T–operators can be used to get the relations

$$\begin{aligned}0 = \{(k_1 q) - (k_1 q)\} &= \left\{q^2 \mathbf{D}^+ \mathbf{Q}_1 - \frac{1}{2}\left(q^2 + \mathbf{1}^- - \mathbf{3}^-\right)\right\} \circ [abcde, xyz] \\ 0 = \{(k_2 q) - (k_2 q)\} &= \left\{q^2 \mathbf{D}^+ \mathbf{Q}_2 - \frac{1}{2}\left(q^2 + \mathbf{2}^- - \mathbf{4}^-\right)\right\} \circ [abcde, xyz] \\ 0 = \{(k_1 v) - (k_1 v)\} &= \left\{\mathbf{D}^+ \mathbf{Q}_3 - \mathbf{S}_1^-\right\} \circ [abcde, xyz] \\ 0 = \{(k_2 v) - (k_2 v)\} &= \left\{\mathbf{D}^+ \mathbf{Q}_4 - \mathbf{S}_2^-\right\} \circ [abcde, xyz]\,.\end{aligned} \tag{2.75}$$

The operators $\mathbf{Q}$ are the functions Q given in eq. (2.19), understood at $\alpha_j \to \nu_j \mathbf{J}^+$.

The last relation useful for deriving the recurrence relations can be obtained from eq. (2.17) and reads

$$0 = \{1 - 1\} = \left\{\mathbf{D}^+ \mathbf{f}_2 - 1\right\} \circ [abcde, xyz]\,. \tag{2.76}$$

Again, the operator $\mathbf{f}_2$ denotes f_2 of eq. (2.1.3) at $\alpha_j \to \nu_j \mathbf{J}^+$.

As an example, consider the recurrence relation used to reduce the source–index of a $\mathrm{J}_{14,x}$–type integral, eq. (2.65). It is derived by a straightforward evaluation of the derivatives in the following relation:

$$\begin{aligned} 0 \;=\; & \Big\{ -\partial_{k_{2,\mu}} \Big(k_{2,\mu}(b+1)\mathbf{2}^+ + (k_1-k_2)_\mu e \mathbf{5}^+ \Big)\, b\mathbf{2}^+ \frac{x-1}{2}\mathbf{D}^+ + (1+b+e-D)(x-1)\Big\{\mathbf{D}^+\mathbf{f}_2 - 1\Big\} \\ & + \Big((2+2b-D) b\mathbf{2}^+ + 2(1+b+e-D) c\mathbf{3}^+ \Big)\, \mathbf{S}_1^- \Big\{ \mathbf{D}^+\mathbf{Q}_3 - \mathbf{S}_1^- \Big\} \Big\} \circ [0bc0e, x00]\,. \end{aligned} \tag{2.77}$$

Here, all three kinds of relations, eqs. (2.71), (2.75) and (2.76), are used to build up the needed recurrence relation.

To end this section, it should be emphasized that relations are not always as compact as the few examples given here. Combining partial integrations and the T–relations in a way to give useful recurrence relations is sometimes more an 'art'. Hence, an elegant automatization of the derivation of the complete set of recurrence relations (see the very recent proposition [29] and references therein) would be most welcome.

Chapter 3

Results

Here, we utilize the results derived in the preceding two chapters to obtain expressions for the static potential in four and three dimensions. We have to compute the set of Feynman diagrams contributing to the potential up to two loops, cf. figs. 1.3 and 1.4. The method employed can be briefly summarized as follows:

- All dimensionally regulated (tensor-) integrals are reduced to pure propagator integrals by a generalization of the method of T–operators [22]. The resulting expressions are then mapped to a minimal set of five scalar integrals by means of recurrence relations, again generalizing [22] as well as [20] to the case including static (non-covariant) propagators. The generalized T–operators as well as the generalized recurrence relations were discussed in detail in chapter 2. These two steps have been implemented into a FORM [30] package. Thus, we constructed our method to be complementary to the calculation in ref. [9], assuring a truly independent check of the four–dimensional result presented therein. At this stage, one obtains analytic coefficient functions (depending on the generic space–time dimension D as well as on the color factors and the bare coupling), multiplying each of the basic integrals. Results are given below in section 3.1.
- The basic scalar integrals are then solved analytically, see appendix B. Expanding the result around $D = 4$ (which is done in both MAPLE [31] and Mathematica [32] considering the complexity of the expressions) and renormalizing, one obtains the final results. The four– and three–dimensional cases are discussed in sections 3.2 and 3.3, respectively.

Important checks of the calculation include

- gauge independence of appropriate classes of diagrams, in D dimensions,
- confirmation of cancelation of infrared divergences,
- correct renormalization properties.

These points will be addressed below, where appropriate.

3.1 D Dimensions

Let us finally present results for the static potential. All calculations are performed as outlined above, allowing an automated algebraic reduction of every diagram to the minimal set of basic integrals in a generic dimension D. The bare momentum–space potential is obtained after summing all exchange diagrams contributing to the potential. The relevant set of diagrams was discussed in chapter 1.2. There it was demonstrated that, due to the logarithm in the definition of the static potential, a large class of diagrams cancels exactly against iterations of lower–order ones, such that only a subset has to be considered for the potential. These subsets of non–iterative diagrams are shown in figs. 1.3 and 1.4. The two-loop potential can be written as

$$V_0(\boldsymbol{q}^2; g_0^2, D) \;=\; -\frac{g_0^2 C_F}{\boldsymbol{q}^2}\left\{1 + g_0^2\, c_1(\boldsymbol{q}^2, D) + g_0^4\, c_2(\boldsymbol{q}^2, D) + \mathcal{O}(g_0^6)\right\}\,. \tag{3.1}$$

The coefficients c_i, being functions of the momentum exchange $\boldsymbol{q}$ and the generic dimension D, are obtained directly from the diagrams, i.e. c_1 results from summing the set of one-loop diagrams displayed in fig. 1.3 and c_2 represents the two-loop ones of fig. 1.4. Employing dimensional regularization [33], the only dimensionful parameter is $\boldsymbol{q}$, so the c_i exhibit a trivial scale dependence

$$c_i(\boldsymbol{q}^2, D) \;=\; \left(\frac{|\boldsymbol{q}|^{D-4}}{(4\pi)^{D/2}}\right)^i \tilde{c}_i(D)\,. \tag{3.2}$$

This becomes clear by noting that the gauge coupling acquires a dimension for D≠4. Counting mass dimensions, we thus have

$$g_0^2 \sim 4 - D \quad , \quad (g_0^2)^i c_i(\boldsymbol{q}^2, D) \sim 0 \quad , \quad V(\boldsymbol{q}) \sim 2 - D\,, \tag{3.3}$$

such that the coordinate–space potential $V(r) \propto \int \mathrm{d}^{D-1}\boldsymbol{q}\, V(\boldsymbol{q})$ has the correct mass dimension of one. The perturbative coefficients c_i can be further classified according to their color structure. We define

$$c_1 \;=\; c_{11} C_A + c_{12} T_F n_f\,, \tag{3.4}$$

$$c_2 \;=\; c_{21} C_A^2 + c_{21} C_A T_F n_f + c_{23} C_F T_F n_f + c_{24} T_F^2 n_f^2\,. \tag{3.5}$$

Working in the linear covariant gauge with arbitrary gauge parameter, and performing the calculations as described above, we get the following results for the coefficients $c_{ij}(\boldsymbol{q}^2, D)$

$$c_{11} \;=\; \frac{(4D-5)(D-2)}{2(D-1)} \tag{3.6}$$

$$c_{12} = -\frac{2(D-2)}{D-1}$$  (3.7)

$$c_{21} = -\frac{7D^4-19D^3-156D^2+740D-776}{4(D-5)(D-4)(D-1)^2}$$ 

$$+\frac{27D^9\text{-}705D^8+8012D^7\text{-}51866D^6+210247D^5\text{-}552129D^4+936394D^3\text{-}983620D^2+574696D\text{-}139520}{(D-5)^2(D-1)^2(D-3)(D-4)^2}\frac{1}{q^2}$$ 

$$+\frac{D^5-11D^4+59D^3-223D^2+484D-374}{(D-5)^2(D-1)(D-3)(D-4)}$$ 

$$+\frac{(D-1)(3D-11)(D-4)}{(D-5)^2}$$  $$-\frac{3D-11}{4(D-5)}\,q^2$$  (3.8)

$$c_{22} = \frac{(D^4-10D^3+33D^2-14D-64)}{(D-4)(D-1)^2}$$ 

$$-\frac{4(14D^5-155D^4+672D^3-1415D^2+1412D-496)}{(D-4)(D-3)(D-1)^2}\,\frac{1}{q^2}$$ 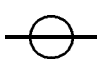

$$+\frac{2(D^2-D-8)}{(D-1)(D-3)(D-4)}$$  (3.9)

$$c_{23} = -\frac{2(D-2)(D^2-7D+16)}{(D-1)(D-4)}$$ 

$$+\frac{8(D-2)(D-3)(D^2-4D+8)}{(D-1)(D-4)^2}\,\frac{1}{q^2}$$  (3.10)

$$c_{24} = \frac{4(D-2)^2}{(D-1)^2}$$  (3.11)

The small pictures denote the set of basic scalar integrals, discussed in appendix B. There, generic solutions in terms of Gamma functions can be found. As expected, every coefficient c_{ij} is gauge independent separately. By far the most work had to be done for c_{21}, while the other three two-loop coefficients are obtained from the subset of diagrams containing internal fermion loops. The coefficient c_{24} could have been obtained from the one-loop result already, by squaring c_{12}.

3.2 Four Dimensions

In this section, renormalization as well as infrared cancelations for the four–dimensional static potential will be discussed. We will find that the constant part of the two-loop coefficient differs from the previously known one [9], and pin down the origin of this discrepancy. It is interesting to note that this difference, being due to the omission of certain diagrams in the calculation of

ref. [9], can be detected best keeping the gauge parameter arbitrary throughout the calculation, which in turn needs a fairly sophisticated method, like the one we have presented. Finally, results are presented for the coupling in the so–called V–scheme, as well as in coordinate space.

3.2.1 Renormalization

In $D = 4-\epsilon$ dimensions, the renormalized potential V_R as well as the renormalized strong gauge coupling a_R are defined by

$$V_0 \equiv \mu^\epsilon V_R \quad , \quad \frac{g_0^2}{16\pi^2} \equiv Z\mu^\epsilon a_R \; , \tag{3.12}$$

where the subscript 0 denotes the bare quantities. Note the difference in the normalization of a_R compared with the usual strong coupling constant $\alpha_s = \frac{g_0^2}{4\pi}$. It is chosen such as to keep formulae more compact, avoiding e.g. an accumulation of factors of 4π in the definition of the renormalization group β function, see below. The factor Z is assumed to have an expansion in the renormalized coupling,

$$Z \;=\; 1 + a_R Z^{'}(\epsilon) + a_R^2 Z^{''}(\epsilon) + ... \; , \tag{3.13}$$

and we choose to work in the $\overline{\rm MS}$ scheme, related to the MS scheme by the scale redefinition $\mu^2 = \bar{\mu}^2 e^\gamma/4\pi$.

One the one hand, the factor Z is well known in QCD. The coefficients of the Beta function are defined by the running coupling,

$$\mu^2\partial_{\mu^2}\, a_R \;=\; -\beta_0 a_R^2 - \beta_1 a_R^3 - ... \; , \tag{3.14}$$

$$\beta_0 = \frac{11}{3}C_A - \frac{4}{3}T_F n_f \quad , \quad \beta_1 = \frac{34}{3}C_A^2 - 4C_F T_F n_f - \frac{20}{3}C_A T_F n_f \; . \tag{3.15}$$

Hence, the coefficients in the expansion of Z are given by

$$Z^{'}_{\overline{\rm MS}}(\epsilon) = -\frac{2}{\epsilon}\beta_0 \quad , \quad Z^{''}_{\overline{\rm MS}}(\epsilon) = \frac{4}{\epsilon^2}\beta_0^2 - \frac{1}{\epsilon}\beta_1 \; . \tag{3.16}$$

On the other hand, Z can be obtained from the bare potential by requiring that the UV divergences be canceled. To do so, suppose we did not know about the Beta function. In terms of renormalized quantities, the potential can be written as

$$V_R(\boldsymbol{q}^2) \;=\; -\frac{C_F 16\pi^2}{\boldsymbol{q}^2}\, a_{\overline{\rm MS}} \left\{1 + a_{\overline{\rm MS}}\, c_{1\,\overline{\rm MS}}(\bar{\mu}^2/\boldsymbol{q}^2) + a^2_{\overline{\rm MS}}\, c_{2\,\overline{\rm MS}}(\bar{\mu}^2/\boldsymbol{q}^2) + \mathcal{O}(a^3_{\overline{\rm MS}})\right\} \; , \tag{3.17}$$

where $a_{\overline{\rm MS}} = a_{\overline{\rm MS}}(\mu^2)$ is understood. The $\overline{\rm MS}$ coefficients c_1 and c_2 can be obtained from the bare ones given in eqs. (3.6) – (3.11) by comparing renormalized and bare potentials, using eq. (3.12). The result is

$$\begin{aligned} c_{1\,\overline{\rm MS}}(\bar{\mu}^2/\boldsymbol{q}^2) \;&=\; \left(\frac{e^\gamma\bar{\mu}^2}{\boldsymbol{q}^2}\right)^{\frac{\epsilon}{2}} \tilde{c}_1(4-\epsilon) + Z^{'}_{\overline{\rm MS}}(\epsilon) \; , \\ c_{2\,\overline{\rm MS}}(\bar{\mu}^2/\boldsymbol{q}^2) \;&=\; \left(\frac{e^\gamma\bar{\mu}^2}{\boldsymbol{q}^2}\right)^{\epsilon} \tilde{c}_2(4-\epsilon) + 2Z^{'}_{\overline{\rm MS}}(\epsilon)\left(\frac{e^\gamma\bar{\mu}^2}{\boldsymbol{q}^2}\right)^{\frac{\epsilon}{2}} \tilde{c}_1(4-\epsilon) + Z^{''}_{\overline{\rm MS}}(\epsilon) \; . \end{aligned} \tag{3.18}$$

Now, requiring these coefficients to be finite, Z' and Z'' are fixed by the one-loop and two-loop terms, respectively. In fact, the anticipated result (3.16) is reproduced exactly, which gives an important check of the calculation. As a further check on the pole terms, the vertex and gluon wave function renormalization constants (Z_1 and Z_3^{-1}, respectively) have been extracted separately from the diagrams. They depend on the gauge parameter and agree with the ones given in [34]. The relation to the coupling renormalization constant as defined above is $Z = Z_1^2 Z_3^{-3}$.

An important question that needs to be asked at this point is how one assures that all ϵ–poles arising from expanding the bare coefficients $\tilde{c}_{ij}$ around $D = 4$ correspond to ultraviolet divergences only (remember that, in dimensional regularization, infrared divergences will be regulated automatically by the same parameter ϵ, which is a potential source of unwanted cancelations between UV and IR poles). To answer this question, i.e. proving IR finiteness, one has to perform a full calculation using a different regularization scheme. Details will be presented in the next subsection.

Infrared Behaviour

To regulate the infrared divergences, we choose a massive scheme. All propagators are supplied with an artificial 'mass' term, $1/k^2 \to 1/(k^2+m^2)$. As an immediate consequence, the recurrence relations presented in chapter 2 are no longer valid. Also, the set of basic integrals is enlarged, since vacuum–like integrals do no longer vanish. We will calculate the poles of these mass–regulated integrals by expanding around D=4. Next, letting $m \to 0$ in the prefactors of the poles, we recover the pure UV divergences of the original, massless, diagram. These can then be compared with the ϵ–poles of the massless calculation, exposing the IR divergences whenever a difference shows up. If the difference is a simple pole $1/\epsilon$, it corresponds to a pure IR divergence, which we will then term $-1/\epsilon_{ir}$, such that IR divergences would be regulated by $D = 4 + \epsilon_{ir}$ [6].

For the one-loop case, we have obtained an alternative, complete set of recurrence relations, which is given in appendix A.2. Using the same strategy as for the massless case, the bare one-loop contribution $(-g_0^2 C_F/\boldsymbol{q}^2)\, g_0^2\, c_1(\boldsymbol{q}^2, m^2, D)$ can be calculated for every single one-loop diagram, see fig. 1.3, in terms of the massive basic integrals A and B, as given in appendix B.3. Let us not give the full results here, since we will be interested in the poles only. Using the strategy outlined above for every diagram, namely first expanding in ϵ, then letting the auxiliary mass vanish and finally comparing the emerging UV–pole–terms with the poles of the massless calculation, we discover two infrared divergent diagrams. Displaying the IR poles only and omitting an overall factor of $(-g_0^4 C_F C_A/16\pi^2\boldsymbol{q}^2)$,

$$\text{diag.}(A) = \frac{4-2\xi}{-\epsilon_{ir}} \quad , \quad \text{diag.}(B) = \frac{-4+2\xi}{-\epsilon_{ir}} \, . \tag{3.19}$$

Here, the gauge parameter ξ is defined as being zero for the Feynman gauge. It is related to the one introduced in the Feynman rules (see appendix D) by $\xi = \eta - 1$. As already observed in [6], the IR divergences cancel in the sum[1], such that the remaining divergences are of pure UV type, indeed.

At the two-loop level, consider the self-energy contributions to the potential, diagrams (i) of fig. 1.4, first. Since they do not contain static propagators, we can take full advantage of the algorithm presented in [23], and its implementation in the Mathematica [32] package TARCER [36]. After this reduction step, one obtains analytic results for the bare coefficient $(-g_0^2 C_F/\boldsymbol{q}^2)\, g_0^4\, c_2(\boldsymbol{q}^2, m^2, D)$ of each diagram in terms of basic massive scalar integrals. The minimal set of integrals is listed in appendix B.3. Expanding the coefficients in $D = 4 - \epsilon$, the UV poles are obtained. Comparing with the poles of the massless diagrams, one finds a perfect match, to conclude that no single two-loop self-energy diagram exhibits an infrared divergence. Cancelation of IR divergences in the remaining diagrams, i.e. those containing at least one static propagator, was already shown in ref. [6] explicitly. As in the one-loop case, it turned out that the different topological classes form IR finite sets of diagrams.

To conclude this subsection, it has been demonstrated that IR divergences *do* occur in single diagrams (involving static propagators) at D=4, but cancel in the sum. Hence, the above procedure of extracting the renormalization constants from the massless calculation leads to correct results.

3.2.2 Renormalized Potential

Expanding eq. (3.18) up to constant terms, we get the coefficients in the renormalized potential, cf. eq. (3.17), as

$$c_{1\,\overline{\rm MS}}(x) = a_1 + \beta_0 \ln(x)\,, \tag{3.20}$$

$$c_{2\,\overline{\rm MS}}(x) = a_2 + \beta_0^2 \ln^2(x) + (\beta_1 + 2\beta_0 a_1)\ln(x) \tag{3.21}$$

with

$$a_1 = \frac{31}{9} C_A - \frac{20}{9} T_F n_f\,, \tag{3.22}$$

$$a_2 = \left(\frac{4343}{162} + 4\pi^2 - \frac{\pi^4}{4} + \frac{22}{3}\zeta(3)\right) C_A^2 - \left(\frac{1798}{81} + \frac{56}{3}\zeta(3)\right) C_A T_F n_f - \left(\frac{55}{3} - 16\zeta(3)\right) C_F T_F n_f + \frac{400}{81} T_F^2 n_f^2\,. \tag{3.23}$$

These constants constitute the main result of the two-loop calculation [35]. Comparing them with the results given in ref. [9], we find a discrepancy of $2\pi^2$ in the pure Yang–Mills term

[1] In fact, IR finiteness occurs on the level of topological classes already, since both diagrams $A, B \in$.

($\propto C_A^2$) of a_2. This amounts to a 30% decrease of a_2 for the case of $n_f = 0$, and a 50% decrease for $n_f = 5$ (for $SU(3)$), which is the case needed for $t\bar{t}$ threshold investigations. This difference can be traced back to a specific set of diagrams, as outlined below.

Comparison

The origin of the discrepancy is eq. (14) in the second paper of ref. [9]. To explain the crucial point, let us add the diagrams in question, using the notation explained in appendix B. Neglecting the overall minus sign, the couplings and the color factors, they give

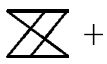

$$\begin{aligned} &= \int_1\int_2 (D_{235}S_{1125} + D_{145}S_{1125} + D_{235}S_{1122}) \\ &= \int_1\int_2 (D_{145}S_{1125} + D_{235}S_{1225}) \\ &= \int_1\int_2 D_{145}S_{112}\,(S_5 + S_{\bar{5}}) \ , \end{aligned} \tag{3.24}$$

where the identity $S_1S_2 = S_5(S_2 - S_1)$ (compare [9], sect. 4) was used for the last term of the first line, and the trivial exchange of loop variables $k_1 \leftrightarrow k_2$ was done in the last term of line two. In the last line, $S_{\bar{5}} = S(-k_5)$. One then obtains

$$\begin{aligned} S_5 + S_{\bar{5}} &= \frac{1}{(k_{10} - k_{20}) + i\varepsilon} + \frac{1}{-(k_{10} - k_{20}) + i\varepsilon} \\ &= -\frac{2i\varepsilon}{(k_{10} - k_{20})^2 + \varepsilon^2} \quad \stackrel{\varepsilon\to 0^+}{\longrightarrow} \quad -2\pi i\delta\,(k_{10} - k_{20}) \ , \end{aligned} \tag{3.25}$$

cf. eq. (2.12). Hence, contrary to the assumption in [9], the sum of the integrands in eq. (3.24) reduces to a delta distribution multiplying the remaining propagators.

Now, considering the color traces as well as the gluon-source couplings and the overall sign, one gets as a contribution to the bare static potential (for simplicity, we use the Feynman gauge here to make the point clear)

$$\begin{aligned} \text{diag.}(a6) + \text{diag.}(b3) &= -\frac{g^6}{4} C_F C_A^2 \Big(\quad + \quad \Big) - \frac{g^6}{2} C_F C_A^2 \\ &= -\frac{g^6}{4} C_F C_A^2 \quad - \frac{g^6}{4} C_F C_A^2 \Big(\quad + \quad + \quad \Big) \ . \end{aligned}$$

While in [9] the latter term was discarded, we evaluate it in $D = 4 - \epsilon$ dimensions to give

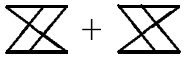

$$\begin{aligned} &= \frac{6(D-4)(3D-11)}{(D-5)} \frac{1}{\boldsymbol{q}^2} \\ &= -\frac{1}{32\pi^2}\frac{1}{\boldsymbol{q}^2} + O(\epsilon) \ . \end{aligned} \tag{3.26}$$

Note that the factor of $(D-4)$ in the numerator cancels the single pole in the scalar integral, such that only the constant part of a_2 is affected by this discussion, while the pole terms are not changed by the omission of this term. Hence, dividing out the overall factor $\left(-\frac{C_F g^6}{(16\pi^2)^2 \boldsymbol{q}^2}\right)$, we identify the $2\pi^2 C_A^2$ difference with respect to ref. [9].

V–Scheme

The static potential can be used for a definition of an effective 'physical' charge, which is conventionally called a_V [1]. Defining

$$V(\boldsymbol{q}^2) = -C_F \, \frac{16\pi^2 \, a_V(\boldsymbol{q}^2)}{\boldsymbol{q}^2} \; , \tag{3.27}$$

its expansion in terms of the $a_{\overline{\rm MS}}$ is given by eqs. (3.17), (3.20) and (3.21). Concerning the convergence of this series, let us give some numbers. For SU(3) and $T_F = \frac{1}{2}$, we have

$$a_V(\boldsymbol{q}^2) = a_{\overline{\rm MS}} \left\{ 1 + a_{\overline{\rm MS}}(10.33 - 1.11 n_f) + a^2_{\overline{\rm MS}}(456.75 - 66.35 n_f + 1.23 n_f^2) + \ldots \right\} \; . \tag{3.28}$$

Here, $a_{\overline{\rm MS}} = a_{\overline{\rm MS}}(\boldsymbol{q}^2)$ is understood. In ref. [9], the first number in the two-loop term was 634.40. One could have written the expansion in terms of $\alpha_{\overline{\rm MS}}/\pi$ $(= 4a_{\overline{\rm MS}})$, as is usually done, but apparently the convergence properties do not look very promising in either case. Knowledge of the three-loop coefficient $\beta_2^{\overline{\rm MS}}$ [34] can be used to derive the corresponding coefficient in the V–scheme from eq. (3.17). While β_0 and β_1 are universal, one finds

$$\begin{aligned} \beta_2^V &= \beta_2^{\overline{\rm MS}} - a_1\beta_1 + (a_2 - a_1^2)\beta_0 & (3.29) \\ &= \left(\frac{206}{3} + \frac{44\pi^2}{3} - \frac{11\pi^4}{12} + \frac{242}{9}\zeta(3) \right) C_A^3 \\ &\quad - \left(\frac{445}{9} + \frac{16\pi^2}{3} - \frac{\pi^4}{3} + \frac{704}{9}\zeta(3) \right) C_A^2 T_F n_f + \left(\frac{2}{9} + \frac{224}{9}\zeta(3) \right) C_A T_F^2 n_f^2 \\ &\quad - \left(\frac{686}{9} - \frac{176}{3}\zeta(3) \right) C_A C_F T_F n_f + 2 C_F^2 T_F n_f + \left(\frac{184}{9} - \frac{64}{3}\zeta(3) \right) C_F T_F^2 n_f^2 \; . & (3.30) \end{aligned}$$

The new value for a_2 leads, for $SU(3)$ and $n_f = 5$, to a 50% decrease of β_2^V compared to the formula given in ref. [9]. Still, β_2^V is much larger than $\beta_2^{\overline{\rm MS}}$, and hence the effective coupling defined by the potential runs faster than the $\overline{\rm MS}$ coupling.

3.2.3 Fourier Transform

The strictly perturbative potential of eq. (3.17) can be transformed to coordinate space. For this purpose, we need Fourier transforms of terms having the form $\ln^n(\boldsymbol{q}^2)/\boldsymbol{q}^2$. Writing

$$\ln^n\left(\frac{\bar\mu^2}{\boldsymbol{q}^2}\right) = \left[\partial_u^n \left(\frac{\bar\mu^2}{\boldsymbol{q}^2}\right)^u \right] \Bigg|_{u=0} \tag{3.31}$$

and defining the auxiliary function [9]

$$\mathcal{F}(r,\bar\mu,u) = \bar\mu^{2u} \int \frac{{\rm d}^3\boldsymbol{q}}{(2\pi)^3} \, \frac{\exp(i\boldsymbol{q}\boldsymbol{r})}{(\boldsymbol{q}^2)^{1+u}} \; , \tag{3.32}$$

we can re-express the Fourier transforms, which we need, as

$$\int \frac{\mathrm{d}^3\boldsymbol{q}}{(2\pi)^3}\,\ln^n\left(\frac{\bar{\mu}^2}{\boldsymbol{q}^2}\right)\,\frac{\exp(i\boldsymbol{q}\boldsymbol{r})}{\boldsymbol{q}^2} = \left[\,\partial_u^n \mathcal{F}(r,\bar{\mu},u)\,\right]\Big|_{u=0}\ . \tag{3.33}$$

Using a Schwinger parameter

$$\frac{1}{(\boldsymbol{q}^2)^{1+u}} = \frac{1}{\Gamma(1+u)}\int_0^\infty \mathrm{d}x\, x^u\,\exp(-x\boldsymbol{q}^2)\ , \tag{3.34}$$

the auxiliary function can be evaluated for $|u| < \frac{1}{2}$ to give [37]

$$\mathcal{F}(r,\bar{\mu},u) = \frac{(\bar{\mu}re^\gamma)^{2u}}{4\pi r}\,\exp\left(\sum_{n=2}^\infty \frac{\zeta(n)u^n}{n}\,(2^n-1-(-1)^n)\right)\ . \tag{3.35}$$

We obtain, as our final result for the two-loop static potential in coordinate space,

$$V(r) = \int \frac{\mathrm{d}^3\boldsymbol{q}}{(2\pi)^3}\,\exp(i\boldsymbol{q}\boldsymbol{r})\,V_R(\boldsymbol{q}^2) = -C_F\,\frac{4\pi a_V(1/r^2)}{r}\ , \tag{3.36}$$

with

$$\begin{aligned} a_V(1/r^2) \;=\; & a_{\overline{\mathrm{MS}}}\,\Big\{\,1 + a_{\overline{\mathrm{MS}}}(a_1+\beta_0 L) \\ & + a_{\overline{\mathrm{MS}}}^2\left(a_2+\beta_0^2(L^2+\frac{\pi^2}{3})+(\beta_1+2\beta_0 a_1)L\right) + \mathcal{O}(a_{\overline{\mathrm{MS}}}^3)\,\Big\}\ , \end{aligned} \tag{3.37}$$

where $L = 2\ln(\bar{\mu}re^\gamma)$ and again $a_{\overline{\mathrm{MS}}} = a_{\overline{\mathrm{MS}}}(\bar{\mu}^2)$. Note the appearance of the new term $\frac{\pi^2}{3}\beta_0^2$ in the two-loop coefficient as compared to eq. (3.21).

There are now numerous concepts for a 'renormalization group improvement', i.e. for an 'optimal' choice of the $\overline{\mathrm{MS}}$ scale parameter $\bar{\mu}$ in order to reduce large logarithmic corrections. Examples include the 'natural choice' $\bar{\mu} = e^{-\gamma}/r$ and the choice $\bar{\mu} = \exp(-\gamma - a_1/2\beta_0)/r$, which eliminates the one-loop coefficient completely. Due to this freedom, it is not very illuminating to present plots of the coordinate space potential. A general feature is that, at increasing distance, the large two-loop coefficient begins to dominate quite soon, even causing the potential to decrease again above some r_{crit}, to signal that the perturbative approach can be followed up to this critical distance at most. For a discussion of a variety of scale choices we refer to ref. [9]. The smaller coefficient a_2 found in our calculation does not change the plots presented there qualitatively. The reason is that the term $\frac{\pi^2}{3}\beta_0^2$, which shows up as a result of the Fourier transform as shown above, is of the same order as a_2. A comparison with four–dimensional quenched lattice results is given in ref. [38]. There, it is concluded that the perturbative potential already fails to describe the slope of the lattice potential at the smallest distances that are numerically tractable, hence invalidating the possibility to match the two potentials at small distances.

3.3 Three Dimensions

In three dimensions, one obtains a gauge–invariant, infrared finite result for the potential at the one-loop level. Fourier transforming back to coordinate space, the one-loop correction contributes a linear term to the potential. The size of this term is compared with lattice simulations. For the two-loop case, after discussing the renormalization, we will turn to the problematic infrared (IR) sector. Although a mechanism will be presented that cancels IR divergent contributions from the self-energy, the overall sum of exchange diagrams is shown to be IR singular and hence non–physical.

3.3.1 One-Loop Result

This section is based on our publication [39]. Let us briefly recapitulate the results given there. From eqs. (3.1), (3.6) and (3.7), and plugging in the basic integral from the appendix, the bare one-loop potential reads

$$V(\boldsymbol{q}^2) = -\frac{g^2 C_F}{\boldsymbol{q}^2}\left\{1 + g^2\,\left[(4D-5)C_A - 4T_F n_f\right]\mu^{2\varepsilon}\frac{(\boldsymbol{q}^2)^{\frac{D-4}{2}}}{(16\pi)^{\frac{D-1}{2}}}\frac{\Gamma\left(\frac{4-D}{2}\right)\Gamma\left(\frac{D}{2}\right)}{\Gamma\left(\frac{D+1}{2}\right)} + \ldots\right\} \quad (3.38)$$

One clearly sees that the dimensionally regulated potential is perfectly finite in $D = 3$ dimensions. Hence, setting $D = 3$, no renormalization is needed ($Z^{'} = 0$ in the language of section 3.2.1) and one obtains

$$V^{3D}(\boldsymbol{q}^2) = -\frac{g^2 C_F}{\boldsymbol{q}^2}\left\{1 + \frac{g^2}{32|\boldsymbol{q}|}(7C_A - 4T_F n_f) + \ldots\right\}\,. \quad (3.39)$$

Concerning the possible cancelation of IR and UV divergences, both (if present) showing up as poles in ϵ, the three-dimensional one-loop case proves harmless. Using the massive coefficients of section 3.2.1 and expanding them around $D = 3 - \epsilon$, none of the one-loop diagrams shows a UV divergence, and since they are finite in the massless calculation also, there are no poles in ϵ_{ir}. This is due to the fact that the leading IR behaviour shows up as $1/m$ poles in the coefficient of ϵ^0 when letting the auxiliary mass $m \to 0$, while dimensional regularization (DR) absorbs these power divergences. In contrast, the diagrams that exhibit single poles in ϵ_{ir} in the $4D$ case started with a logarithmic divergence $\ln(m)$, to which DR is sensitive.

In two (spatial) dimensions the Fourier transforms, which we need, read $-2\pi/\boldsymbol{q}^2 \to \ln(r/r_0)$ and $-2\pi/|\boldsymbol{q}|^3 \to r$. They can be derived within distribution theory, since the potential is understood as an operator acting on wave functions which fall off fast enough. The scale r_0 introduced in the above is purely arbitrary. Since the potential is defined only up to a constant, a change in r_0 is irrelevant. Hence, let us choose the only natural scale at hand, $r_0 = 1/g^2$, to

obtain for the perturbative potential in coordinate space

$$V^{3D}_{\rm pert}(r) = \frac{g^2 C_F}{2\pi}\ln(g^2 r) + \sigma r + \mathcal{O}(g^4 r^2)\,, \tag{3.40}$$

$$\text{with } \sigma = \frac{g^4 C_F}{64\pi}\left(7C_A - 4T_F n_f\right)\,. \tag{3.41}$$

The first term constitutes the well–known Coulomb potential in two space–dimensions, while the linear part is the new information added by this investigation.

The linear term can be compared with lattice results [40]. There, $\sqrt{\sigma}/g^2$ is measured in the 3D pure $SU(N_c)$ theory for $N_c = 2, 3, 4, 5$ using smeared Polyakov loops. Specializing our result (3.41) to this case ($T_F = 1/2$, $C_F C_A = (N_c^2 - 1)/2$, $n_f = 0$), it reads

$$\text{pure } SU(N_c)\ : \qquad \sqrt{\sigma}/g^2 = \sqrt{\frac{7(N_c^2-1)}{128\pi}} \approx 0.132\sqrt{N_c^2 - 1}\,. \tag{3.42}$$

The comparison (see table 3.1) shows qualitative agreement, especially concerning N_c–dependence.

N_c	$\sqrt{\sigma}/g^2\|_{lat}$	$\sqrt{\sigma}/g^2\|_{pert}$	lat/pert
2	.34	.23	1.47
3	.55	.37	1.48
4	.76	.51	1.48
5	.97	.65	1.49

Table 3.1: *Comparison of lattice and analytical results*

The lattice results are, at least in the range of the parameter N_c covered, larger by a factor of 3/2. The outcome of this calculation suggests that the perturbative part of the potential may constitute a sizeable part of the full potential.

As is to be expected from the dimensional considerations, the next coefficient in the 3D coordinate space potential will, if it exists, contribute a quadratic term λr^2. Considering the concavity and monotony of the potential [41], it will therefore bear information on the range of validity of the perturbative potential. While this argument was a main part of the motivation that led us to investigate the two-loop potential, let us discuss the expansion of the two-loop coefficient around D=3 in the next section.

3.3.2 Two-Loop Infrared Problems

To analyze the structure of counterterms, let us start the discussion by the power–counting method, as usually used in proofs of renormalizability. If the superficial degree of divergence d of any Feynman diagram (defined by the number of loop momenta in the numerator minus the

number of loop momenta in the denominator) is negative, there are no ultraviolet divergences. If this number turns out to be zero (or greater), the diagram is expected to have a logarithmic (or higher) divergence, which has to be regulated by the counterterms. At one loop, we have $d = D-6$ for our diagrams. As usual, D denotes the number of space–time dimensions. It is useful to define the number of 'external legs' in our case as the number of propagators that carry the exchange momentum $\boldsymbol{q}$ only, since these lines do not contribute to the UV behaviour inside the loop integrals. Hence, we conclude that for diagrams with 0 (1,2,..) 'external legs', D has to be greater or equal 6 (4,2,..) to make the diagram potentially UV divergent. At two loops, $d = 2D-10$, such that for 0 (1,2,..) 'external legs', we need $D \geq 5$ $(4, 3, ..)$ for potential UV divergences. It is now clear that the general condition for UV divergences is

- n–loop diagram $\Longrightarrow d = nD - 2(2n+1) = n\,[\,D - (4 + 2/n)\,]$,
- e 'external legs' $\Longrightarrow D \geq 4 + \frac{2-2e}{n}$ for UV divergence .

For D=3, it follows from the above general inequality that UV divergences can occur only if the condition $2e \geq n+2$ is satisfied. This means that only self-energy diagrams (for which $e=2$; cf. diags.(i1))[2] at $n \leq 2$ loops are potentially UV divergent, while vertex corrections ($e=1$; as an example,see diag.(b1)) as well as the ladder diagrams ($e=0$; cf. diag.(a6)) are ultraviolet finite. It has become clear now that the 3D theory is superrenormalizable (there are only a finite number of potentially UV divergent diagrams), and that there is no vertex renormalization needed. The wave–function renormalization is completely fixed by one– and two-loop self-energy diagrams, and hence the Beta function will be known exactly after calculating these diagrams (it will turn out to vanish identically, i.e. the 3D coupling does not run).

Consider the self-energy diagrams (diags.(i) of fig. 1.4) in massive regularization first. Along the lines of section 3.2.1, one can express them in terms of the basic massive integrals, listed in appendix B.3. Expanding the coefficients as well as the integrals around $D = 3 - \epsilon$ while keeping the mass regulator finite, the UV divergences are extracted. They cancel in the sum, so there is no wave function renormalization at two loops. Comparing with the poles of the massless diagrams, we find the following IR divergences:

$$\text{diag.}(i1.b) \;=\; \frac{(\xi+5)\,[\,((\xi+2)^2+10)\,C_A - 8T_F n_f\,]}{6(-\epsilon_{ir})}\,, \tag{3.43}$$

$$\text{diag.}(i1.c) \;=\; \frac{-2\,[\,((\xi+2)^2+10)\,C_A - 8T_F n_f\,]}{6(-\epsilon_{ir})}\,. \tag{3.44}$$

An overall factor of $g^6 C_F C_A/16\pi\boldsymbol{q}^4$ was omitted here. The two terms do not cancel in the sum, leaving the class (2) IR divergent in three dimensions. The form of the IR divergence has been obtained before, cf. ref. [15], where it was noticed that the infrared divergences of the two-loop

[2] Note that diagrams with $e > 2$ are not one-particle irreducible, cf. diag.(i2), and are hence renormalized automatically as pure iterations.

self-energy in pure gauge theory disappear by choosing the gauge $(\eta+1)^2 = -10$ (note that our $\xi = \eta - 1$).

To motivate the mechanism that leads to the cancelation of IR divergences originating from the self-energy diagrams, it is instructive to investigate a simpler, exactly solvable problem first, namely the one-loop potential for $D = 2 - \epsilon$. Employing the strategy explained in section 3.2.1 once more, we find four diagrams being infrared divergent. Omitting an overall factor of $(-g_0^4 C_F C_A/4\pi \boldsymbol{q}^2)$, and again denoting $\epsilon = -\epsilon_{ir}$ for pure IR terms, they read

$$\text{diag.}(A) = \frac{8 - 4\xi - \xi^2}{-\epsilon_{ir}} \quad , \quad \text{diag.}(C) = \frac{10\xi + 2\xi^2}{-\epsilon_{ir}} \, , \tag{3.45}$$

$$\text{diag.}(a) = \frac{-10 - 7\xi - \xi^2}{-\epsilon_{ir}} \quad , \quad \text{diag.}(b) = \frac{2 + \xi}{-\epsilon_{ir}} \, . \tag{3.46}$$

In the sum, they cancel, but note that already in this two-dimensional case, the self-energy by itself is not IR finite. Depicting the minimal IR finite set on the level of the topological classes introduced in the first chapter, we can write

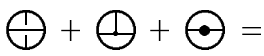

(3.47)

Thus, for the first time, we observe a cancelation that goes beyond just adding topological classes, which was the mechanism that emerged in the 4D case, put forward in [6].

Returning to D=3 after this short digression, we note that infrared divergences in the non–self-energy type diagrams can be obtained by setting $\epsilon = -\epsilon_{ir}$ in the usual expansion of the analytic two-loop coefficients (i.e. by expanding around $D = 3 + \epsilon_{ir}$), since it it clear from the above power–counting arguments that no UV divergences are present ($e \in \{0, 1\}$ here). The IR divergences are collected in appendix C and include in particular (omitting the same factor as above)

$$\text{diag.}(f1) \;=\; \frac{(\xi - 5)\,\left[\,((\xi+2)^2 + 10)\,C_A - 8T_F n_f\,\right]}{6(-\epsilon_{ir})} \, , \tag{3.48}$$

$$\text{diag.}(g2) \;=\; \frac{-2(\xi - 1)\,\left[\,((\xi+2)^2 + 10)\,C_A - 8T_F n_f\,\right]}{6(-\epsilon_{ir})} \, . \tag{3.49}$$

With diags.(f2),(f3),(g1) being (IR) finite, we can construct an IR finite set of diagrams in a fashion similar to (3.47), adding

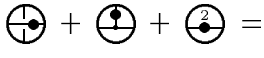

(3.50)

The potential thus seems to have the nice feature of absorbing the bad behaviour of the self-energy in a well-defined way.

Summing up the remaining IR divergences, we notice that they do not cancel completely. We are left with the divergent part which, using the notation introduced in eq. (3.2), is given

by

$$\tilde{c}_2(D = 3 + \epsilon_{ir}) = -\frac{16\pi^2 C_A^2}{\epsilon_{ir}^2} + \frac{24\pi^2 C_A^2}{\epsilon_{ir}} + \mathcal{O}(\epsilon_{ir}^0) \; . \tag{3.51}$$

All dependence on the gauge parameter ξ, present in the individual contributions displayed in app. C, has canceled, so that we are left with a gauge independent infrared pole structure. A closer look on the IR structure of the involved diagrams is unavoidable now. It is possible that these divergences are specific to the momentum space treatment, in the sense that they are induced by the exchange of limit and summation in the original definition of the static potential, which had to be done to derive the set of p–space Feynman rules (see appendix D.1). This potentially dangerous step can be circumvented by performing an analysis in coordinate space directly, which will be done in the next chapter.

Chapter 4

Coordinate Space

To understand the origin of the infrared problems that occurred in the momentum space calculations, one needs to go back to coordinate space. The vacuum expectation value of the Wilson–loop, defined with finite temporal extension T is not divergent. However, divergences can be introduced by the limit $T \to \infty$, in which the static potential is extracted.

The problem in momentum space is that the limit has to be performed before the integrations are done, in order to get Feynman rules with energy–momentum conservation at the vertices (keeping T finite destroys translational invariance).

Hence, let us aim at calculating the finite Wilson–loop directly in coordinate space, and performing the large–T limit at the very end. It is clear from the outset that such a calculation is much more involved compared to the momentum–space approach, since there is one more scale.

4.1 Dimensional Analysis

To illustrate the structures to be met, let us start with some general dimensional considerations. Displaying the relevant parameters only, the potential is defined as

$$V = -\lim_{T\to\infty} \frac{1}{T} W(g^2; T, r) \,. \tag{4.1}$$

In a perturbative analysis, the dimensionless function W will be expanded in powers of the coupling,

$$W(g^2; T, r) = g^2 \, F_{g^2}(T, r) + g^4 \, F_{g^4}(T, r) + \dots \,. \tag{4.2}$$

Since the gauge coupling is dimensionless in four dimensions only, in general the functions F carry dimension. The appropriate dimensionless expansion parameter would be $g^2 r^{4-D}$, so

writing

$$F_{g^2}(T,r) = r^{4-D}\, f_{g^2}\,(T/r) \quad , \quad F_{g^4}(T,r) = \left(r^2\right)^{4-D}\, f_{g^4}\,(T/r) \quad , \quad \text{etc.} \tag{4.3}$$

defines dimensionless functions f, which as a consequence can only depend on the ratio T/r. Aiming towards extracting the potential, the large–T asymptotics of these functions has to be found. In general, we will find powers as well as logarithms, so the situation is as follows:

$$\begin{aligned} f(x) \quad &\overset{x\gg 1}{=} \quad \sum_{i=\infty}^{-\infty} \sum_{j=0} c_{ij}\, x^i\, \ln^j x \\ &= \quad \underbrace{\sum_{i=\infty}^{2} \sum_{j=0} c_{ij}\, x^i\, \ln^j x + \sum_{j=1} c_{1j}\, x\, \ln^j x}_{\text{diverge in limit}} + c_{10}\, x + \underbrace{\sum_{i=0}^{-\infty} \sum_{j=0} c_{ij}\, x^i\, \ln^j x}_{\text{vanish in limit}} \; . \end{aligned} \tag{4.4}$$

The divergent terms have to cancel in the sum of all diagrams. This is to be shown below. It is clear now, that enforcing the limit *before* adding all diagrams can lead to infrared problems, which is exactly the situation encountered in the momentum–space calculation. The only terms in $f(T/r)$ contributing to the potential are the linear ones. There is one important exception to the structure depicted in the last formula, namely the tree-level (g^2) contribution for D=3. In this case, since we had pulled out a factor of r, the c_{10}–contribution to the potential is a constant (with respect to r), and thus can be dropped. Instead, the c_{11}–term gets important here:

$$\begin{aligned} V_{g^2}^{D=3} \quad &= \quad -\lim_{T\to\infty} \frac{r}{T}\, f_{g^2}(T/r) = -\lim_{T\to\infty} \left\{ \ldots + c_{11} \ln(T/r) + c_{10} + \ldots \right\} \\ &= \quad -\lim_{T\to\infty} \left\{ \underbrace{\ldots}_{\text{div.}} + \underbrace{c_{11} \ln(T/r_0)}_{\text{const}_r} - c_{11} \ln(r/r_0) + \underbrace{c_{10}}_{\text{const}_r} + \underbrace{\ldots}_{\text{vanish}} \right\} . \end{aligned} \tag{4.5}$$

Note that this clarifies the appearance of the logarithmic Coulomb potential as well as the need to introduce the arbitrary scale r_0 in 2+1 dimensions.

4.2 Results

One should realize that it is very easy to get lost in a lot of work when diving into the two-loop coordinate space calculation. On top of having the additional scale T (compared to the p–space calculation), there is no simple UV regularization scheme [1] (like $\overline{\text{MS}}$). So the real structure of terms to be expected is slightly more complicated than sketched above, since an UV cutoff scale has to be introduced. Furthermore, one has to deal with a large number of integrals to be expanded quite far (up to seventh order in some cases, which would even make a numerical treatment very delicate), if one wants to prove the IR cancelations analytically. Finally, things

[1] See e.g. [42] and references therein for the differential renormalization method for one-loop calculations.

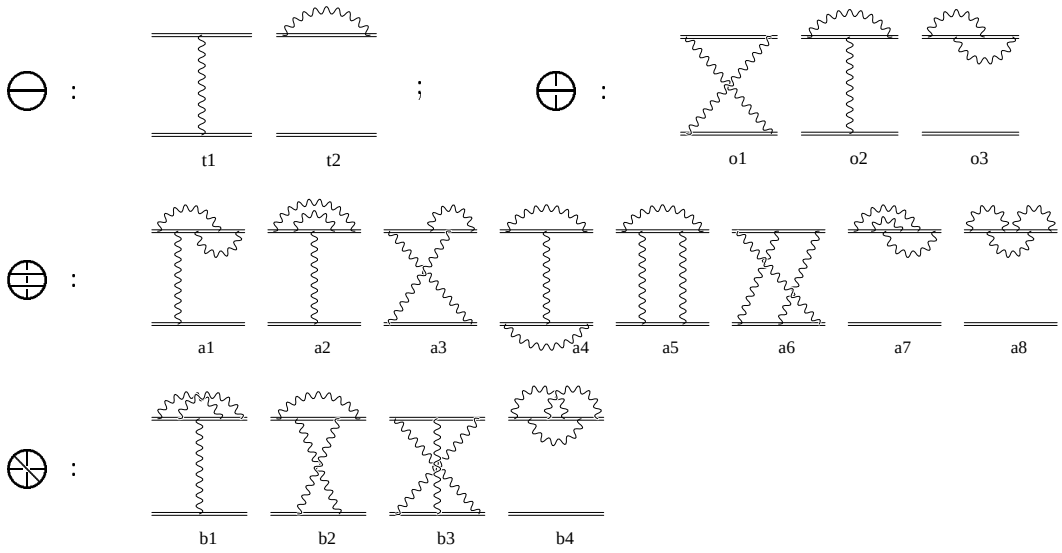

Figure 4.1: *Diagrams discussed in this chapter. Mirror diagrams as well as rotated ones are not shown, but are understood to be included where appropriate.*

are completely different in 4D and 3D. This gets immediately clear by noting the different structures of the gluon propagator [2], cf. eq. (D.3).

These preliminary warnings should serve as an excuse for not (yet) being able to discuss the complete infrared sector at this place. Below, some results obtained so far will be presented. All calculations are done in the Feynman gauge, and only the diagram classes without internal gluon–couplings are treated, see fig 4.1.

4.2.1 Tree-Level

As a simple example, let us start by evaluating the tree-level class (⊖). Using the x–space Feynman rules given in eqs. (D.2) and (D.3), the tree-level contribution can be evaluated for D=4 and D=3 as follows.

D=4. In four dimensions, the situation is clear:

$$t_1 \;=\; \overset{x}{\underset{y}{\vcenter{\hbox{\includegraphics{}}}}} \;\overset{D=4}{=}\; \frac{g^2}{4\pi^2}\int_{-\frac{T}{2}}^{\frac{T}{2}}\mathrm{d}x_0\int_{-\frac{T}{2}}^{\frac{T}{2}}\mathrm{d}y_0\,\frac{1}{(y_0-x_0)^2+r^2}$$

$$= \frac{g^2}{4\pi^2}\left[\frac{T}{r}\left(\frac{\pi}{2}+\arctan(T/r)-\arctan(r/T)\right)-\ln\left((T/r)^2+1\right)\right]$$

[2] This is exactly what makes a momentum–space calculation more universal: Feynman rules in p–space have the same form for any dimension, while only at a late stage of any calculation, i.e. when expanding/calculating integrals or when doing the Fourier-transform back to x–space, one 'feels' the dimension.

$$\stackrel{T\gg r}{=} \frac{g^2}{4\pi^2}\left[\underbrace{\pi}_{c_{10}}\frac{T}{r}+\mathcal{O}(T^0)\right], \tag{4.6}$$

so an attractive Coulomb–potential

$$-\lim_{T\to\infty}\frac{1}{T}\{t_1\} = -\frac{g^2}{4\pi r} \tag{4.7}$$

results from the gluon exchange diagram (note that color factors, like C_F in this case, are suppressed in this chapter). There is no danger in performing the limit. This will no longer be true in three dimensions, so let us turn to that case immediately.

D=3. For the exchange diagram, a comparably simple integration gives

$$\begin{aligned} t_1 &\stackrel{D=3}{=} \frac{g^2}{4\pi}\int_{-\frac{T}{2}}^{\frac{T}{2}}\mathrm{d}x_0\int_{-\frac{T}{2}}^{\frac{T}{2}}\mathrm{d}y_0\frac{1}{\sqrt{(y_0-x_0)^2+r^2}} \\ &= -\frac{g^2 r}{4\pi}\left[2\sqrt{(T/r)^2+1}-\frac{T}{r}\ln\left(\frac{\sqrt{(T/r)^2+1}+T/r}{\sqrt{(T/r)^2+1}-T/r}\right)-2\right] \\ &\stackrel{T\gg r}{=} -\frac{g^2 r}{4\pi}\left[\underbrace{-2}_{c_{11}}\frac{T}{r}\ln(T/r)+\underbrace{(2-2\ln(2))}_{c_{10}}\frac{T}{r}+\mathcal{O}(T^0)\right]. \end{aligned} \tag{4.8}$$

Proceeding in the way outlined above, the c_{11}–term can be split,

$$\text{eq.(4.8)} = -\frac{g^2 r}{4\pi}\left[-2\frac{T}{r}\ln(T/r_0)+2\frac{T}{r}\ln(r/r_0)+(2-2\ln(2))\frac{T}{r}+\mathcal{O}(T^0)\right], \tag{4.9}$$

where the first term will be dropped in the potential as a (infinite, but r–independent) constant, the second term gives the Coulomb potential, and the last one can be dropped as a (finite) constant. Alternatively, one can calculate the r–independent diagrams of this class (here, an UV cutoff a has to be introduced),

$$\begin{aligned} (t_2+\text{rotated}) &\stackrel{D=3}{=} -2\frac{g^2}{4\pi}\int_{-\frac{T}{2}}^{\frac{T}{2}}\mathrm{d}x_0\int_{-\frac{T}{2}}^{\frac{T}{2}}\mathrm{d}y_0\frac{\theta(y_0-x_0)}{\sqrt{(y_0-x_0)^2}} \\ &\stackrel{\text{UV reg.}}{\longrightarrow} -2\frac{g^2}{4\pi}\int_{-\frac{T}{2}}^{\frac{T}{2}}\mathrm{d}x_0\int_{-\frac{T}{2}}^{\frac{T}{2}}\mathrm{d}y_0\frac{\theta(y_0-x_0-a)}{\sqrt{(y_0-x_0)^2}} \\ &= -\frac{g^2 r}{4\pi}\left[(2\ln(T/a)-2)\frac{T}{r}+2\frac{a}{r}\right], \end{aligned} \tag{4.10}$$

and observe that the overall sum gives a manifestly IR finite contribution to the potential,

$$\begin{aligned} -\lim_{T\to\infty}\frac{1}{T}\bigominus &= -\lim_{T\to\infty}\frac{1}{T}\Big\{t_1+(t_2+\text{rotated})\Big\} \\ &= \lim_{T\to\infty}\frac{1}{T}\frac{g^2 r}{4\pi}\left[2\frac{T}{r}\ln(r/a)-2\frac{T}{r}\ln(2)+\mathcal{O}(T^0)\right] = \frac{g^2}{2\pi}\ln(r/2a) \end{aligned} \tag{4.11}$$

Now, the UV cutoff a sets the scale of the Coulomb potential, and one can identify $r_0 \leftrightarrow 2a$.

4.2.2 One-Loop

It is no longer possible to obtain closed analytic expressions for the integrals occurring here, but the asymptotic T–expansion for members of the one-loop class $\bigoplus$ can be driven to the needed accuracy.

D=4. Introducing the UV regulator a as above,

$$o_1 = \frac{g^4}{(4\pi^2)^2}\left[\underbrace{2\pi}_{c_{11}}\frac{T}{r}\ln(T/r)\underbrace{-2\pi\,(\ln(2)+1)}_{c_{10}}\frac{T}{r}+\mathcal{O}(T^0)\right], \tag{4.12}$$

$$(o_2+\text{rotated}) = \frac{g^4}{(4\pi^2)^2}\left[\underbrace{-2\pi}_{c_{11}}\frac{T}{r}\ln(T/r)+\underbrace{2\pi\,(-\ln(r/a)+\ln(2)+2)}_{c_{10}}\frac{T}{r}+\mathcal{O}(T^0)\right] \tag{4.13}$$

$$\text{sum} = \frac{g^4}{(4\pi^2)^2}\left[2\pi\,(-\ln(r/a)+1)\,\frac{T}{r}+\mathcal{O}(T^0)\right]. \tag{4.14}$$

The disconnected diagram o_3 is UV divergent, but IR finite in the limit, and since it does not depend on r, it can be omitted here. Like in the tree-level case, the sum of the exchange diagrams has an IR–finite limit.

D=3. The individual diagrams contribute

$$o_1 = \frac{g^4r^2}{(4\pi)^2}\left[\underbrace{2}_{c_{21}}\frac{T^2}{r^2}\ln(T/r)+\underbrace{\left(2\ln(2)-5+\frac{\pi^2}{6}\right)}_{c_{20}}\frac{T^2}{r^2}+\mathcal{O}(T^0)\right], \tag{4.15}$$

$$(o_2+\text{rotated}) = \frac{g^4r^2}{(4\pi)^2}\left[\underbrace{-2}_{c_{21}}\frac{T^2}{r^2}\ln(T/r)+\underbrace{\left(-2\ln(2)+5-\frac{\pi^2}{3}\right)}_{c_{20}}\frac{T^2}{r^2}+\mathcal{O}(T^0)\right], \tag{4.16}$$

$$(o_3+\text{rotated}) = \frac{g^4r^2}{(4\pi)^2}\left[\underbrace{\frac{\pi^2}{6}}_{c_{20}}\frac{T^2}{r^2}\right]. \tag{4.17}$$

Like in the 3–dimensional tree-level case, only the sum permits a finite limit,

$$\begin{aligned} -\lim_{T\to\infty}\frac{1}{T}\bigoplus &= -\lim_{T\to\infty}\frac{1}{T}\left\{o_1+(o_2+\text{rotated})+(o_3+\text{rotated})\right\} \\ &= -\lim_{T\to\infty}\frac{1}{T}\frac{g^4r^2}{(4\pi)^2}[\,0\,]=0\,. \end{aligned} \tag{4.18}$$

In this case, the only contribution (in Feynman gauge) to the potential comes from the one–gluon–exchange diagram, $\bigodot$.

4.2.3 Two-Loop

Omitting an overall factor of $-g^6r^3/(4\pi)^3$, the known two-loop coefficients of the functions $f_{g^6}\,(T/2r)$ are displayed as a set $\{c_{32},c_{31},c_{30};c_{2j};c_{13},c_{12},c_{11},c_{10}\}$. While c_{32}, corresponding to

$T^3 \ln^2 T$, is the highest divergence to occur, the terms beyond c_{10} vanish in the potential, like discussed above.

For the class  , we have obtained

$$\begin{aligned}
a_1 &= \{0, \tfrac{16}{9}(-6+\pi^2), -\tfrac{8}{27}(138-5\pi^2-72\ln 2+12\pi^2\ln 2-90\zeta(3)); [0]; [0], [-.4], \ldots\} \\
a_2 &= \{0, \tfrac{8}{3}, -\tfrac{4}{9}(-20+3\pi^2+12\ln 2-12\zeta(3)); 0; 0, 0, 0, \ldots\} \\
a_3 &= \{0, -16, \tfrac{8}{3}(-22+\pi^2+12\ln 2+4\zeta(3)); 0; [3.2], \ldots\} \\
a_4 &= \{0, -\tfrac{8}{9}(-15+\pi^2), -\tfrac{8}{27}(-168+10\pi^2+90\ln 2-6\pi^2\ln 2+45\zeta(3)); 0; [0], [0], [3.15], \ldots\} \\
a_5 &= \{\tfrac{16}{3}, -\tfrac{16}{9}(-20+\pi^2+12\ln 2), \tfrac{4}{27}(530-25\pi^2-480\ln 2+24\pi^2\ln 2+144\ln^2 2-108\zeta(3)); 0; [2], \ldots\} \\
a_6 &= \{-\tfrac{16}{3}, \tfrac{8}{9}(-28+\pi^2+24\ln 2), -\tfrac{8}{27}(127-7\pi^2-168\ln 2+6\pi^2\ln 2+72\ln^2 2+9\zeta(3)); [0]; [-6], \ldots\} \\
a_7 &= \{0, 0, \tfrac{8}{9}(\pi^2-6\zeta(3)); 0; 0, 0, 0, 0\} \\
a_8 &= \{0, 0, \tfrac{8}{9}(\pi^2-6\zeta(3)); 0; 0, 0, 0, 0\} \\
\text{sum} &= \{0, 0, 0; [0]; [-.8], \ldots\}
\end{aligned} \tag{4.19}$$

Numbers in square brackets were obtained only numerically, using the Monte–Carlo integration routine Vegas [43]. The leading IR divergences, c_{3j}, cancel analytically. The sub-leading divergences are not known analytically.

The class  has been calculated to the same precision,

$$\begin{aligned}
b_1 &= \{0, \tfrac{8}{9}(12-\pi^2), \tfrac{4}{27}(-704+39\pi^2+312\ln 2-12\pi^2\ln 2-360\ln^2 2+144\ln^3 2+252\zeta(3)); [0]; 0, 0, 0, [-.88]\} \\
b_2 &= \{0, \tfrac{8}{9}(-30+2\pi^2), -\tfrac{4}{27}(182-9\pi^2-132\ln 2+12\pi^2\ln 2-180\ln^2 2+72\ln^3 2+18\zeta(3)); 0; [-1.16], \ldots\} \\
b_3 &= \{0, \tfrac{8}{9}(18-\pi^2), \tfrac{16}{27}(99-5\pi^2-54\ln 2+3\pi^2\ln 2-18\zeta(3)); 0; [.67], \ldots\} \\
b_4 &= \{0, 0, \tfrac{8}{27}(245-14\pi^2-114\ln 2+6\pi^2\ln 2+90\ln^2 2-36\ln^3 2-81\zeta(3)); 0; 0, 0, 0, 0\} \\
\text{sum} &= \{0, 0, 0; [0]; [-.49], \ldots\}
\end{aligned} \tag{4.20}$$

Like above, the leading divergences c_{3j} cancel analytically, while the further numerical treatment points towards the non–cancelation of c_{13}–terms, corresponding to $T \ln^3 T$.

4.3 A New Type of Diagrams

We are now in a position to discuss the long–standing question of the role of the end–pieces of the Wilson–loop. For brevity, we will call these the 'vertical' source–lines (see fig. 1.1), as opposed to the 'horizontal' source–lines considered so far for the '*traditional*' diagrams. Again, the Feynman gauge will be used here.

Let us first analyze the set of possible new diagrams. First, there is a new class of diagrams involving gluons coupled to the vertical pieces only. These we will call '*dual*' diagrams, since their contributions can be obtained from the traditional set by interchanging $T \leftrightarrow r$. An example

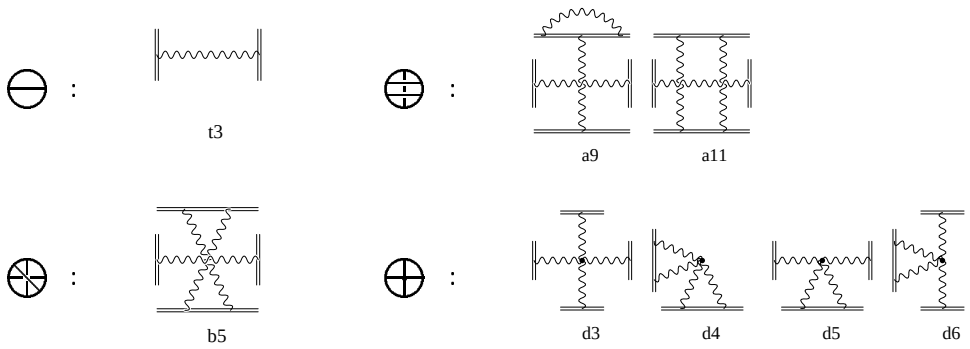

Figure 4.2: *Examples of new diagrams that are nonzero in Feynman gauge.*

is provided by the diagram t_3 of fig. 4.2. Second, there are new diagrams in which vertical and horizontal source–lines are connected. We will call them '*mixed*' diagrams. Examples are $d_3..d_6$ of fig. 4.2. Due to the diagonal Lorentz structure of the gluon propagator, it is easy to see that all mixed diagrams containing direct gluon exchange between horizontal and vertical source–lines vanish in Feynman gauge (this is not the case if the gluon is dressed, since the self-energy insertion leads to non–diagonal terms). Third, we identify a new class of '*factorized*' diagrams, in which horizontal and vertical source–lines are connected among themselves only, like a_9, a_{11} and b_5 of fig. 4.2. Their contributions can be obtained by simply multiplying lower–order traditional and dual diagrams.

Dual diagrams. This class of diagrams can be shown to not contribute in the limit of large T. The argument is the following. If the diagram is disconnected, it cannot depend on T, so it is suppressed by the overall $1/T$ coming from the definition of the potential. For the connected diagrams, a propagator connecting the 'vertical' source–lines at $+T/2$ and $-T/2$ vanishes asymptotically like $1/T$ ($1/T^2$) in D=3 (D=4). Nevertheless, let us give the leading terms of the lowest–order dual diagram, since, besides supporting the above dimensional argument, it will play an important role for the two-loop factorized diagrams. From eqs. (4.6) and (4.8), by interchanging $T \leftrightarrow r$, we get for $T \gg r$

$$t_3 = \begin{cases} \dfrac{g^2}{4\pi^2}\left[\dfrac{r^2}{T^2} + \mathcal{O}\left(T^{-4}\right)\right] & (D=4) \\ \dfrac{g^2 r}{4\pi}\left[\dfrac{r}{T} + \mathcal{O}\left(T^{-3}\right)\right] & (D=3) \end{cases} \tag{4.21}$$

Mixed diagrams can contribute to the potential. While the one-loop mixed diagrams vanish in pairs due to symmetry reasons, we have analyzed one two-loop class (in D=3) so far. Consider the diagram class involving the gluon–4–vertex. In a numerical treatment, one can see that each of the diagrams starts with a c_{10}–term, giving a contribution to the potential in the limit of large T, while being IR finite. Suppressing a common overall factor, the relative

strengths of the coefficients c_{10} are

$$d_3 \sim [4] \quad , \quad d_4 \sim [-4] \quad , \quad d_5 \sim [-2] \quad , \quad d_6 \sim [-4] \, . \tag{4.22}$$

There are, of course, many more mixed two-loop diagrams. Considering all of them, it might happen that their sum does not contribute. The above example is given here only to make a first case for a non–vanishing non–traditional diagram.

Factorized diagrams. Recalling the above argument for dual diagrams, it is immediately clear that for D=4 the factorized diagrams cannot contribute. The reason is the $1/T^2$ suppression factor coming from any dual diagram, so the multiplying traditional diagram would have to exhibit a T^3 divergence, which is not the case according to the explicit calculation above. In D=3 dimensions, the situation is much more interesting. Here, the dual diagrams vanish like $1/T$ only, so any traditional diagram with a T^2–divergence (or worse) at $(n-1)$ loops will lead to an n–loop factorized diagram that can potentially contribute to the potential. Such traditional diagrams are immediately recognized from the above calculation: $o_1..o_3$, cf. eqs. (4.15) – (4.17). While folding o_3 with t_3 (which is the tree-level diagram dual to t_1) falls into an abelian class of diagrams and hence is part of the exponentiated tree-level potential, folding o_1 and o_2 with t_3 does have non–abelian parts. We thus have

$$\begin{aligned} b_5 &= t_3 \otimes o_1 \\ &\stackrel{D=3}{=} \frac{g^6 r^3}{(4\pi)^3} \left[2\frac{T}{r} \ln(T/r) + \left(2\ln(2) - 5 + \tfrac{\pi^2}{6} \right) \frac{T}{r} + \mathcal{O}\left(T^{-1}\right) \right] \, , \end{aligned} \tag{4.23}$$

$$\begin{aligned} a_9 &= t_3 \otimes (o_2 + \text{rot.}) \\ &\stackrel{D=3}{=} \frac{g^6 r^3}{(4\pi)^3} \left[-2\frac{T}{r} \ln(T/r) + \left(-2\ln(2) + 5 - \tfrac{\pi^2}{3} \right) \frac{T}{r} + \mathcal{O}\left(T^{-1}\right) \right] \, . \end{aligned} \tag{4.24}$$

Considering cancelations, note that there is one important difference to the one-loop case, where in the sum of o_1 and o_3 the leading IR divergences cancel. Here, after folding with the dual tree-level diagram, the resulting terms b_5 and a_9 do not belong to the same color–class anymore. In fact, the color factors are $C_F C_A^2/2$ and $C_F C_A^2/4$ respectively (cf. eq. (1.21)), leaving IR divergences even in the sum of b_5 and a_9. Another diagram shows an even worse behaviour,

$$\begin{aligned} a_{11} = t_3 \otimes \quad \stackrel{D=3}{=} \quad & \frac{g^6 r^3}{(4\pi)^3} \left[2\frac{T}{r} \ln^2(T/r) + (-6 + 4\ln 2) \frac{T}{r} \ln(T/r) \right. \\ & \left. + \left(7 - \tfrac{\pi^2}{6} - 6\ln(2) + 2\ln^2 2 \right) \frac{T}{r} + \mathcal{O}\left(T^0\right) \right] \, , \end{aligned} \tag{4.25}$$

where

$$\begin{aligned} \quad \stackrel{D=3}{=} \quad & \frac{g^4 r^2}{(4\pi)^2} \left[2\frac{T^2}{r^2} \ln^2(T/r) + (-6 + 4\ln 2) \frac{T^2}{r^2} \ln(T/r) + \left(7 - \tfrac{\pi^2}{6} - 6\ln(2) + 2\ln^2 2 \right) \frac{T^2}{r^2} \right. \\ & \left. + 4\frac{T}{r} \ln(T/r) + (-4 + 4\ln 2) \frac{T}{r} + \mathcal{O}\left(T^0\right) \right] \end{aligned} \tag{4.26}$$

was used.

The surprising result of this analysis is that in D=3, the omission of diagrams containing gluons coupling to the end–pieces of the Wilson–loop is no longer justified, as opposed to the 4D case. It was proven that these new types of diagrams first occur in a two-loop calculation. Whether or not they will solve the IR problem of the two-loop calculation in D=3 remains an open question.

4.4 Discussion

As seen above, the general mechanism for IR cancelations in three dimensions is that the *leading* divergences (which are of power type) are canceled inside the topological classes. This is in accordance with the situation in D=4, where (at one loop) Fischler [6] pointed out that the (leading) IR divergent term of a given diagram, stemming from a gluon coupling to the source at large times, is canceled by a diagram where the same gluon couples to the source of opposite charge, thereby introducing a relative minus sign.

Concerning the cancelation of *sub-leading* divergences, this simple argument cannot be applied. At present, no firm comment can be made on this point, since the coefficients c_{1j} are not yet known analytically. In a numerical analysis, they do not seem to cancel inside the classes.

What has become clear now is that the IR poles in ϵ, as seen in the 3D two-loop calculation in p–space (cf. sect. 3.3.2 and app.C), did not have to cancel inside the topological classes, since they are not the leading divergences. Instead, they correspond to the c_{1j}–terms in the x–space language, which collect the logarithmic divergences. The leading IR divergences found here turned out to be power–like, and hence could not be observed in p–space since they are suppressed by the chosen (dimensional) regularization scheme.

Furthermore, the x–space analysis has lead to the unexpected (but, considering the IR problems in p–space, most welcome) conclusion that in D=3, there is a new class of diagrams. While for D=4, it was shown here that the vertical pieces of the Wilson–loop do not contribute to the potential up to two loops, we have discussed some new diagrams that include gluon–exchange with the vertical pieces and survive the limit of large T in D=3. It was shown that on the two-loop level, these new structures contribute to the IR sector as well as to the finite part of the potential, and hence cannot be omitted in a three–dimensional calculation.

Chapter 5

Further Results for the Static $V_{\rm pert}$

This chapter is organized in two separate parts. In the first section, we discuss problems arising in higher orders of the four–dimensional (4D) perturbative static singlet potential. The material presented is entirely based on the literature, and we will give the main arguments only. The second section documents work we have done on the one-loop potential in a massive theory, the SU(N) Higgs model. The results are used for a proof of infrared finiteness of the QCD potential in dimensions $D \geq 2$. After completion of this work, an interesting application of the full SU(N) Higgs potential has appeared [44], where in the context of finite temperature dimensional reduction the static potential is used for a matching of the renormalized gauge coupling in the broken phase.

5.1 Logarithms of the Coupling in Higher Orders

The Wilson–loop definition of the static potential suffers from IR divergences when computed at finite orders of perturbation theory, i.e. in a power series in the strong–coupling constant α_s. In a 4D analysis, this was first shown by Appelquist, Dine and Muzinich (ADM) [7]. The leading IR singularities of the static Wilson–loop were found at a relative order α_s^3, corresponding to three-loop contributions to the potential. It was argued that these singularities can be regulated by resumming a certain class of diagrams, giving rise to terms logarithmic in the coupling and leading to a breakdown of the power–series expansion at three-loop order. Thus, the problem was posed of whether the static potential could be defined in some way at any order in perturbation theory. This problem was attacked very recently in [11]. Before describing the redefinition proposed in [11], let us illustrate the main argument for the occurrence of the above–mentioned divergences.

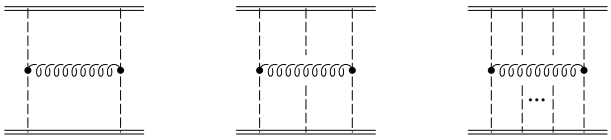

Figure 5.1: *Series of infrared divergent diagrams that need to be resummed. Dashed lines denote Coulomb exchange.*

5.1.1 The Main Argument

In this section, we will give the main argument of ref. [7] for the breakdown of the naive perturbative expansion. Working in Coulomb gauge, the gluon propagator splits into instantaneous and transverse parts, $D_{00} \sim 1/\boldsymbol{k}^2$ and $D_{ij} \sim (\delta_{ij} - k_i k_j/\boldsymbol{k}^2)/k^2$. The FP–ghosts couple to the transverse gluons only, so they do not play a role in the discussion of this section. Consider now the first diagram of fig. 5.1, the so–called H–diagram. Working in coordinate space, simple dimensional considerations suggest that, after the two spatial integrations coming from the internal vertices have been performed, it is proportional to

$$\text{diag.(1)} \quad \propto \quad \int_{-T/2}^{T/2} \mathrm{d}t_1 \int_{-T/2}^{T/2} \mathrm{d}t_2 \, \frac{\alpha_s^3 C_F C_A^2}{(t_2 - t_1)^2 + r^2} \; , \tag{5.1}$$

where $(T \times r)$ is the dimension of the rectangular Wilson–loop, as usual. For this single diagram, the leading term for large T (i.e. $T \gg r$, to be exact) is easily obtained, and the result is proportional to $\alpha_s^3 \, T/r$, hence contributing as $\alpha_s^3 \, T/r$ to the potential.

Next, consider a single additional Coulomb gluon to be exchanged, as shown in the second diagram of fig. 5.1. Using eq. (D.16) and remembering that the three–gluon–vertex is totally antisymmetric, one can convince oneself that the non–abelian part of the new contribution gives an additional factor of $-C_A/2 \cdot \alpha_s(t_2 - t_1)/r$ in the above integral. The leading term then has the form

$$\text{diag.(2)} \quad \propto \quad \alpha_s^4 \, \frac{T \ln(T)}{r} + \mathcal{O}(T \ln^0 T) \; , \tag{5.2}$$

contributing a divergent term to the potential. This divergence, which originates from the integration region of large relative time component $(t_2 - t_1) \propto T$, but finite spatial coordinates $|\boldsymbol{x}| < r$, signals the breakdown of the perturbative expansion for the potential. However, since the divergence is only logarithmic, it can be dealt with by a selective resummation.

Summing over any number of internal Coulomb gluons, an exponential builds up as an additional factor inside the integral (5.1). One obtains

$$\text{diag.(3)} \quad \propto \quad \int_{-T/2}^{T/2} \mathrm{d}t_1 \int_{-T/2}^{T/2} \mathrm{d}t_2 \, \exp\left(-\frac{C_A}{2} \, \frac{\alpha_s}{r} \, (t_2 - t_1) \right) \, \frac{\alpha_s^3 C_F C_A^2}{(t_2 - t_1)^2 + r^2}$$

$$
\begin{aligned}
&= T\int_0^T \mathrm{d}t\,\left(1-\frac{t}{T}\right)\exp\left(-\frac{C_A}{2}\,\frac{\alpha_s}{r}\,t\right)\,\frac{\alpha_s^3 C_F C_A^2}{t^2+r^2}\\
&= \alpha_s^3 C_F C_A^2\,\frac{T}{r}\int_0^{T/r}\mathrm{d}y\,\left(1-\frac{r}{T}\,y\right)\,\frac{\exp(-ay)}{1+y^2}\,, \qquad (5.3)
\end{aligned}
$$

where $a=\frac{C_A}{2}\,\alpha_s$. While the second term is suppressed at large T, the first one can be evaluated taking the upper integration limit to infinity. Using $\int_0^\infty \mathrm{d}y\,\exp(-ay)/(1+y^2)=\ln(a)\sin(a)+g(a)$, where the function g(a) is analytic at $a=0$, the large–T result is

$$
\begin{aligned}
\text{diag.(3)} &\sim \alpha_s^3 C_F C_A^2\,\frac{T}{r}(\ln(a)\sin(a)+g(a))\\
&= \alpha_s^3 C_F C_A^2\,\frac{T}{r}\left(\frac{\pi}{2}+\frac{C_A}{2}\,\alpha_s\ln\left(\alpha_s\right)+\mathcal{O}(\alpha_s\ln^0\alpha_s)\right)\,. \qquad (5.4)
\end{aligned}
$$

The first term simply reproduces the well-behaved contribution of diagram (1), while the following term, being proportional to $\alpha_s^4\ln\alpha_s$, spoils the naive perturbative series. In ref. [7] it is conjectured, though, that the static potential can in principle be computed at small α_s even beyond the two-loop level, if the expansion is organized in a double series of the form $\alpha_s^n\ln^m\alpha_s$ with $m<n$.

5.1.2 A Novel Definition

Led by the fact that the IR divergences originate from massless gluons that are allowed to self-interact at arbitrarily small energy scales, and noting that the potential can be defined rigorously as a matching coefficient in an effective field theory approach, the authors of ref. [11] resolve the problem described above. Keeping the mass of the $q\bar{q}$ pair large but finite, they construct a series of effective theories, exploiting the scale hierarchy $m\gg mv\gg\Lambda_{\mathrm{QCD}}$, where m and v are the heavy–quark mass and velocity, respectively. The procedure is well–known. Starting with QCD and integrating out the hard scale first, one arrives at non–relativistic QCD (NRQCD) [45]. Next, integrating out the soft degrees of freedom defines what they call potential NRQCD (pNRQCD) [46], leaving only ultrasoft degrees of freedom with energies much smaller than mv.

It turns out that the definition of the static potential as a matching coefficient in pNRQCD does not coincide with the Wilson–loop definition, since the latter does not exclude ultrasoft contributions. The matching of pNRQCD and NRQCD has to be performed at a scale μ that lies in between the soft and ultrasoft scales, and since $\mu>\Lambda_{\mathrm{QCD}}$, it can be done perturbatively. As a result of this matching, a correction term to the Wilson–loop definition emerges. As given in ref. [11], this additional term depends on the dynamical scale generated by the difference of octet and singlet potential, which to leading order equals $[V_o(r)-V_s(r)]=\frac{C_A}{2}\,\frac{\alpha_s}{r}$, and exactly cancels the $\alpha_s^4\ln\alpha_s$–term (5.4) arising from the Wilson–loop. For more details, we refer to the original paper [11].

The long–standing issue of how to define the perturbative potential in higher orders seems to clarified. Let us remark, however, that the proposed redefinition does not play a role below the three-loop level, hence justifying the Wilson–loop definition in lower orders and, in particular, leaving the two-loop results presented in this work valid.

5.2 One-Loop Potential in a Massive Model

As an example for the calculation of the static potential in a massive theory, let us choose the SU(N) Higgs model. While staying close to the notation of ref. [47], where the SU(2) model was examined, we present and discuss our generalized lagrangian in appendix D. Shifting the Higgs field around its non–trivial vacuum expectation value, all fields acquire a mass term, allowing for a manifestly infrared finite calculation.

In the massless limit, and omitting all diagrams containing scalar particles, the QCD potential (with $n_f = 0$) can be rederived. The new feature in such a procedure is the separate treatment of UV– and IR–singularities, the former showing up as poles in the ϵ–parameter of dimensional regularization, and the latter giving rise to divergent terms in the massless limit only. Calculating the full SU(N) Higgs potential seems to be superfluous at first sight, but since the number of additional diagrams to be calculated is small, adding them to the QCD–like ones provides important checks (gauge independence!).

All Feynman rules for the model are collected in appendix D. The calculation can be done using the same strategy as for the massless case treated in the rest of this work, i.e. by first removing all numerators using the T–operators, then using a set of recurrence relations to reduce the scalar integrals to a basic set, next solving the basic integrals, and finally expanding them in the dimension of interest and identifying the renormalization constants. While the T–operators are universal in the sense that they work for massless as well as massive propagators, the recurrence relations need to be modified compared to the massless case. For the one-loop case, we have again found a complete set, which is displayed in appendix A.2.

At the one-loop level, the additional scalars only come in as new contributions to the one-loop self-energy, see fig. 5.2. Let us come to the results in terms of basic integrals immediately. Summing up all one-loop diagrams, fig. 1.3 and fig. 5.2, the gauge independent result reads

$$\begin{aligned} V(\boldsymbol{q}^2) \;=\; & -\frac{g^4 C_F}{(\boldsymbol{q}^2+m_W^2)^2}\,\frac{1}{D-1}\left\{\left[(2C_A-4C_F)\left(\frac{\boldsymbol{q}^2-m_W^2+m_H^2}{4\boldsymbol{q}^2}+C_F C_A\frac{(D-1)^2 m_W^2}{m_H^2}\right)\right.\right. \\ & \left.\left.+\,C_A\frac{4m_W^2(-21+25D-7D^2)-\boldsymbol{q}^2(39-52D+16D^2)}{4(\boldsymbol{q}^2+4m_W^2)}\right]A\left(m_W^2\right)\right. \\ & \left.+\,(2C_A-4C_F)\frac{m_W^2-m_H^2+(2D-1)\boldsymbol{q}^2}{4\boldsymbol{q}^2}\,A\left(m_H^2\right)\right. \end{aligned}$$

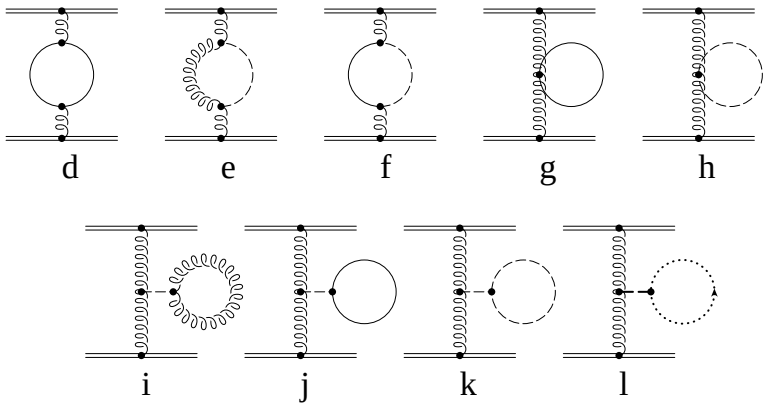

Figure 5.2: *Additional one-loop vector self-energy diagrams for the SU(N) Higgs model. Solid and dashed lines denote Goldstone and Higgs bosons, respectively.*

$$+ C_A \left(\frac{12m_W^2(3-2D) + 3\boldsymbol{q}^2(4D-3)}{8} + \frac{2(\boldsymbol{q}^2+m_W^2)^2(D-1)(D-3)}{\boldsymbol{q}^2+4m_W^2} \right) B\left(m_W^2, m_W^2\right)$$
$$+ (2C_A - 4C_F) \frac{-m_W^4+2m_W^2((2D-3)\boldsymbol{q}^2+m_H^2)-(\boldsymbol{q}^2+m_H^2)^2}{4\boldsymbol{q}^2} B\left(m_W^2, m_H^2\right) \Bigg\} \quad (5.5)$$

For the above–mentioned massless limit, we need results on the level of individual diagrams. Omitting an overall factor of

$$-\frac{g^4 C_F}{(\boldsymbol{q}^2+m_W^2)^2} \frac{C_A}{D-1}\,, \quad (5.6)$$

the contributions of the three diagrams involving source propagators are

$$\begin{aligned}
(A) \;=\; & \frac{(\boldsymbol{q}^2+m_W^2)^2}{4m_W^2} \left\{ \frac{4m_W^2(1-\eta)+\boldsymbol{q}^2(9+4D(D-3)-\eta)}{\boldsymbol{q}^2(\boldsymbol{q}^2+4m_W^2)} A\left(m_W^2\right) \right. \\
& + \frac{\eta-1}{\boldsymbol{q}^2} A\left(\eta m_W^2\right) + \frac{16m_W^4 D(D-2)+8m_W^2\boldsymbol{q}^2(D-2)-\boldsymbol{q}^4}{2m_W^2(\boldsymbol{q}^2+4m_W^2)} B\left(m_W^2, m_W^2\right) \\
& + \frac{m_W^4(\eta-1)^2-2m_W^2\boldsymbol{q}^2(2D-3-\eta)+\boldsymbol{q}^4}{\boldsymbol{q}^2 m_W^2} B\left(m_W^2, \eta m_W^2\right) \\
& \left. + \frac{-\boldsymbol{q}^2-4\eta m_W^2}{2m_W^2} B\left(\eta m_W^2, \eta m_W^2\right) \right\} \quad (5.7)
\end{aligned}$$

$$(B) \;=\; \frac{(D-1)(\boldsymbol{q}^2+m_W^2)}{m_W^2} \left\{ (1-D) A\left(m_W^2\right) + A\left(\eta m_W^2\right) \right\} \quad (5.8)$$

$$\begin{aligned}
(C) \;=\; & \frac{\boldsymbol{q}^2+m_W^2}{2m_W^2} \left\{ \frac{(\eta-1)m_W^2+\boldsymbol{q}^2(4D-6+\eta)}{\boldsymbol{q}^2} \left[A\left(m_W^2\right) - A\left(\eta m_W^2\right) \right] \right. \\
& + \frac{8m_W^4(2-D)+2m_W^2\boldsymbol{q}^2(7-4D)+\boldsymbol{q}^4}{2m_W^2} B\left(m_W^2, m_W^2\right) \\
& \left. + \frac{(\boldsymbol{q}^2+m_W^2)\left(-(\eta-1)^2 m_W^4+2m_W^2\boldsymbol{q}^2(2D-3-\eta)-\boldsymbol{q}^4\right)}{\boldsymbol{q}^2 m_W^2} B\left(m_W^2, \eta m_W^2\right) \right\}
\end{aligned}$$

$$+\frac{\boldsymbol{q}^2(\boldsymbol{q}^2+4\eta m_W^2)}{2m_W^2}\,B\left(\eta m_W^2,\eta m_W^2\right)\Bigg\} \tag{5.9}$$

Now, let us analyze the limit $m_W \to 0$ of the above expressions, which corresponds to the IR behaviour of the massless calculation. Although individual diagrams are singular in this limit,

$$(A),(B) \;\sim\; (D-2)\frac{A(m_W^2\to 0)}{m_W^2}+B(0,0)\;, \tag{5.10}$$

their sum is better–behaved,

$$\begin{aligned}(A)+(B)+(C) \;\stackrel{m_W^2\to 0}{\longrightarrow}\; & -\frac{g^4C_F}{\boldsymbol{q}^4}\,\frac{C_A}{D-1}\Bigg\{-3(D-1)(D-2)A(0)\\ & +\frac{\boldsymbol{q}^2}{4}(27-32D+8D^2-2\eta-\eta^2)B(0,0)\Bigg\}\;.\end{aligned} \tag{5.11}$$

The power divergences $\propto 1/m_W^2$ cancel between diagrams A and B.

The remaining diagrams contributing to the one-loop potential are of self-energy type. Owing to the transversality of q and v, only the transverse part of the self-energy tensor contributes,

$$(D) = -\frac{g^2C_F}{(\boldsymbol{q}^2+m_W^2)^2}\,\Pi_T(\boldsymbol{q}^2)\;. \tag{5.12}$$

The function Π_T, expressed in terms of basic integrals, is listed below for completeness.

$$\Pi_T(\boldsymbol{q}^2) = \Pi_T^{a..c}(\boldsymbol{q}^2)+\Pi_T^{d}(\boldsymbol{q}^2)+\Pi_T^{e,f}(\boldsymbol{q}^2)+\Pi_T^{g,j}(\boldsymbol{q}^2)+\Pi_T^{i,l}(\boldsymbol{q}^2)+\Pi_T^{h}(\boldsymbol{q}^2)+\Pi_T^{k}(\boldsymbol{q}^2) \tag{5.13}$$

$$\begin{aligned}\Pi_T^{a..c}(\boldsymbol{q}^2) = & \frac{g^2C_A}{D-1}\Bigg\{\frac{\boldsymbol{q}^4(7-4D-\eta)-\boldsymbol{q}^2m_W^2(7-12D+4D^2+2\eta)-m_W^4(\eta-1)}{4\boldsymbol{q}^2m_W^2}\,A\left(m_W^2\right)\\ & +\frac{\boldsymbol{q}^4(4D-7+\eta)+\boldsymbol{q}^2m_W^2(4D-9+2\eta)+m_W^4(\eta-1)}{4\boldsymbol{q}^2m_W^2}\,A\left(\eta m_W^2\right)\\ & +\frac{(\boldsymbol{q}^2+4m_W^2)(-\boldsymbol{q}^4+4\boldsymbol{q}^2m_W^2(2D-3)-4m_W^4(D-1))}{8m_W^4}\,B\left(m_W^2,m_W^2\right)\\ & +\frac{(\boldsymbol{q}^2+m_W^2)^2(\boldsymbol{q}^4-2\boldsymbol{q}^2m_W^2(2D-3-\eta)+m_W^4(\eta-1)^2)}{4\boldsymbol{q}^2m_W^4}\,B\left(m_W^2,\eta m_W^2\right)\\ & +\frac{(2m_W^4-\boldsymbol{q}^4)(\boldsymbol{q}^2+4\eta m_W^2)}{8m_W^4}\,B\left(\eta m_W^2,\eta m_W^2\right)\Bigg\}\end{aligned} \tag{5.14}$$

$$\Pi_T^{d}(\boldsymbol{q}^2) = \frac{g^2C_A}{D-1}\left\{\frac{1}{4}\,A\left(\eta m_W^2\right)+\frac{-\boldsymbol{q}^2-4\eta m_W^2}{8}\,B\left(\eta m_W^2,\eta m_W^2\right)\right\} \tag{5.15}$$

$$\begin{aligned}\Pi_T^{e,f}(\boldsymbol{q}^2) = & \frac{g^2(2C_A-4C_F)}{D-1}\Bigg\{\frac{\boldsymbol{q}^2-m_W^2+m_H^2}{4\boldsymbol{q}^2}\,A\left(m_W^2\right)+\frac{\boldsymbol{q}^2+m_W^2-m_H^2}{4\boldsymbol{q}^2}\,A\left(m_H^2\right)\\ & +\frac{-\boldsymbol{q}^4+2\boldsymbol{q}^2((2D-3)m_W^2-m_H^2)-(m_W^2-m_H^2)^2}{4\boldsymbol{q}^2}\,B\left(m_W^2,m_H^2\right)\Bigg\}\end{aligned} \tag{5.16}$$

$$\Pi_T^{g,j}(\boldsymbol{q}^2) = 0 \tag{5.17}$$

$$\Pi_T^{i,l}(\boldsymbol{q}^2) = \frac{g^2 C_F C_A (2C_A - 4C_F)}{D-1} \left\{ \frac{(D-1)^2 m_W^2}{m_H^2} A\left(m_W^2\right) \right\} \tag{5.18}$$

$$\Pi_T^{h}(\boldsymbol{q}^2) = \frac{g^2 (2C_A - 4C_F)}{D-1} \left\{ -\frac{D-1}{4} A\left(m_H^2\right) \right\} \tag{5.19}$$

$$\Pi_T^{k}(\boldsymbol{q}^2) = \frac{g^2 (2C_A - 4C_F)}{D-1} \left\{ \frac{3(D-1)}{4} A\left(m_H^2\right) \right\} \tag{5.20}$$

Note that this is not an entirely new result. Compare, for example, ref. [47] (where Π_T was given for N=2, D=3) and ref. [44] (diagrams for the potential, for N=2). Whenever possible, gauge independent subgroups of diagrams were presented in the above.

For $\Pi_T^{a..c}$, the part collecting the Yang–Mills type diagrams, the limit $m_W \to 0$ gives

$$\Pi_T^{a..c} \overset{m_W^2 \to 0}{\longrightarrow} \frac{g^2 C_A}{D-1} \left\{ -(D-2)^2 A(0) + \frac{\boldsymbol{q}^2}{4} (6D - 7 + 2\eta + \eta^2) B(0,0) \right\} . \tag{5.21}$$

Combining with the above result for the source–type diagrams, eq. (5.11), we get

$$V^{YM} = -\frac{g^4 C_A C_F}{\boldsymbol{q}^2} \frac{(4D-5)(D-2)}{2(D-1)} \left\{ -\frac{2}{\boldsymbol{q}^2} A(0) + B(0,0) \right\} \tag{5.22}$$

for the one-loop static potential in pure Yang–Mills theory. The special combination of basic integrals occurring in the above curly brackets is perfectly IR finite for all D, as can be seen in a regularization–scheme independent way by performing the k_0–integration first:

$$\begin{aligned} \mu^\epsilon \int \frac{d^D k}{(2\pi)^D} \left\{ -\frac{2}{\boldsymbol{q}^2} \frac{1}{k^2} + \frac{1}{k^2} \frac{1}{(k-q)^2} \right\} &= \mu^\epsilon \int \frac{d^{D-1}\boldsymbol{k}}{(2\pi)^{D-1}} \left\{ -\frac{2}{\boldsymbol{q}^2} \frac{1}{2|\boldsymbol{k}|} + \frac{1}{|\boldsymbol{k}|(\boldsymbol{q}^2 + 4\boldsymbol{k}^2)} \right\} \\ &= -\frac{4}{\boldsymbol{q}^2} \mu^\epsilon \int \frac{d^{D-1}\boldsymbol{k}}{(2\pi)^{D-1}} \frac{|\boldsymbol{k}|}{\boldsymbol{q}^2 + 4\boldsymbol{k}^2} \\ &= -2\mu^\epsilon \frac{(\boldsymbol{q}^2)^{\frac{D-4}{2}}}{(16\pi)^{\frac{D-1}{2}}} \frac{\Gamma\left(\frac{D}{2}\right) \Gamma\left(\frac{2-D}{2}\right)}{\Gamma\left(\frac{D-1}{2}\right)} . \end{aligned} \tag{5.23}$$

In the last line, to obtain the result, dimensional regularization was chosen. It coincides with eq. (B.3) (setting $b = 4\pi^2$ there), of course, since $A(0) = 0$ in dimensional regularization. Ultraviolet divergences in the potential (5.22), arising for $D \geq 4$ only, are canceled by the counterterms.

To complete the collection of massive one-loop results, let us give the fermionic contribution

$$\Pi_T^{\mathrm{fer}} = \sum_{i=1}^{n_f} \Pi_T^{\mathrm{fer}}(\boldsymbol{q}^2, m_i^2) \tag{5.24}$$

$$\Pi_T^{\mathrm{fer}}(\boldsymbol{q}^2, m_i^2) = \frac{g^2 T_f}{D-1} \left\{ 4(D-2)\, A(m_i^2) - 2(D-2)(\boldsymbol{q}^2 + 4m_i^2)\, B(m_i^2, m_i^2) \right\} \tag{5.25}$$

In the limit where all quark masses be negligible (i.e. $m_i^2 \ll \boldsymbol{q}^2$), the familiar IR–finite combination of massless integrals occurs again. Adding the gluonic part V^{YM}, as given in eq. (5.22),

the one-loop result for the static QCD potential, eq. (3.38), is rederived as

$$V^{QCD} = -\frac{g^4 C_F}{\boldsymbol{q}^2} \frac{D-2}{2(D-1)} \left[(4D-5)C_A - 4T_f n_f \right] \left\{ -\frac{2}{\boldsymbol{q}^2} A(0) + B(0,0) \right\} . \qquad (5.26)$$

The special combination of massless basic integrals A and B is manifestly infrared finite, as demonstrated above.

Conclusions

We have analyzed in detail the perturbative static potential in QCD, defined by the Wilson–loop formula. A full two-loop calculation of the class of contributing exchange diagrams has been performed. Working in the linear covariant gauge, and keeping the gauge–parameter arbitrary throughout the calculation, we have shown analytically that this class of diagrams forms a gauge–independent set.

To perform the necessary analytic reduction of the individual diagrams, we have derived an algorithm that is suited to cope with the special type of integrals occurring in the calculation, namely massless two–point functions involving boson–type as well as static (non–covariant) propagators, hence depending on two orthogonal momenta. The reduction method is kept very general, and is shown to be complete in the sense that neither limitations concerning the possible tensor structures in the numerators nor restrictions on the maximal powers of individual propagators are present. Hence, it could be well used to treat the two-loop subgraphs occurring in higher–order calculations of the potential. This new calculation method has enabled us to present, for the first time, analytical results for the two-loop coefficients in the static potential in arbitrary dimensions.

Specializing to four dimensions, we have presented results on the potential in momentum as well as in coordinate space. The two-loop coefficient a_2 that we have obtained [35] gives an important check on results presented before by other groups. Finding a (numerically) quite substantial discrepancy, we have compared the two approaches and agreed with the author of the original calculation on the origin of this difference, which has turned out to be due to the omission of specific contributions in his work. Furthermore, it has been shown that the bad convergence of the perturbative series does not improve considerably taking into account the new value of a_2. Hence, the use of a physical coupling, defined by the potential, as expansion parameter seems to be disfavored. Further studies are clearly needed to clarify the role of higher–order corrections, which have been shown to be potentially infrared divergent.

In three dimensions, the static potential exhibits a linear term in coordinate space. The size of this term has been compared with existing lattice calculations in pure $\mathrm{SU}(\mathrm{N}_c)$ gauge theory, and has been found be of the same order of magnitude, while showing the correct

N_c dependence. Considering the two-loop coefficient resulting from the exchange diagrams, we have demonstrated that the result (although being gauge independent) is infrared divergent. In a subsequent analysis directly in coordinate space, non–exchange type diagrams have been shown to contribute to the Wilson–loop defined potential in three dimensions, while they vanish for the four–dimensional case, as we have shown explicitly on the two-loop level.

Finally, since we have demonstrated that the mechanism which controls infrared cancelations in the two–dimensional one-loop potential is in operation for the corresponding three–dimensional two-loop subclass of diagrams also, one might hope that a further examination of these infrared problems in three dimension may yield interesting results for the more complicated four–dimensional case also.

Appendix A

One-Loop Reduction Formulae

In the one-loop case, it is possible to achieve a complete reduction even for integrals involving static as well as massive boson–type propagators. The necessary relations will be presented in this appendix.

A.1 One-Loop T–Operators

Here, the one-loop T–operators are documented for completeness. The notation used, as well as the derivation, is analogous to the two-loop case, cf. sections 2.1.3 and 2.1.4.

The one-loop tensor T–operator reads:

$$\begin{aligned}\int_1 \frac{(k_1)_{\mu_1}...(k_1)_{\mu_\tau}}{c_1^{\nu_1} c_3^{\nu_3} c_6^{\nu_6}} &= \partial_{a_{1,\mu_1}}...\partial_{a_{1,\mu_\tau}} \int_1 \frac{\exp\{(a_1 k_1)\}}{c_1^{\nu_1} c_3^{\nu_3} c_6^{\nu_6}}\Big|_{a_1=0} \\ &= T^{\text{1-loop}}_{\mu_1..\mu_\tau}(\mathbf{J}^+, \mathbf{D}^+) \int_1 \frac{1}{c_1^{\nu_1} c_3^{\nu_3} c_6^{\nu_6}} \end{aligned} \tag{A.1}$$

$$T^{\text{1-loop}}_{\mu_1...\mu_\tau} = \partial_{a_{1,\mu_1}}...\partial_{a_{1,\mu_\tau}} \exp\left\{\frac{b\mathbf{D}^+}{\pi}\left[(a_1 q)\alpha_3 + (a_1 v)(-\frac{1}{2}\alpha_6) + a_1^2 \frac{1}{4}\right]\right\}\Big|_{\substack{a_1=0 \\ \alpha_j=\nu_j \mathbf{J}^+}} \tag{A.2}$$

The one-loop scalar T–operators are:

$$\begin{aligned}\int_1 \frac{(k_1 q)^r (k_1 v)^t}{c_1^{\nu_1} c_3^{\nu_3} c_6^{\nu_6}} &= q_{\mu_1}..q_{\mu_r} v_{\mu_{r+1}}..v_{\mu_{r+t}}\, T^{\text{1-loop}}_{\mu_1...\mu_{r+t}}(\mathbf{J}^+, \mathbf{D}^+) \int_1 \frac{1}{c_1^{\nu_1} c_3^{\nu_3} c_6^{\nu_6}} \\ &= T_r(\mathbf{J}^+, \mathbf{D}^+)\, \widetilde{T}_t(\mathbf{J}^+, \mathbf{D}^+) \int_1 \frac{1}{c_1^{\nu_1} c_3^{\nu_3} c_6^{\nu_6}} \end{aligned} \tag{A.3}$$

$$T_r = \partial_x^r \exp\left\{\frac{b\mathbf{D}^+}{\pi} q^2 \left[\frac{1}{4}x^2 + x\alpha_3\right]\right\}\Big|_{\substack{x=0 \\ \alpha_3=\nu_3 \mathbf{3}^+}} \tag{A.4}$$

$$\widetilde{T}_t = \partial_y^t \exp\left\{\frac{b\mathbf{D}^+}{\pi} v^2 \left[\frac{1}{4}y^2 - \frac{1}{2}y\alpha_6\right]\right\}\Big|_{\substack{y=0 \\ \alpha_6=\nu_6 \mathbf{6}^+}} \tag{A.5}$$

As explained in the two-loop case, these T–operators are valid for massless as well as massive integrals.

A.2 Massive One-Loop Relations

For the case of massive propagators, as e.g. used in section 5.2, the reduction formulae given in chapter 2 have to be modified as follows. Replacing the relations of eq. (2.6), the numerators of massive scalar integrals can be simplified according to

$$k_1^2 D_1 = 1 - m_1^2 D_1 \,, \tag{A.6}$$

$$k_1^2 D_3 = 1 + (2k_1 q - q^2 - m_3^2) D_3 \,, \tag{A.7}$$

$$2k_1 q D_1 D_3 = D_3 - D_1 + (q^2 - m_1^2 + m_3^2) D_1 D_3 \,. \tag{A.8}$$

Instead of eqs. (2.41)-(2.47), one can then use the following recurrence relations for massive one-loop propagator integrals:

$$(x-1)[ac,x] = \left\{-2\left(a\mathbf{1}^+ + c\mathbf{3}^+\right)\mathbf{S}_1^{--}\right\}[ac,x] \tag{A.9}$$

$$(a-1)c_1[ac,x] = \left\{c_2\mathbf{1}^- + (a-1)(\boldsymbol{q}^2 + m_1^2 + m_3^2)\mathbf{3}^- - 2cm_3^2\mathbf{3}^+\mathbf{1}^{--}\right\}[ac,x] \tag{A.10}$$

$$2(a-1)m_1^2[a0,x] = \left\{-(D-2a-x+2)\mathbf{1}^-\right\}[a0,x] \tag{A.11}$$

$$c_3\boldsymbol{q}^2\mathbf{D}^+[11,x] = \left\{-c_1 + (\boldsymbol{q}^2 + m_1^2 - m_3^2)\mathbf{1}^- + (\boldsymbol{q}^2 - m_1^2 + m_3^2)\mathbf{3}^-\right\}[11,x] \tag{A.12}$$

$$c_4\mathbf{D}^+[a0,x] = \left\{-2m_1^2\right\}[a0,x] \tag{A.13}$$

with $c_1 = (m_1^2 - m_3^2)^2 + \boldsymbol{q}^2(\boldsymbol{q}^2 + 2m_1^2 + 2m_3^2)$, $c_2 = 2m_3^2(D-2a-c-x+2) - (\boldsymbol{q}^2 + m_1^2 + m_3^2)(D-a-2c-x+1)$, $c_3 = 2(D-x-1)$ and $c_4 = (D-2a-x+2)$. Three more relations are obtained by interchanging $1 \leftrightarrow 3$ (and $a \leftrightarrow c$, of course) in the above. For the case $x = 0$, the last four relations can be checked against the one-loop relations found in section 4.5 of Tarasov's paper [23][1].

[1] Note that Tarasov works with Minkowskian metrics, such that for a comparison one needs to do the replacements $\boldsymbol{q}^2 \to -\boldsymbol{q}^2$ and $\mathbf{1}^- \to -\mathbf{1}^-$ etc.

Appendix B

Basic Integrals

Here, we collect the results for the integral basis that occurs in the calculation of the static potential. We adopt the dimensional regularization scheme and work with Euclidean metrics, diag(1,**1**). Our notation is as follows: We have two types of denominators, $D_i \equiv D(k_i) = \frac{1}{k_i^2}$, stemming from gluon, ghost and fermion propagators, and $S_i \equiv S(k_i) = \frac{1}{v\cdot k_i + i\varepsilon}$, with $v = (1, \mathbf{0})$, stemming from the source propagators. The loop momenta are k_1, k_2, $k_3 = k_1 - q$, $k_4 = k_2 - q$, $k_5 = k_1 - k_2$, where $q = (0, \boldsymbol{q})$ is the external momentum. We abbreviate the D–dimensional integration measure as $\int_i \equiv \mu^\epsilon \int \frac{d^D k_i}{\sqrt{i}^D}$, while products of propagators will be written like $D_1 D_2 \equiv D_{12}$. The integrals have been calculated by introducing Feynman parameters for bosonic propagators in the usual way,

$$\frac{1}{x^n y^m} = \frac{\Gamma(n+m)}{\Gamma(n)\Gamma(m)} \int_0^1 \mathrm{d}z \, \frac{z^{n-1} z^{m-1}}{[zx + (1-z)y]^{m+n}} \,, \tag{B.1}$$

and by rewriting source propagators in the more suitable representation

$$\frac{1}{x^n y^m} = \frac{\Gamma(n+m)}{\Gamma(n)\Gamma(m)} \int_0^\infty \mathrm{d}z \, \frac{z^{m-1}}{[x + zy]^{m+n}} \,. \tag{B.2}$$

In the first two sections, we will list the one-loop– and two-loop basic integrals. Since all integrals are massless two-point functions, there exist analytical results in terms of Gamma functions. The last section collects the massive two-point integrals needed for the discussion of infrared divergences.

B.1 One-Loop Basis

The basic set of massless scalar one-loop two–point integrals consists of two members only. This is due to the well–known fact that massless tadpole integrals vanish in dimensional regulariza-

tion.

$\left(\frac{1}{|\boldsymbol{q}|}\right)$ $= \frac{1}{|\boldsymbol{q}|}\int_1 D_{13} = \frac{8(1-D)}{(2-D)(4-D)}\,\frac{\Gamma(\frac{6-D}{2})\Gamma(\frac{D}{2})^2}{\Gamma(D)}\,G_D$ (B.3)

 $= \int_1 D_{13}S_1 = i\sqrt{\pi}\,\frac{16(2-D)}{(1-D)(3-D)}\,\frac{\Gamma(\frac{1+D}{2})^2\Gamma(\frac{5-D}{2})}{\Gamma(D)}\,G_D$ (B.4)

$$G_D = \frac{1}{|\boldsymbol{q}|^5}\mu^\epsilon \left(\frac{\pi \boldsymbol{q}^2}{b}\right)^{\frac{D}{2}} \tag{B.5}$$

Even though the integral (B.4) does not occur in the one-loop part, it is listed here because it will be needed for the one-loop–iteration part of the two-loop calculation. Integrating out the zero–component of eq. (B.4) first, one gets the nice relation

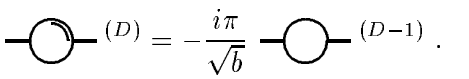 $= -\frac{i\pi}{\sqrt{b}}$. (B.6)

The expansions in four and three dimensions read (with the Euler number $\gamma = 0.5772..$)

	$D = 4-\epsilon$	$D = 3-\epsilon$
$\left(\frac{1}{\lvert\boldsymbol{q}\rvert}\right)$ 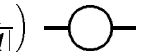	$\left(\frac{2}{\epsilon} + 2 + \left(2 - \frac{\pi^2}{24}\right)\epsilon + O(\epsilon^2)\right)\widetilde{G}$	$\left(\pi + O(\epsilon)\right)\sqrt{\pi}\,\widetilde{G}$
	$\left(-\pi^2 + O(\epsilon)\right) i\,\widetilde{G}$	$\left(\frac{4}{\epsilon} - \frac{\pi^2}{12}\epsilon + O(\epsilon^2)\right) i\sqrt{\pi}\,\widetilde{G}$
$\widetilde{G} = e^{-\frac{\gamma\epsilon}{2}}\,G_D$	$\frac{1}{\lvert\boldsymbol{q}\rvert}\left(\frac{\pi}{b}\right)^2\left(\frac{b\mu^2}{\pi e^\gamma \boldsymbol{q}^2}\right)^{\frac{\epsilon}{2}}$	$\frac{1}{\boldsymbol{q}^2}\left(\frac{\pi}{b}\right)^{\frac{3}{2}}\left(\frac{b\mu^2}{\pi e^\gamma \boldsymbol{q}^2}\right)^{\frac{\epsilon}{2}}$

(B.7)

B.2 Two-Loop Basis

As detailed in chapter 2, the complete set of basic scalar integrals for massless two-loop two–point functions involving boson–type as well as static propagators contains the following members (compare the chart on page 19):

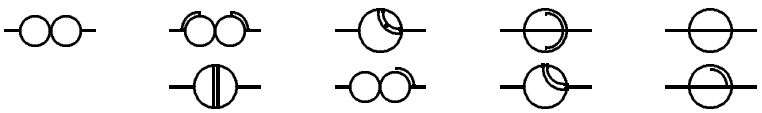 (B.8)

 (B.9)

Note that all integrals displayed in the first line have an even dimension, while those in the second line are odd-dimensional. For the calculation of V_{static} only the first line of integrals is

needed, while the second line will contribute to higher–order calculations only. This 'decoupling' can be best understood by a simple dimensional argument: Due to the orthogonality of q and v, the only dimensional parameter that can occur in the prefactors of the integrals is q^2. Hence, even– and odd–dimensional basic integrals can never 'mix' and contribute to the same quantity.

The analytic results, given for generic dimensions D, read

$\left(\frac{1}{q^2}\right)$ 

$$\equiv D_q \int_1 \int_2 D_{1234}$$

$$= \frac{64(D-1)^2}{(D-2)^2(D-4)^2} \frac{\Gamma(\frac{6-D}{2})^2\Gamma(\frac{D}{2})^4}{\Gamma(D)^2} {G_D}^2 \qquad \text{(B.10)}$$

$\left(\frac{1}{q^2}\right)^2$

$$\equiv D_q^2 \int_1 \int_2 D_{235}$$

$$= \frac{12}{(D-2)^2(D-3)(D-4)} \frac{\Gamma(5-D)\Gamma(\frac{D}{2})^3}{\Gamma(\frac{3D-4}{2})} {G_D}^2 \qquad \text{(B.11)}$$

$\left(\frac{1}{q^2}\right)$ 

$$\equiv D_q \int_1 \int_2 D_{123} S_{55}$$

$$= \frac{64(2D-1)(2D-3)(2D-5)}{(1-D)(D-2)^2(D-3)(D-4)^2} \frac{\Gamma(5-D)\Gamma(\frac{6-D}{2})\Gamma(D)^2\Gamma(\frac{D}{2})}{\Gamma(2D)} G_D^2 \qquad \text{(B.12)}$$

$\left(\frac{1}{q^2}\right)$ 

$$\equiv D_q \int_1 \int_2 D_{235} S_{12}$$

$$= 48\pi^2 \frac{(3D-1)(3D-5)(3D-7)}{(D-1)^2(D-3)^2(D-4)} \frac{\Gamma(5-D)\Gamma(D)^3\Gamma(\frac{3D}{2})}{\Gamma(\frac{D}{2})^3\Gamma(3D)} {G_D}^2 \qquad \text{(B.13)}$$

$$\equiv \int_1 \int_2 D_{1234} S_{12}$$

$$= -\frac{4^{2-D}\pi^4(D-2)^2}{(D-1)^2(D-3)^2} \frac{\Gamma(5-D)^2\Gamma(D)^2}{\Gamma(\frac{6-D}{2})^2\Gamma(\frac{D}{2})^4} {G_D}^2 \qquad \text{(B.14)}$$

The expansions in four and three dimensions are given by

	$D = 4 - \epsilon$	$D = 3 - \epsilon$
$\left(\frac{1}{q^2}\right)$ 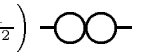	$\left(\frac{4}{\epsilon^2} + \frac{8}{\epsilon} + 12 - \frac{\pi^2}{6} + O(\epsilon)\right) \widetilde{G}^2$	$\left(\pi^2 + O(\epsilon)\right) \pi \widetilde{G}^2$
	$\left(-\pi^4 + O(\epsilon)\right) \widetilde{G}^2$	$\left(-\frac{16}{\epsilon^2} + \frac{2\pi^2}{3} + O(\epsilon)\right) \pi \widetilde{G}^2$
$\left(\frac{1}{q^2}\right)$ 	$\left(-\frac{4}{\epsilon^2} - \frac{8}{\epsilon} - 16 + \frac{\pi^2}{6} + O(\epsilon)\right) \widetilde{G}^2$	$\left(\frac{4}{\epsilon} + O(\epsilon)\right) \pi \widetilde{G}^2$
$\left(\frac{1}{q^2}\right)$ 	$\left(-\frac{4\pi^2}{3\epsilon} - 4\pi^2 + O(\epsilon)\right) \widetilde{G}^2$	$\left(-\frac{8}{\epsilon^2} + \frac{\pi^2}{3} + O(\epsilon)\right) \pi \widetilde{G}^2$
$\left(\frac{1}{q^2}\right)^2$ 	$\left(-\frac{1}{2\epsilon} - \frac{13}{8} + O(\epsilon)\right) \widetilde{G}^2$	$\left(\frac{2}{\epsilon} + 6 + O(\epsilon)\right) \pi \widetilde{G}^2$
$\widetilde{G}^2 = e^{-\gamma\epsilon} {G_D}^2$	$\frac{1}{q^2}\left(\frac{\pi}{b}\right)^4 \left(\frac{b\mu^2}{\pi e^\gamma q^2}\right)^\epsilon$	$\frac{1}{(q^2)^2}\left(\frac{\pi}{b}\right)^3 \left(\frac{b\mu^2}{\pi e^\gamma q^2}\right)^\epsilon$

(B.15)

B.3 Massive Integrals

When the propagators become massive, vacuum integrals no longer vanish in dimensional regularization, such that the set of basic integrals has to be enlarged. The following two massive one-loop integrals are needed:

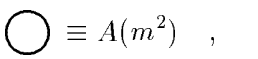

$$\equiv A(m^2) \quad , \quad \equiv B(m_1^2, m_2^2) \ . \tag{B.16}$$

In dimensional regularization, they can be evaluated as

$$A(m^2) = \mu^\epsilon \int \frac{\mathrm{d}^D k}{(2\pi)^D} \frac{1}{k^2+m^2} = \mu^\epsilon \frac{m^{D-2}}{(4\pi)^{\frac{D}{2}}} \Gamma\left(\frac{2-D}{2}\right) \tag{B.17}$$

$$\begin{aligned} B(m_1^2, m_2^2) &= \mu^\epsilon \int \frac{\mathrm{d}^D k}{(2\pi)^D} \frac{1}{k^2+m_1^2} \frac{1}{(k-q)^2+m_2^2} \\ &= \mu^\epsilon \frac{|\boldsymbol{q}|^{D-4}}{(4\pi)^{\frac{D}{2}}} \Gamma\left(\frac{4-D}{2}\right) \int_0^1 \mathrm{d}z \left(z(1-z) + z\frac{m_1^2}{\boldsymbol{q}^2} + (1-z)\frac{m_2^2}{\boldsymbol{q}^2} \right)^{\frac{D-4}{2}} \\ &= \mu^\epsilon \frac{|\boldsymbol{q}|^{D-4}}{(4\pi)^{\frac{D}{2}}} \Gamma\left(\frac{4-D}{2}\right) \times \begin{cases} D=4-\epsilon: \ 1 - \frac{\epsilon}{2} \left[-2 + \frac{m_2^2-m_1^2}{\boldsymbol{q}^2} \ln\left(\frac{m_1}{m_2}\right) + \ln\left(\frac{m_1 m_2}{\boldsymbol{q}^2}\right) \right. \\ \qquad \left. + \frac{\boldsymbol{q}^2+m_1^2+m_2^2}{2\boldsymbol{q}^2} x \ln\left(\frac{1+x}{1-x}\right) \right] + O(\epsilon^2) \\ D=3-\epsilon: \ 2 \arctan\left(\frac{|\boldsymbol{q}|}{m_1+m_2}\right) + O(\epsilon) \\ D=2-\epsilon: \ \frac{\boldsymbol{q}^2}{\boldsymbol{q}^2+m_1^2+m_2^2} \frac{1}{x} \ln\left(\frac{1+x}{1-x}\right) + O(\epsilon) \end{cases} \end{aligned} \tag{B.18}$$

where $x = \sqrt{1-y^2}$ with $y = \frac{2m_1 m_2}{\boldsymbol{q}^2+m_1^2+m_2^2}$.

Correspondingly, the minimal set of static massive two-loop integrals has to be enlarged also. According to ref. [23], it contains the two-loop integrals

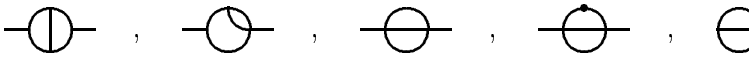

, , , , , (B.19)

as well as products of the above one-loop integrals. Here, every line is understood to represent a massive propagator $1/(k^2+m^2)$, all masses being equal, while a dot on a line means it is squared.

Results for these integrals in $D = 4-\epsilon$ dimensions can be found in ref. [48]. For other cases, which are however not relevant for the discussion of section 3.2.1, see e.g. the overview [49]. While the first integral of the list (B.19) is finite, the others exhibit double and simple poles.

For $D = 3-\epsilon$, results are given in ref. [50]. For the use in section 3.3.2, it suffices to know the pole terms, to which only two of the integrals contribute:

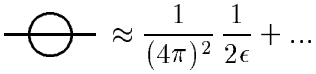

$$\approx \frac{1}{(4\pi)^2} \frac{1}{2\epsilon} + \ldots \quad , \quad \approx \frac{1}{(4\pi)^2} \frac{1}{2\epsilon} + \ldots \ . \tag{B.20}$$

The other six integrals are finite in dimensional regularization.

Appendix C

Infrared Poles in Three Dimensions

Here, the infrared poles of all two-loop non–self-energy diagrams are collected, as needed in section 3.3.2. Expanding the individual diagrams in $D = 3 + \epsilon_{ir}$ and omitting an overall factor of $\frac{C_F C_A g^6}{16\pi \boldsymbol{q}^4} \left(\frac{4\pi\mu^2}{\boldsymbol{q}^2}\right)^{-\epsilon_{ir}}$, they read

$$\text{diag.}(a3) = \frac{(8-8\xi)C_A}{\epsilon_{ir}^2} + \frac{(12-12\xi-2\xi^2)C_A}{-\epsilon_{ir}} + \mathcal{O}(1) \tag{C.1}$$

$$\text{diag.}(a5) = \frac{(4-4\xi)C_A}{\epsilon_{ir}^2} + \frac{(6-6\xi-\xi^2)C_A}{-\epsilon_{ir}} + \mathcal{O}(1) \tag{C.2}$$

$$\text{diag.}(a6) = \frac{(-16+16\xi)C_A}{\epsilon_{ir}^2} + \frac{(-32+32\xi+\xi^2)C_A}{-\epsilon_{ir}} + \mathcal{O}(1) \tag{C.3}$$

$$\text{diag.}(b2) = \frac{(-8+8\xi)C_A}{\epsilon_{ir}^2} + \frac{(-12+12\xi+2\xi^2)C_A}{-\epsilon_{ir}} + \mathcal{O}(1) \tag{C.4}$$

$$\text{diag.}(b3) = \frac{(8-8\xi)C_A}{\epsilon_{ir}^2} + \frac{(16-16\xi-2\xi^2)C_A}{-\epsilon_{ir}} + \mathcal{O}(1) \tag{C.5}$$

$$\text{diag.}(c2) = \frac{-4\xi C_A}{\epsilon_{ir}^2} + \frac{(-7\xi-\xi^2)C_A}{-\epsilon_{ir}} + \mathcal{O}(1) \tag{C.6}$$

$$\text{diag.}(c3) = \frac{8\xi C_A}{\epsilon_{ir}^2} + \frac{(14\xi+2\xi^2)C_A}{-\epsilon_{ir}} + \mathcal{O}(1) \tag{C.7}$$

$$\text{diag.}(c4) = \frac{-24\xi C_A}{\epsilon_{ir}^2} + \frac{-48\xi C_A}{-\epsilon_{ir}} + \mathcal{O}(1) \tag{C.8}$$

$$\text{diag.}(c6) = \frac{12\xi C_A}{\epsilon_{ir}^2} + \frac{(27\xi+4\xi^2)C_A}{-\epsilon_{ir}} + \mathcal{O}(1) \tag{C.9}$$

$$\text{diag.}(e1) = \frac{(12+8\xi)C_A}{\epsilon_{ir}^2} + \frac{(25+15\xi-\xi^2)C_A}{-\epsilon_{ir}} + \mathcal{O}(1) \tag{C.10}$$

$$\text{diag.}(e3) = \frac{(-4-4\xi)C_A}{\epsilon_{ir}^2} + \frac{(-9-11\xi-2\xi^2)C_A}{-\epsilon_{ir}} + \mathcal{O}(1) \tag{C.11}$$

$$\text{diag.}(f1) = \frac{0}{\epsilon_{ir}^2} + \frac{(\xi-5)((14+4\xi+\xi^2)C_A - 8T_F n_f)}{-6\epsilon_{ir}} + \mathcal{O}(1) \tag{C.12}$$

$$\text{diag.}(g2) \;=\; \frac{0}{\epsilon_{ir}^2} + \frac{(1-\xi)((14+4\xi+\xi^2)C_A - 8T_F n_f)}{-3\epsilon_{ir}} + \mathcal{O}(1) \qquad \text{(C.13)}$$

The poles of the self-energy diagrams have already been given sect. 3.3.2, while the remaining diagrams of fig. 1.4 are not IR singular.

What seems surprising at first sight is the non–cancelation of the leading $1/\epsilon_{ir}^2$ poles inside the topological classes. Guided by a simple argument given in the 4D treatment of ref. [6] (see sect. 4.4), such a cancelation of *leading* IR divergences can be expected to occur in the three–dimensional case also. However, as is explained in chapter 4, there is no contradiction. It turns out in the coordinate–space calculation that the leading IR divergences are power–like, and while they *do* cancel inside the classes, the ϵ_{ir}–poles seen in momentum space correspond to the *sub-leading* (logarithmic) divergences and hence their cancelation is *not* guaranteed by the above–mentioned argument.

Appendix D

Feynman Rules

In this chapter, all Feynman rules needed in this thesis are summarized. We work in Euclidean space, $g_{\mu\nu} = \mathrm{diag}(1,1,1,1)$. Integrals are often abbreviated as

$$\int_x = \int \mathrm{d}^D x \quad , \quad \int_{\not q} = \int \frac{\mathrm{d}^D q}{(2\pi)^D} \quad , \quad \int_{\boldsymbol{x}} = \int \mathrm{d}^{D-1}\boldsymbol{x} \quad , \quad \int_{\not{\boldsymbol{q}}} = \int \frac{\mathrm{d}^{D-1}\boldsymbol{q}}{(2\pi)^D}; . \tag{D.1}$$

In the same fashion, a slashed delta–function carries the appropriate power of 2π in the numerator, e.g. $\not\delta(\boldsymbol{q}) = \delta(\boldsymbol{q})/(2\pi)^{D-1}$.

The 'non–standard' rules (arising from the perturbative expansion of the Wilson–loop) are derived and explained in detail, including some specialties concerning the transformation from coordinate to momentum space. This is done in the first section. In the second section, the SU(N) Higgs model is explicited, to introduce notation for the 'standard' Feynman rules listed here. From the rules of the massive theory, one immediately deduces those for QCD by omitting all scalar particles and setting the masses to zero. The fermionic rules are given also. Finally, dropping the color structure, QED rules can be obtained. Hence, we will not list the cases of QCD and QED explicitly in this appendix.

D.1 Non–Standard Feynman Rules

From the Wilson–loop formula eq. (1.13), it is straightforward to derive a set of Feynman rules in coordinate space. Represented in a graphical notation already, the result is

$$V(\boldsymbol{r}) \;=\; -\lim_{T\to\infty}\frac{1}{T}\sum_{\text{diags.}}\widetilde{\mathrm{tr}}\int_x \ldots \int_x \times$$

$$\Big[\;\; \underset{\mathrm{x}\qquad\qquad \mathrm{y}}{=\!=\!=} \;,\; \underset{\mathrm{x}\qquad\qquad \mathrm{y}}{=\!=\!=\!\!\rightarrow} \;: \theta(y_0 - x_0)\;,$$

$$\underset{\mu\;\mathrm{a}}{\overset{\mathrm{x}}{\overset{=\!=\!=}{\sim\!\sim\!\sim}}} \;: -igT^a\delta_{\mu 0}\delta(\boldsymbol{x}-\boldsymbol{r})\theta(T^2/4 - x_0^2)\;,$$

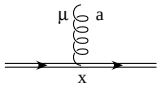

$$: igT^a\delta_{\mu 0}\delta(\boldsymbol{x})\theta(T^2/4 - x_0^2)\ , \quad + \text{standard rules} \Big] \tag{D.2}$$

Inside the brackets, it is understood to insert all diagrams contributing to the potential. These were already detailed in section 1.2, when discussing the expansion of the logarithm in the original Wilson–loop formula. The full set of coordinate–space 'standard rules', like e.g. the gluon propagator (in Feynman gauge)

$$\delta^{ab}D_{\mu\nu}(x-y) \;=\; \begin{cases} \dfrac{\delta^{ab}g_{\mu\nu}}{4\pi^2(y-x)^2} & (\mathrm{D}=4) \\ \dfrac{\delta^{ab}g_{\mu\nu}}{4\pi\sqrt{(y-x)^2}} & (\mathrm{D}=3) \end{cases} \tag{D.3}$$

will not be given here.

From eq. (D.2), one can derive a set of momentum–space Feynman rules. The sign–convention for Fourier transforms we use is given by $f(x) = \int \frac{\mathrm{dk}}{2\pi} \exp(-ikx)\, f(k)$. This convention manifests itself in the sign of the causal $i\epsilon$ in the source–'propagator' below, which is nothing but the Fourier transform of the θ–function. Plugging in the momentum–space representations, we get

$$\begin{aligned} V(\boldsymbol{q}) \;&=\; \int_{\boldsymbol{r}} \exp(i\boldsymbol{q}\boldsymbol{r})V(\boldsymbol{r}) \\ &=\; -\lim_{T\to\infty}\frac{1}{T}\sum_{\text{diags.}}\tilde{\text{tr}}\int_{\not k}\ldots\int_{\not k}\int_{\not p_0}\ldots\int_{\not p_0} \not\delta(\Sigma\boldsymbol{k}_{(\text{upper line})} - \boldsymbol{q})\,\not\delta_{\prime\text{inner vertices}'} \times \\ &\Bigg[\quad \underset{\text{p}}{\longrightarrow}\ , \quad \underset{\text{p}}{\longrightarrow} \ : \frac{i}{p_0 + i\epsilon}\ , \end{aligned}$$

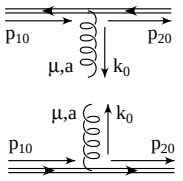

$$: -igT^a\delta_{\mu 0}\,\frac{\sin\left((p_{10}-p_{20}-k_0)T/2\right)}{(p_{10}-p_{20}-k_0)/2}\ ,$$

$$: igT^a\delta_{\mu 0}\,\frac{\sin\left((p_{10}-p_{20}-k_0)T/2\right)}{(p_{10}-p_{20}-k_0)/2}\ , \quad + \text{st. rules} \Bigg] \tag{D.4}$$

The first delta–function guarantees that the net momentum transfer from the quark– to the antiquark–line equals $\boldsymbol{q}$, while the trigonometric functions originate from the factors of $\theta(T^2/4 - x_0^2)$ at each vertex in x–space. They are very disturbing in a momentum–space calculation, since as a result of keeping the time–extension T of the Wilson–loop finite, there is no energy–conservation at the source–gluon vertices.

The standard procedure to extract practical Feynman rules is to exchange limit and summation now. One immediately recognizes that the needed energy–conserving delta–functions build up at each vertex according to

$$\lim_{T\to\infty}\frac{\sin(p_0T/2)}{p_0/2} = \not\delta(p_0)\ . \tag{D.5}$$

These delta–functions can then be used to solve the remaining p_0–integrals. Finally, the overall factor of $\frac{1}{T}$ gets canceled by a delta–function with zero argument, which becomes clear remembering the origin of this function,

$$\frac{\not{\delta}(0)}{T} = \lim_{T\to\infty} \frac{1}{T} \int_{-T/2}^{T/2} \mathrm{d}t \, \exp(it \cdot 0) = \lim_{T\to\infty} \frac{T}{T} = 1 \, . \tag{D.6}$$

Along these lines, one arrives at the 'asymptotic' Feynman rules

$$V(\boldsymbol{q}) = -\sum_{\text{diags.}} \widetilde{\mathrm{tr}} \int_{\not k} \ldots \int_{\not k} \not{\delta}(\Sigma k_{(\text{upper line})} - q)\Big|_{q_0=0} \times$$

$$\Big[\quad , \quad : \frac{i}{p_0 + i\epsilon} \, , \quad : -igT^a\delta_{\mu 0} \, ,$$

$$: igT^a\delta_{\mu 0} \, , \quad + \text{standard rules} \Big] \, , \tag{D.7}$$

where now E–p–conserving delta functions are implied at each vertex. It is this set of Feynman rules that is used for calculations of the static p–space potential. By convention, the normalized color trace $\widetilde{\mathrm{tr}}\{T^{\cdots}\} = \mathrm{tr}\{T^{\cdots}\}/\mathrm{tr}\mathbb{1}$ has to be taken in the direction opposite to the arrows on the source–lines.

Using the 'asymptotic' Feynman rules, it is thus possible to calculate contributions to the potential in momentum space directly, without having to perform the limit of large times in the end. However, it is important to keep in mind that exchanging limit and summation is defined only if no divergences are present, a feature that cannot be guaranteed on the level of individual diagrams. Such large–time divergences correspond to infrared divergences in momentum–space. Hence, it should be expected that the contributions of individual diagrams to $V(\boldsymbol{q})$ can be IR singular, making the use of an IR regularization scheme necessary. Note that dimensional regularization regulates not only the UV divergences, but also the IR ones with the same parameter, such that in integrals with both types of divergences it will be necessary to extract the IR divergences beforehand, e.g. by employing a massive regularization, as is done in this work, cf. sections 3.2.1 and 3.3.2.

D.2 SU(N)

Some useful formulae concerning the group SU(N) (or any other compact semi–simple Lie group) are collected here.

T^a are the (hermitean and traceless) generators of the fundamental representation, normalized by

$$\mathrm{tr}(T^a T^b) = T_f \, \delta^{ab} \, . \tag{D.8}$$

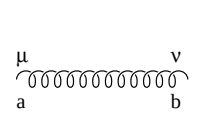

$$\frac{1}{p^2+m_W^2}\left(g_{\mu\nu}-\frac{p_\mu p_\nu}{p^2}\right)\delta^{ab}+\frac{\eta}{p^2+\eta m_W^2}\frac{p_\mu p_\nu}{p^2}\,\delta^{ab}$$
$$=\frac{1}{p^2+m_W^2}\,g_{\mu\nu}\,\delta^{ab}+\left(\frac{1}{p^2+m_W^2}-\frac{1}{p^2+\eta m_W^2}\right)\frac{p_\mu p_\nu}{m_W^2}\,\delta^{ab}$$

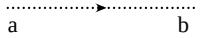

$$\frac{1}{p^2+\eta m_W^2}\,\delta^{ab}$$

$$\frac{1}{p^2+\eta m_W^2}\,\delta^{ab}$$

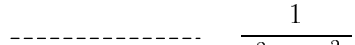

$$\frac{1}{p^2+m_H^2}$$

Figure D.1: *Euclidean Feynman rules for two–point functions. Curly, dotted, plain and dashed lines denote gluons, ghosts, Goldstone and Higgs bosons, respectively.*

The totally antisymmetric structure constants are defined by the Lie algebra

$$[T^a,T^b]=if^{abc}\,T^c\;, \tag{D.9}$$

while the Casimir operators of the fundamental and adjoint representation are

$$T^aT^a=C_F\qquad,\qquad f^{acd}\,f^{cdb}=C_A\,\delta^{ab}\;, \tag{D.10}$$

respectively. For the group SU(N), it is common to set $T_f=\frac{1}{2}$, so their values are

$$C_F=\frac{N^2-1}{2N}\qquad,\qquad C_A=N\qquad(\mathrm{SU(N)})\;. \tag{D.11}$$

The totally symmetric structure constants d^{abc} can be defined by the anticommutator,

$$\{T^a,T^b\}\;=\;(C_A-2C_F)\,\delta^{ab}\,\mathbb{1}+d^{abc}\,T^c\quad,\quad d^{abc}=\frac{1}{T_f}\,\mathrm{tr}(\{T^a,T^b\}T^c)\;. \tag{D.12}$$

For the group SU(2), d^{abc}=0. Useful relations include

$$d^{aac}=0\qquad,\qquad d^{abc}d^{abd}=(8C_F-3C_A)\,\delta^{cd}\;. \tag{D.13}$$

With the help of both types of structure constants, products of generators can be rewritten as

$$T^aT^b\;=\;(\tfrac{1}{2}C_A-C_F)\,\delta^{ab}\,\mathbb{1}+\tfrac{1}{2}(d^{abc}+if^{abc})T^c\;. \tag{D.14}$$

Further useful relations needed for the color sums in this work are

$$T^aT^bT^a\;=\;(C_F-\tfrac{1}{2}C_A)\,T^b \tag{D.15}$$
$$T^aT^bT^cT^a\;=\;(C_F-\tfrac{1}{2}C_A)(T^{bc}-\tfrac{1}{2}C_A\delta^{bc}\,\mathbb{1})\;, \tag{D.16}$$

as well as the Jacobi identity

$$0\;=\;f^{abe}f^{ecd}+f^{bce}f^{ead}+f^{cae}f^{ebd}\;. \tag{D.17}$$

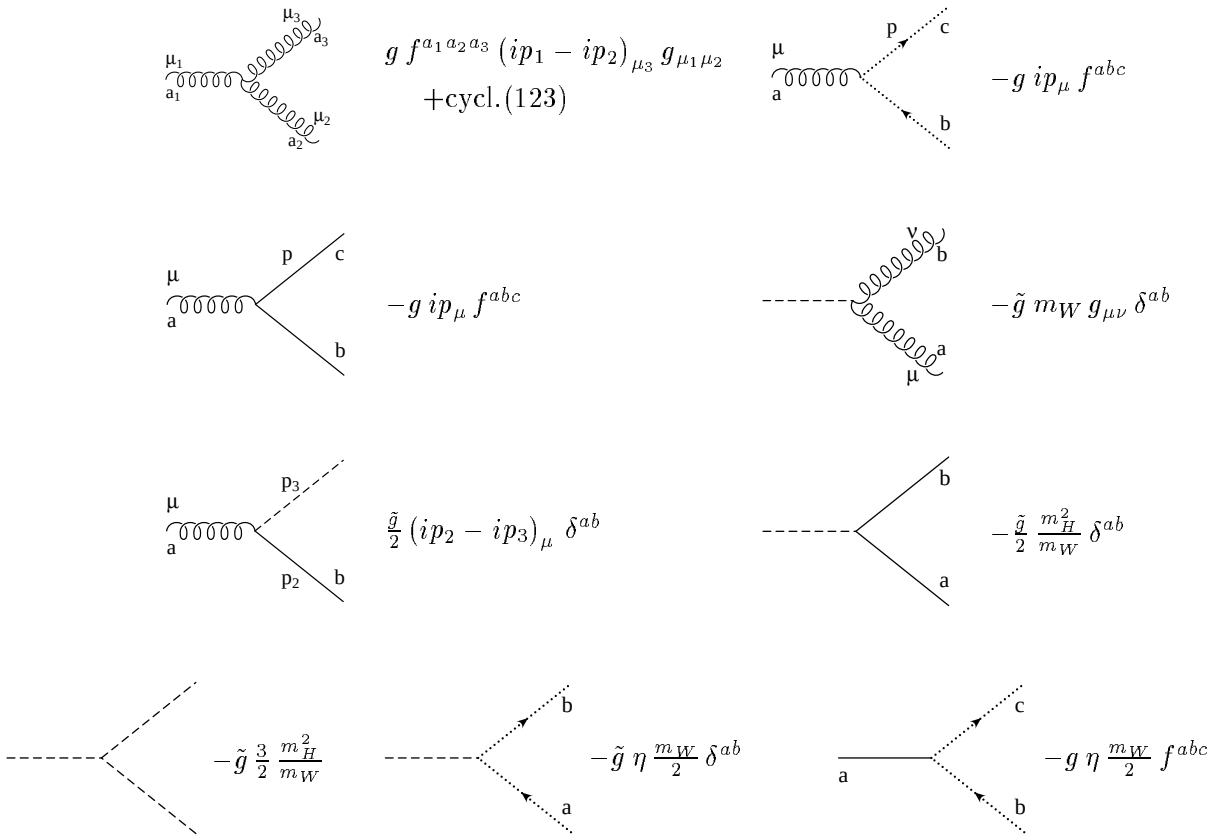

Figure D.2: *Euclidean Feynman rules for three–point functions. All momenta p are defined outgoing. The abbreviation $\tilde{g} = g\sqrt{4T_f/N} = g\sqrt{2C_A - 4C_F}$ is used. Note that $\tilde{g} = g$ for SU(2) with $T_f = \frac{1}{2}$.*

D.3 Standard Feynman Rules

Let us define the SU(N) Higgs model by the action

$$S = \int \mathrm{d}^D x\, \mathcal{L} = \int \mathrm{d}^D x\, \frac{1}{2T_f}\, \mathrm{tr}\, \left[\frac{1}{2} W_{\mu\nu} W_{\mu\nu} + (D_\mu \Phi)^\dagger D_\mu \Phi - \frac{m_H^2}{2}\, \Phi^\dagger \Phi + \frac{g^2 m_H^2}{4 m_W^2}\, (\Phi^\dagger \Phi)^2 \right] \quad \text{(D.18)}$$

where $\Phi = \sqrt{\frac{T_f}{N}}\, \sigma\, \mathbb{1} + i \pi^a\, T^a$ collects the N^2 real scalar fields σ and π^a, and the covariant derivative $D_\mu = \partial_\mu - i g W_\mu$ as well as the adjoint fields $W_\mu = W_\mu^a\, T^a$ are defined in the usual way. For SU(N) relations, like trace normalization etc., see sect. D.2.

The lagrangian has to be supplemented by gauge–fixing and Faddeev–Popov ghost terms,

$$\mathcal{L}_{\mathrm{GF}} = \frac{1}{2\eta}\, (G^a)^2 \quad , \quad G^a = \partial_\mu W_\mu^a - \eta m_W \pi^a\, , \quad \text{(D.19)}$$

$$\mathcal{L}_{\mathrm{FP}} = -(c^a)^*\, M^{ab}\, c^b\, . \quad \text{(D.20)}$$

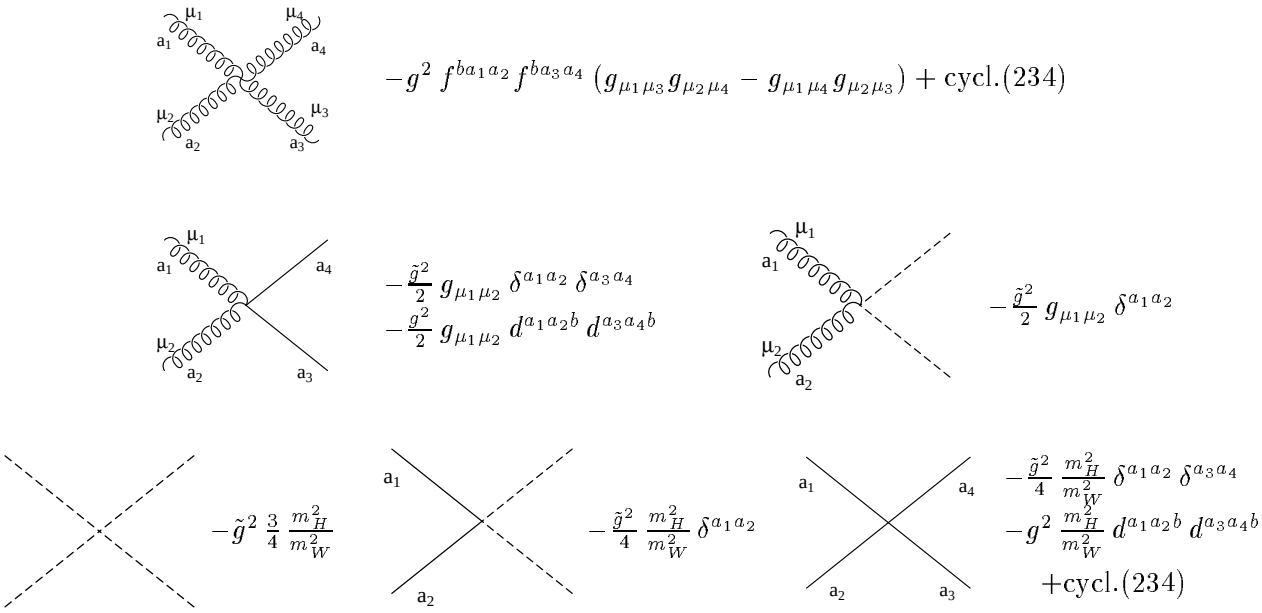

Figure D.3: *Euclidean Feynman rules for four–point functions. For the definition of the totally symmetric constants d^{abc} see App. D.2.*

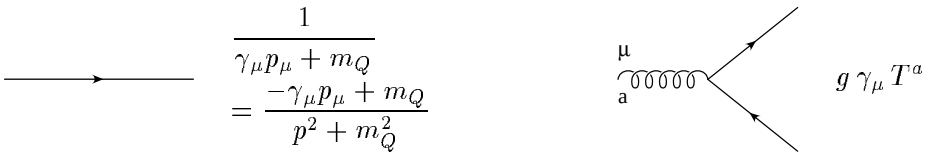

Figure D.4: *Euclidean Feynman rules for quarks. Arrows denote the fermion flow. Traces are to be taken in the opposite direction.*

The gauge–fixing condition G^a is chosen such that the term proportional to $W_\mu \partial_\mu \pi$, which is induced by the shift below, cancels in the action. The matrix appearing in the ghost term is the variation of the gauge–fixing condition, $\delta G^a = M^{ab}\Lambda^b$, under infinitesimal gauge transformations given by $\Phi \to U\Phi$, $W_\mu \to \frac{i}{g} U D_\mu U^\dagger$, $U = \exp(igT^a\Lambda^a)$.

Shifting the Higgs field around the classical minimum of the potential, $\sigma = \sigma' + \frac{m_W}{g}\sqrt{\frac{N}{T_f}}$, the mass term for the vector bosons is generated, and one obtains the set of Feynman rules depicted in this appendix. There are two quartic vertices that contain parts proportional to the not too familiar symmetric structure constants d^{abc} (cf. fig. D.3). However, these parts do not contribute to the one-loop self-energy calculated in section 5.2.

Bibliography

[1] W. Buchmüller, G, Grunberg and S.-H. H. Tye, Phys. Rev. Lett. **45** (1980) 103; S.J. Brodsky, G.P. Lepage and P.B. Mackenzie, Phys. Rev. **D 28** (1983) 228.

[2] W. Bardeen, A. Buras, D. Duke and T. Muta, Phys. Rev. **D 18** (1978) 3998.

[3] G.P. Lepage and P.B. Mackenzie, Phys. Rev. **D 48** (1993) 2250, `hep-lat/9209022`.

[4] L. Susskind, *Coarse grained quantum chromodynamics* in R. Balian and C.H. Llewellyn Smith (eds.), *Weak and electromagnetic interactions at high energy* (North Holland, Amsterdam, 1977).

[5] A. Billoire, Phys. Lett. **B 92** (1980) 343.

[6] W. Fischler, Nucl. Phys. **B 129** (1977) 157.

[7] T. Appelquist, M. Dine and I.J. Muzinich, Phys. Lett. **B 69** (1977) 231; Phys. Rev. **D 17** (1978) 2074.

[8] M. Jeżabek, J.H. Kühn, M. Peter, Y. Sumino and T. Teubner, Phys. Rev. **D 58** (1998) 14006, `hep-ph/9802373`; for a recent review, see A.H. Hoang and T. Teubner, preprint CERN-TH-99-59, `hep-ph/9904468`.

[9] M. Peter, Phys. Rev. Lett. **78** (1997) 602, `hep-ph/9610209`; Nucl. Phys. **B 501** (1997) 471, `hep-ph/9702245`.

[10] M. Melles, Phys. Rev. **D 58** (1998) 114004, `hep-ph/9805216`.

[11] N. Brambilla, A. Pineda, J. Soto and A. Vairo, preprint CERN-TH-99-61, `hep-ph/9903355`.

[12] see, e.g., G. 't Hooft, Acta Phys. Austr. Suppl. **12** (1980) 531 (Schladming lecture 1980); R.P. Feynman, Nucl. Phys. **B 188** (1981) 479.

[13] for textbooks, cf. J.I. Kapusta, *Finite-temperature field theory* (Cambridge University Press, 1989); M. Le Bellac, *Thermal field theory* (*ibid.*, 1996).

[14] D.J. Gross, R.D. Pisarski and L.G. Jaffe, Rev. Mod. Phys. **53** (1981) 43; S. Nadkarni, Phys. Rev. **D 27** (1983) 917; N.P. Landsman, Nucl. Phys. **B 322** (1989) 498.

[15] T. Appelquist and R.D. Pisarski, Phys. Rev. **D 23** (1981) 2305.

[16] K. Wilson and J. Kogut, Phys. Rep. **12C** (1974) 75; A.D. Linde, Phys. Lett. **B 96** (1980) 289.

[17] K. Kajantie, M. Laine, K. Rummukainen and M. Shaposhnikov, Nucl. Phys. **B 458** (1996) 90, `hep-ph/9508379`.

[18] O. Philipsen, M. Teper and H. Wittig, Nucl. Phys. **B 469** (1996) 445, `hep-lat/9602006`; M. Gürtler, E.M. Ilgenfritz, J. Kripfganz, H. Perlt and A. Schiller, Nucl. Phys. **B 483** (1997) 383, `hep-lat/9605042`.

[19] H.G. Dosch, J. Kripfganz, A. Laser and M.G. Schmidt, Phys. Lett. **B 356** (1996) 213, `hep-ph/9509352`; Nucl. Phys. **B 509** (1997) 519, `hep-ph/9612450`; W. Buchmüller and O. Philipsen, Phys. Lett. **B 397** (1997) 112, `hep-ph/9612286`.

[20] K.G. Chetyrkin and F.V. Tkachov, Nucl. Phys. **B 192** (1981) 159.

[21] A.I. Davydychev, Phys. Lett. **B 263** (1991) 107.

[22] O.V. Tarasov, Phys. Rev. **D 54** (1996) 6479, `hep-th/9606018`.

[23] O.V. Tarasov, Nucl. Phys. **B 502** (1997) 455, `hep-ph/9703319`.

[24] E. Eichten and B. Hill, Phys. Lett. **B 234** (1990) 511; for a review and references, see M. Neubert, Phys. Rep. **245C** (1994) 259, `hep-ph/9306320`.

[25] A. Duncan, Phys. Rev. **D 10** (1976) 2866.

[26] E. Eichten and F.L. Feinberg, Phys. Rev. Lett. **43** (1979) 1205; E. Eichten and F.L. Feinberg, Phys. Rev. **D 23** (1981) 2724.

[27] G. Passarino and M. Veltman, Nucl. Phys. **B 160** (1979) 151.

[28] N.N. Bogoliubov and D.V. Shirkov, *Introduction to the Theory of Quantized Fields* (J. Wiley, New York, 1980).

[29] O.V. Tarasov, Acta Phys. Pol. **B 29** (1998) 2655, `hep-ph/9812250`.

[30] J.A.M. Vermaseren, *Symbolic Manipulation with FORM* (CAN, Amsterdam, 1991).

[31] B.W. Char, K.O. Geddes, G.H. Gonnet, B.L. Leong, M.B. Monagan, S.M. Watt, *Maple V* (Springer, New York, 1991).

[32] S. Wolfram, *Mathematica – A System for Doing Mathematics by Computer* (Addison-Wesley, Redwood City, CA, 1988).

[33] G. 't Hooft and M. Veltman, Nucl. Phys. **B 44** (1972) 189; G. 't Hooft, Nucl. Phys. **B 61** (1973) 455.

[34] see, e.g., S.A. Larin and J.A.M. Vermaseren, Phys. Lett. **B 303** (1993) 334, `hep-ph/9302208`; T. v. Ritbergen, J.A.M. Vermaseren and S.A. Larin, Phys. Lett. **B 400** (1997) 379, `hep-ph/9701390`.

[35] Y. Schröder, Phys. Lett. **B 447** (1999) 321, `hep-ph/9812205`.

[36] R. Mertig and R. Scharf, Comput. Phys. Commun. **111** (1998) 265, `hep-ph/9801383`.

[37] I.S. Gradshteyn and I.M. Ryzhik, *Table of Integrals, Series and Products* (Academic Press, New York 1965).

[38] G.S. Bali, preprint HUB-EP-99/23, `hep-ph/9905387`.

[39] Y. Schröder, *The static potential in QCD_3 at one loop* in F. Csikor and Z. Fodor (eds.), *Strong and electroweak matter '97* (World Scientific, 1997).

[40] M. Teper, Phys. Lett. **B 397** (1997) 223, `hep-lat/9701003`; Nucl. Phys. **B** (Proc. Suppl.) **53** (1997) 715, `hep-lat/9701004`; Phys. Rev. **D 59** (1999) 14512, `hep-lat/9804008`.

[41] C. Bachas, Phys. Rev. **D 33** (1986) 2723.

[42] D.Z. Freedman, K. Johnson and J.I. Latorre, Nucl. Phys. **B 371** (1992) 353; F. del Águila, A. Culatti, R. Muñoz Tapia and M. Pérez-Victoria, Nucl. Phys. **B 537** (1999) 561.

[43] G.P. Lepage, J.Comp.Phys. **27** (1978) 192.

[44] M. Laine, preprint CERN-TH-99-62, `hep-ph/9903513`.

[45] W.E. Caswell and G.P. Lepage, Phys. Lett. **B 167** (1986) 437; G.T. Bodwin, E. Braaten and G.P. Lepage, Phys. Rev. **D 51** (1995) 1125, *ibid.* **55** (1997) 5853 (E), `hep-ph/9407339`.

[46] A. Pineda and J. Soto, Nucl. Phys. **B** (Proc. Suppl.) **64** (1998) 428, `hep-ph/9707481`.

[47] W. Buchmüller and O. Philipsen, Nucl. Phys. **B 443** (1995) 47, `hep-ph/9411334`.

[48] R. Scharf and J.B. Tausk, Nucl. Phys. **B 412** (1994) 523; F.A. Berends and J.B. Tausk, Nucl. Phys. **B 421** (1994) 456.

[49] A.I. Davydychev, Acta. Phys. Pol. **B 28** (1997) 841, `hep-ph/9610510`.

[50] A.K. Rajantie, Nucl. Phys. **B 480** (1996) 729, *ibid.* **513** (1998) 761 (E), `hep-ph/9606216`.

Acknowledgments

I would like to thank my advisor, W. Buchmüller, who suggested this investigation, for continuous support and encouragement, as well as for sharing his ideas with me in highly motivating discussions.

At different stages of the work, I have profited from discussions with A. Hebecker, O. Philipsen, A. Gehrmann-De Ridder, M. Peter, M. Spira, T. Teubner, M. Plümacher, T. Plehn, R. Kirchner and O. Bär .

Finally, I would like to thank all my colleagues and friends at DESY for the enjoyable working atmosphere.